Examensarbete
TVVR 12/5006

Flow conditions downstream of Bergeforsen dam

Erik Lidén

Division of Water Resources Engineering
Department of Building and Environmental Technology
Lund University

Avdelningen för Teknisk Vattenresurslära
TVVR 12/5006
ISSN-1101-9824

Flow conditions downstream of Bergeforsen dam

Flödesförhållanden nedströms dammen i Bergeforsen

Erik Lidén

Abstract

Due to the change in climate the design flow for Bergeforsen dam, located at the Indalsälven river mouth, is being revised from 2300 m^3/s to more than 3000 m^3/s. The dam needs to be upgraded with a new gated spillway and repaired in order to increase the safety of the dam. Concerns have been raised about the altered flow conditions that will occur downstream of the dam in connection with that the new spillway is constructed and taken into service. These altered conditions could result in an increased risk for erosion of the channel bed as well as a compromise in the safety of the dam and the future operation of the hydropower facility. Therefore, a detailed analysis of the flow downstream of the dam was carried out using the numerical modeling program SMS. The velocities, water depths, bed shear stresses and critical particle diameters were simulated with the two-dimensional hydraulic model RMA2. This was done for eight different discharge combinations with flows from the existing and new spillway as well as from the power plant.

From the simulation results, it was concluded that the construction of the new spillway would lead to an increase in velocities, shear stresses and critical particle diameters. The increase was most pronounced in the vicinity of the spillways and the power station outlet. Although no clear information regarding the particle size distribution in the investigated area is available, the bed shear stress and critical particle diameter values in the different zones could be related to each other in order to get a feel for the relative erosion potential. They could also work as an indicator of what kind of erosion protection material that needs to be placed in that particular area in order to prevent future erosion. Topics for further investigations are whether the shallow areas about 200 meters downstream of the existing spillway are sufficiently protected against erosion and what the exact decrease in operational head for the power plant after the construction is.

Regarding the numerical model, the capabilities of RMA2 were not enough to completely reflect the flow conditions, especially in the area around the spillways. Even so, the general flow patterns and trends received from the simulations could function as a good complement to the future tests in the physical hydraulic model in the laboratory at Vattenfall Research and Development in Älvkarleby.

Keywords: Bergeforsen, Indalsälven, spillway, dam safety, design flow, flow conditions, erosion, SMS, Surfacewater Modeling System, RMA2

Acknowledgements

I would like to thank my supervisor James Yang at Vattenfall Research and Development AB for giving me the opportunity to conduct this master thesis, be a part of the project regarding the Bergeforsen dam and introducing me to the fascinating and complex fields of numerical and physical hydraulic modeling. Furthermore, I would like to thank my supervisor Magnus Larson at LTH for the guidance and valuable critics and comments throughout the project.

Table of contents

This project was carried out as a master thesis for the Master of Science in Environmental Engineering program at the Division of Water Resources Engineering, Lund Institute of Technology, Lund University, Sweden. The simulations, measurements and analysis were performed at Vattenfall Research and Development AB, Älvkarleby, Sweden.

1 Introduction

1.1 Project description

Due to the change in climate, which is believed to lead to an increase in the annual river discharge, the design flows for several hydropower dams in Sweden are being revised in accordance to the new design flood guidelines. The Bergeforsen dam, located at the Indalsälven river mouth, is one of the dams affected by this revision. The dam needs to be upgraded to increase its design flow and repaired to increase the safety of the dam. Due to these circumstances, a new gated spillway will be constructed in addition to the existing spillway to increase the total discharge capacity.

Concerns have been raised about the altered flow conditions that will occur downstream of the dam in connection with that the new spillway is constructed and taken into service. These altered conditions could result in an increased risk for erosion of the channel bed as well as a compromise in the safety of the dam and the future operation of the hydropower facility. At Vattenfall Research and Development AB hydraulic model tests have been made in order to provide the planning process with the required data. However, due to growing costs and a lack of time, the flow conditions has only been mapped and analyzed in a few sections and a complete picture of the downstream flow conditions is missing. Because of this, it has been concluded that a detailed analysis of the flow downstream of the dam needs to be carried out.

1.1.1 Objectives

The objective of this thesis is to determine the flow conditions downstream of the Bergeforsen dam for the present situation and how they change in connection with the construction of the new spillway. The study will include a detailed investigation of the flow patterns that develop as well as their effects on the erosion potential and the resulting changes in the river bed and water level. Different discharge combinations (DC) of the flows through the hydropower plant, the existing and the new spillway structures are going to be studied.

Situation prior to the construction:

- DC1: The hydropower plant is in operation and the existing spillway gates are closed.
- DC2: The hydropower plant is out of operation due to high flow and the existing spillway gates are open.
- DC3: The hydropower plant is out of operation due to a flow higher than the present design flow causing flooding of the upstream area and the existing spillway gates are open.

Situation after the construction:

- DC4: The hydropower plant is in operation and both the existing and new spillway gates are closed.

- DC5: The hydropower plant is out of operation due to high flow, the existing spillway gates are open and the new spillway gate is closed.
- DC6: The hydropower plant is out of operation due to high flow, the new spillway gate is open and the existing spillway gates are closed.
- DC7: The hydropower plant is out of operation due to high flow and both the existing and the new spillway gates are open.
- DC8: The hydropower plant is out of operation due to a flow higher than the new design flow causing flooding of the upstream area and both the existing and the new spillway gates are open.

1.1.2 Methodology

Prior to the simulations of the downstream flow conditions, a literature study regarding the background theory of dam safety, design flow, erosion as well as physical and numerical hydraulic modeling is performed. Previously obtained background data from the Bergeforsen dam will be reviewed and analyzed in order to provide a general understanding of the flow conditions. The numerical hydraulic modeling program SMS 8.1 will be employed in order to generate, simulate and analyze the different discharge combinations. River bed topography from a digital terrain model and beforehand obtained boundary conditions will be used as input to the program. Verification of the simulations will be carried out using the flow data received from the beforehand carried out model tests at Vattenfall R&D. The potential erosion and the resulting changes in the river bed will be determined from established hydrodynamic theories and relations regarding sediment transport.

2 Dam safety

2.1 Spillways and outlets

In order for dams to pass floods in a safe and controlled manner they are equipped with spillways. During very high flows which the turbines cannot handle, the power plant is usually taken out of operation and the spillway gates are opened to prevent flooding of the upstream area. It is often difficult to dissipate the energy stored by raising the water depth in the reservoir behind the dam which means that the spillways need to be located on the most erosion-resistant foundation material available along the dam axis and constructed in concrete with erosion-resistant surfaces. This makes the spillways one of the most expensive and essential parts of the dam. The Bergeforsen dam is equipped with gated spillways which are reliant on to be free of debris blockage and have a good power supply and management in order to avoid rises in the reservoir level. Since gated spillways are often designed to pass a much higher flow than free flow spillways, the energy dissipation below the spillway in this case pose a much higher challenge (Lysne et al., 2003). More about the Bergeforsen dam and spillways in section 3.

2.2 Design flow

When constructing and operating a dam it is fundamental to determine a design flow. This is the maximum flow the dam should be able to handle at full reservoir retention level (FRRL) without flooding of the surrounding area or breaking of the dam construction. Flooding or breaking of the dam can cause severe economical damage and loss of life and it is therefore crucial to find an acceptable design flow. Doing this is no easy task and the long record of dam safety incidents related to insufficient spillway designs are an indication that this is of major concern worldwide (Bergström et al., 1992).

In Sweden, there are a number of legalizations and recommendations to take into consideration when investigating dam safety. This includes the environmental code 1998:808, regulation 1998:901 on self-monitoring, act 2003:778 on protection against accidents, the Swedish spillway design flood guidelines and RIDAS (Svenska kraftnät, 2011).

2.2.1 Swedish spillway design flood guidelines and RIDAS

In 1990, the Swedish Committee for Design Flood Determination published a set of guidelines for determining the design flow for Swedish waterpower and mining dams. Since then the guidelines has gained acceptance by the industry and the Swedish Meteorological and Hydrological Institute (SMHI) and an updated version was published in 2007. This updated version also discusses the implications of climate change on design flow (see section 2.2.2). Briefly summarized, the guidelines make a classification of dams into two categories depending on the potential consequences of dam failure; flow design class I (FDC I) and II (FDC II). FDC I, which includes the Bergeforsen dam, applies to dams where failure could cause loss of life, injury, damage to infrastructure, property or the environment, or other extensive economic damage. FDC II applies to dams where failure could cause damage to infrastructure, property or the environment. This also means that the design floods for the two categories of dams are determined in different ways (KFR, 2007).

Determination of the design flood for FDC I are based on hydrological simulations using the HBV model, developed by SMHI, where a 14 days long extreme precipitation sequence coincides with heavy snowmelt and wet soils. When all these conditions occur at the same time the result is very high flows, which the dam should be able to withstand without any severe damage to the structure. It has been found that flows received by using this method have a return period of more than 10 000 years on average. Regarding dams of FDC II, they must be able to pass a flow with at least a 100 year return period at FRRL. Here, a frequency analysis should be applied together with a cost-benefit analysis, meaning that a design flood of higher return period than 100 year could be selected as long as the costs are not far greater than the benefits (KFR, 2007).

RIDAS is the Swedish power industry's own set of guidelines to support the work on dam safety. These guidelines were published in 1997, latest updated in 2008 and can be ordered from Svensk energi's homepage (http://www.svenskenergi.se/sv/Kompetens/webbshop/Fakta-pa-webben/RIDAS---Kraftforetagens-riktlinjer-for-dammsakerhet/).

2.2.2 Design flood and climate change

Due to climate change, the conventional way of calculating a design flow may be insufficient. The flows received from historical data might not correlate with future flows and parameters such as snowmelt, soil moisture, precipitation and evapotranspiration are all sensitive to a change in climate. The updated Swedish guidelines from 2007 address these uncertainties regarding climate change and states that the calculated design flows needs to be continuously revisited and margins created where ever possible (Elforsk, 2011).

One investigation of the impact of climate change on peak flows in Sweden were made by Elforsk (2011) where an adaptation of the design flows was made in accordance with the Swedish guidelines. Calculations of new design flows for FDC I was made for 11 different regions with relevance to hydropower and mine industry. The calculations were based upon 16 scenarios with a time period to the year 2050. As with the calculations carried out to determine the original design floods, the HBV model by SMHI was utilized in these simulations as well. The change in magnitude of flows with a 100 year return period was simulated and the results for Torpshammar, a station located in the Ljungan catchment area 40 km to the west of Bergeforsen, is shown in figure 1.

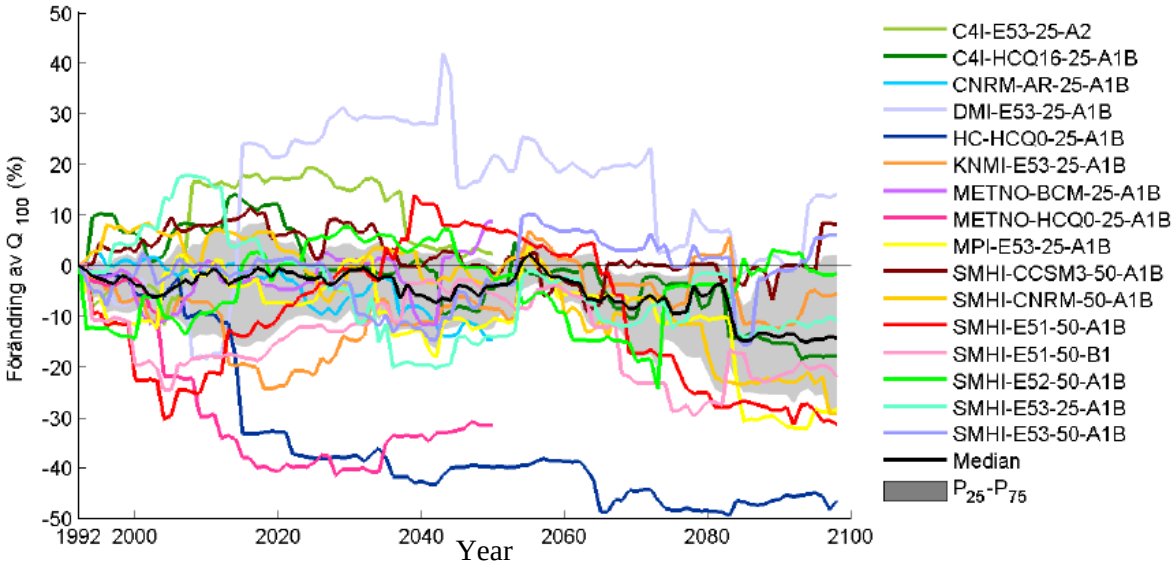

Figure 1. Change in the 100-year flood for Torpshammar. The graph includes 16 climate scenarios relative to the reference period 1963-1992. Each year's value was calculated from the maximum values for the previous 30 years. The gray area shows the variation between the 25th and 75th percentiles. (Elforsk, 2011).

As can be seen in the figure above, the results fluctuate a lot depending on the chosen climate scenario. The change in magnitude of a 100-year flood varies from -50% to +30%, with an average of -5%. The range of uncertainty grows significantly with time.

In another study carried out by Andréasson et al. (2004) the change in total annual runoff was investigated using four different climate scenarios. The hydrological model HBV by SMHI was utilized in this simulation as well. It was concluded that due to the warmer winters the timing of the flows would be more evenly spread out during the year and the mean annual runoff in northern Sweden, including the Indalsälven catchment area, would increase. This can be seen in figure 2 below. This would be mostly due to a decrease in spring flood peaks, increased autumn and winter runoff and an increase of high flow events during autumn.

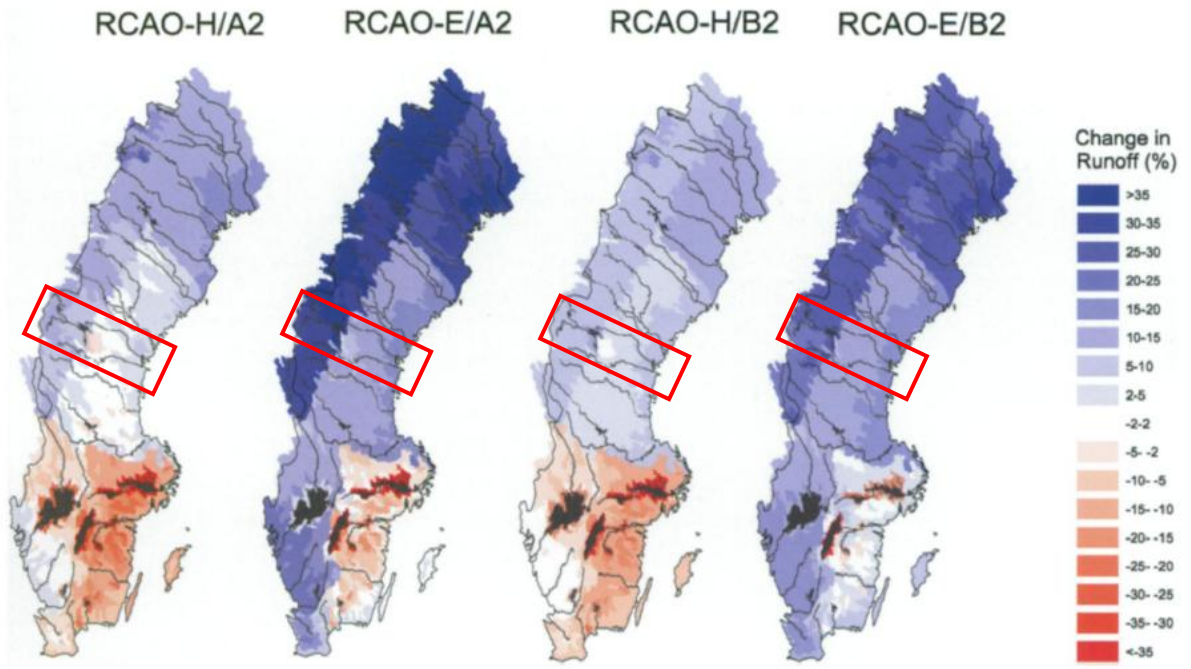

Figure 2. Change in average annual mean runoff for the time period 2071-2100 compared to the time period 1961-1990 for the four RCAO-scenarios. The red box marks the Indalsälven catchment area (Andréasson et al., 2004).

For the Indalsälven catchment area, the magnitude of the mean annual runoff is increased by 5-30%, depending on the climate scenario used.

The results from the climate change simulations above vary a lot and in the end no real conclusions can be drawn. It is however apparent that a change in peak flows and annual runoff will be notable in the future. Due to these uncertainties in the change of climate exemplified in the investigations above, the design flows for several dams in Sweden, including the Bergeforsen dam, are currently being revised.

3 Site description

3.1 The Indalsälven river

Bergeforsen is a small town with around 1600 inhabitants located in Timrå municipality in northern Sweden, approximatley 15 kilometer from the city of Sundsvall (SCB, 2011). Through the town runs the river Indalsälven which has its origin in the mountains to the northwest and reaches the Gulf of Botnia a few kilometers to the southeast of Bergeforsen (Vattenfall, 2012a). At the hydrological measuring station located near the dam the average low flow (MLQ) is 140 m^3/s, the average flow (MQ) 444 m^3/s and the average high flow (MHQ) 1110 m^3/s (SMHI, 2009). The main river catchment and the location of Bergeforsen can be seen in figure 3 below.

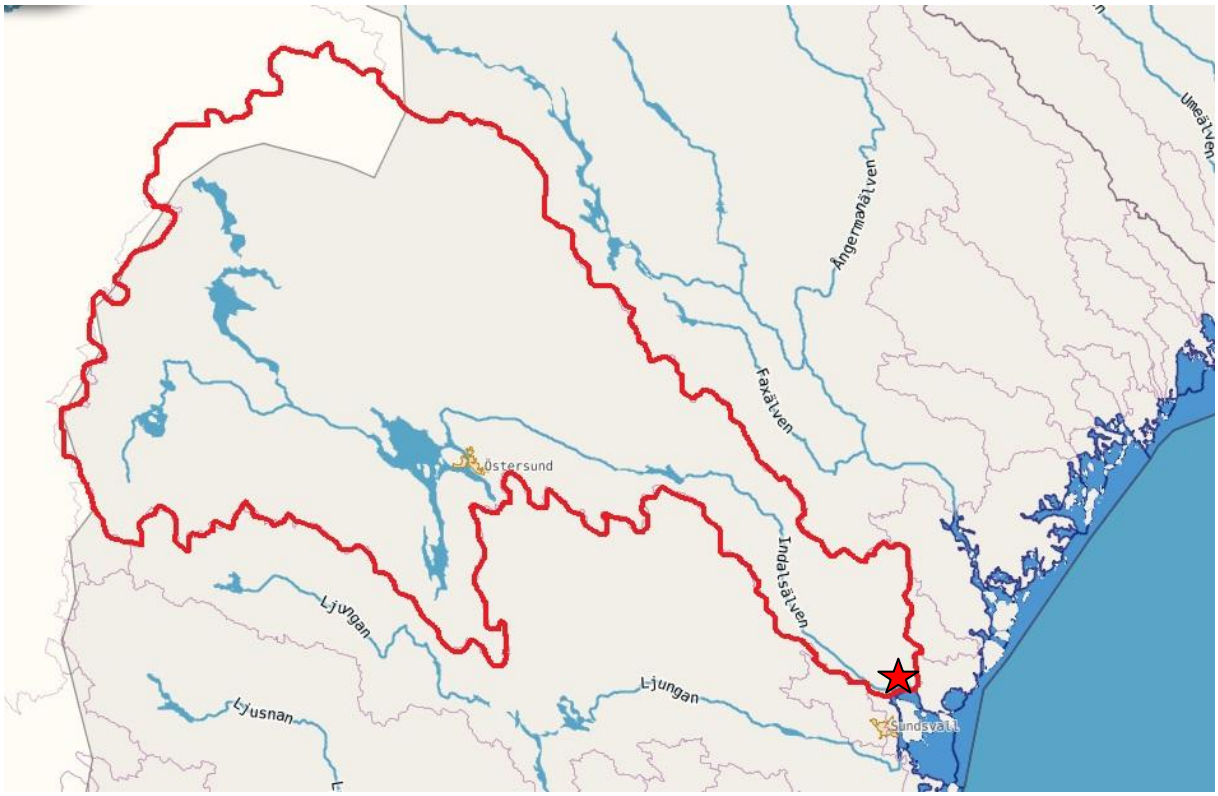

Figure 3. The Indalsälven main catchment area (red line) and the location of Bergeforsen (red star) (SMHI, 2012).

3.2 Existing dam and power plant

There are 31 power plants in operation in Indalsälven, with Vattenfall as the owner or partial owner of eight of them. Most of the dams and power plants were constructed more than 50 years ago and the facility at Bergeforsen, owned by Bergeforsen Kraft with Vattenfall and E.ON as the major shareholders, was put into operation in 1955 (Vattenfall, 2010). The facility consists of an earth fill dam on the left and right side, a disused plugged timber flume, a spillway with chutes and gates and a power station. There is a railroad and a highway (route 331) running across the downstream part of the

dam (Ekström et al., 2011). Both riversides downstream of the dam consist of erosion resistant material. The location of the facility can be seen in figure 4 below.

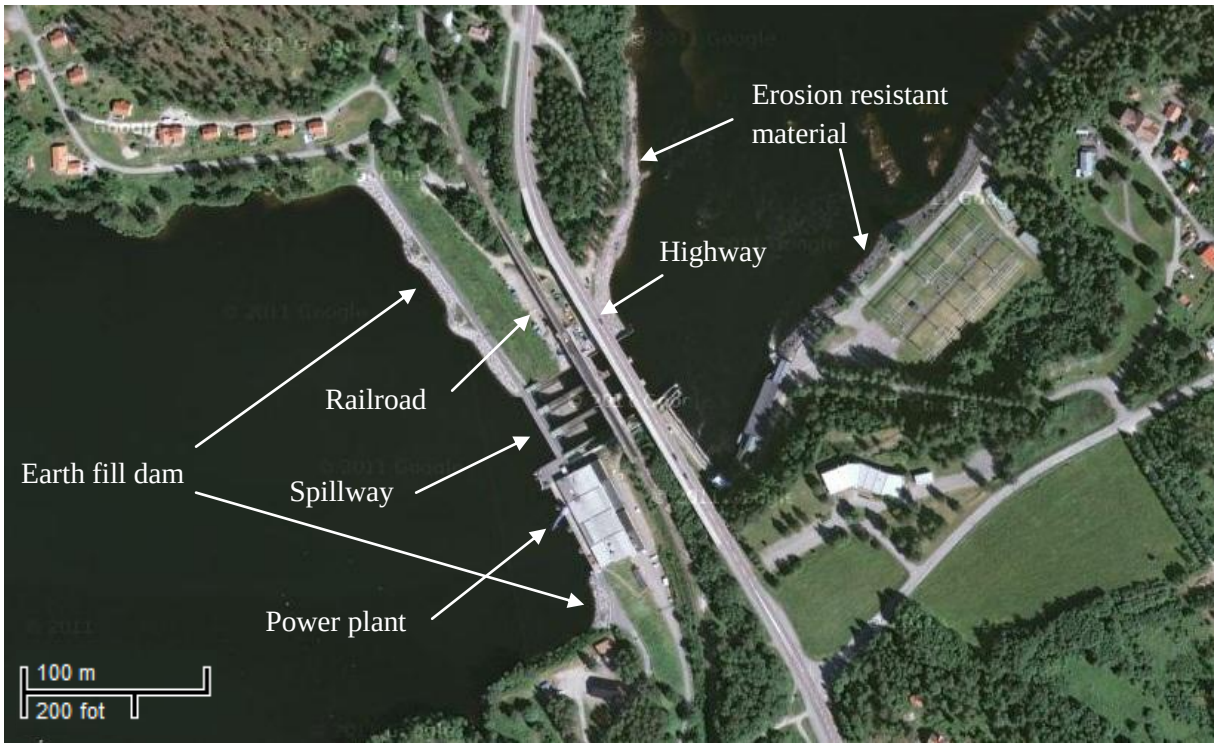

Figure 4. The Bergeforsen dam with the earth fill dam, the location of the power plant, the existing spillway with chutes and the erosion resistant riversides. The railroad and the highway run across the dam on the downstream side (Google, 2011).

3.2.1 Power plant

The power plant is a run-of-the river type, meaning that the dam has little storage capacity. The installed electrical capacity is 168 MW and the average annual production is 735 GWh. In order to generate electricity the plant utilizes four Kaplan turbines which operate at a water head of 23 meters and a total turbine flow of 840 m^3/s (Vattenfall, 2010). In the Kaplan turbine, water flows under pressure parallel to the axis of the machine and is frequently used with heads of between 10 and 50 meters. The turbine has high flexibility and can stay over 90% efficiency with 40% to 100% of full load (Hamill, 2001).

3.2.2 Dam and spillway

The earth fill dam on each side of the power plant and existing spillway has an impervious moraine core and the crest length is approximately 400 meters with a maximum height of 35 meters. The spillway consists of three 15 meters wide openings with upward going radial gates and has a sill elevation of +113,75 meters. It should be noted that the elevations are defined as the meters above sea level plus 100 meters, in order to avoid negative heights. At FRRL, which is +123 meters, the spillway is designed to discharge around 2300 m^3/s. The spillway with associated gates and chutes as well as the right and left downstream river sides can be seen in figure 5 to 8 below.

Figure 5. The spillway with associated gates and chutes together with the railroad and highway bridges seen from downstream (Wänn & Yang, 2010)

Figure 6. The spillway with chutes seen from upstream (Wänn & Yang, 2010)

Figure 7. Left river side downstream of the spillway (Wänn & Yang, 2010).

Figure 8. Right river side downstream of the power station (Wänn & Yang, 2010).

Parts of the earth fill dam as well as the concrete parts of the facility are constructed on bedrock composed of gneiss granite with dikes of alkaline and carbonate. If exposed to permeating water and oxygen, these dikes can dissolve leading to a deterioration of the stability of the structure. Because of this, the underwater structures has been under frequent supervision since the facility was taken into operation and actions have been made to decrease this process and secure the foundation (Ekström et al., 2011).

In accordance with the new Swedish design flood guidelines and RIDAS (see section 2.2.1), the design flood for the Bergeforsen dam has been revised from 2300 m^3/s to 3000-3500 m^3/s in order to pass a flood at FRRL. During the last few years, studies have been carried out to find the optimal solution to meet the new design requirements from both a hydraulic, architectural, economic and environmental perspective. In 2003, the first measures were taken to enhance the safety. This was done by raising the crest of the earth fill dam and fit it with new riprap protection upstream, stabilizing and repair the spillway as well as raising the spillway chute walls. This allowed an increase in FRRL of 2,7 meters up to the present +123 meters without the construction of a supplement spillway (Ekström et al., 2011).

However, due to the sensitivity of the bedrock mentioned above, underwater inspections made since the upgrade in 2003 has indicated that there is a need for additional repairs and reinforcements of the spillway structure in order to safely meet the design flood criteria. It has also been established that there is a need to improve the energy dissipation of the spillway as water at high velocity is released at the end of the spillway in an area where the bedrock contains dissolvable dikes, which undermines the structures stability. Additionally, the pillars of the railroad and the highway are constructed on the spillway chute walls (as can be seen in figure 5 and 6 above) which further increase the safety requirements of the structure. Summing up, an upgrade of the existing spillway is necessary to maintain a high safety level of the dam. However, maintenance of the underwater structure can only be performed with high technical difficulties and it has been recommended that the structure should be taken out of operation during the upgrade to increase the accessibility. To be able to do this it has therefore been suggested to construct a separate secondary spillway which will allow the existing spillway to be repaired and upgraded without taking the power plant out of operation. When the renovation of the existing spillway is complete after one year, the secondary spillway will contribute to meet the new required design flood criteria. (Ekström et al., 2011).

3.3 New spillway

A number of different layouts for the secondary spillway have been suggested and investigations prior to this project have been carried out in the laboratory at Vattenfall R&D in Älvkarleby in order to find the most suitable solution. The final result can be seen in figure 9 below. The spillway consists of an inlet, a stilling basin with aerator, a curved tunnel and an outlet. The railroad will pass over the tunnel at the bend and the highway will run across a part of the channel further downstream. Since the pre-glacial riverbed in the area under the left earth fill dam is not suitable for a spillway structure, the spillway will be located further to the left at the shallow side of the reservoir where the conditions are better. This in turn enables the construction of a cofferdam that seals off permeable soil and fractured surface rock layers in the bottom of the reservoir which allows the power plant to operate during the construction period (Ekström et al., 2011).

The new spillway allows the water to be released at a safe distance from the bedrock with dissolvable dikes where the energy dissipation is easier to control. Furthermore, the new spillway will decrease the operation time of the existing spillway from 40 days to a few hours per year as the majority of the discharge will pass through the new spillway, except during very high flows. This will decrease the need for future maintenance and the risk for additional damage to the existing foundation and spillway chutes. The new spillway will be equipped with a 25 meter wide gate, the largest in Sweden and 10 meters wider than any of the existing sluice gates. At FRRL, the spillway can discharge around 1500 m^3/s which generates a good margin for future additional increase of the design flood criteria. As mentioned above, the discharge capacity of the new spillway also makes it possible to stay within the limits of FRRL, to pass high flows during the time period the existing spillway is taken out of operation and to have a margin when the discharge capacity might be reduced due to debris clogging (Ekström et al., 2011).

Based on the testing of the physical hydraulic model, the sill elevation is determined to +112,75 meters, one meter lower than the existing spillway sill. The stilling basin will be 85 meters long, 35 meters wide and have a bottom elevation of +87,75 meters. Since the new spillway is located relatively far to the left, the tunnel gets a unfavorable sharp bend in order to lead the water back to the river channel. This can lead to unwanted spiral flow and wave motions of the surface water which will affect the flow pattern negatively and reduce the saftey margin. By rounding the transition from the stilling basin to the tunnel this effect is decreased. Due to the bend, the water is non-uniform when exiting the spillway chutes and the flow direction is to the left of the centerline. To prevent erosion, the channel side is protected by riprap which ends 30-40 meters downstream of the tunnel exit. The redundant material which is produced while constructing the spillway is placed downstream between the two spillway structures and will there function as erosion protection. In this way, the circulation zone that is formed on the left side downstream of the existing spillway is removed and the material is distributed on site (Ekström et al., 2011). See figure 9 below for a detailed layout and figure 10 to 12 for animated images of the area after construction.

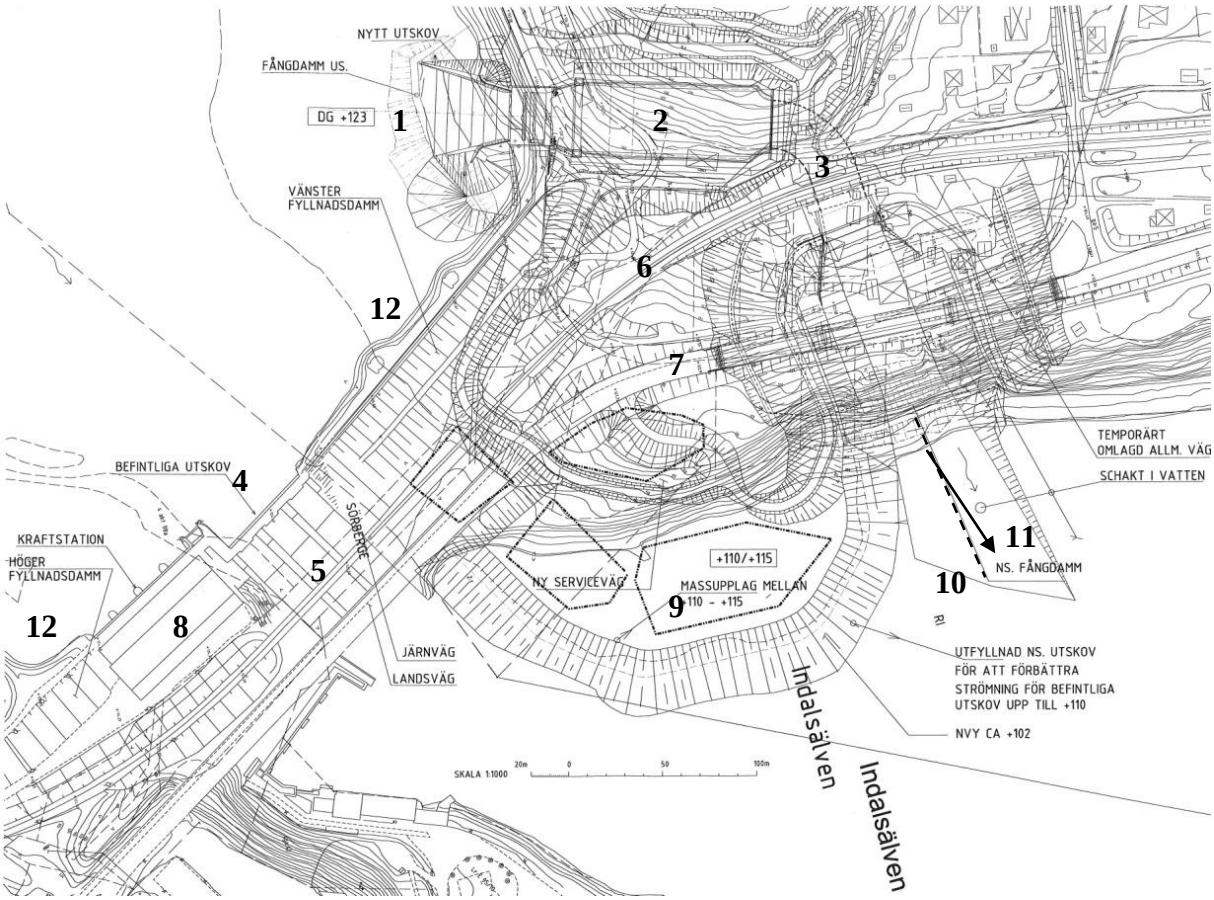

Figure 9. Layout of the new spillway (Ekström et al., 2011).

1. New spillway inlet
2. Stilling basin with energy dissipator
3. Curved tunnel section
4. Existing spillway inlet
5. Existing spillway chutes
6. Railroad.
7. Highway
8. Power plant
9. Excavated material with erosion protection
10. Outlet centerline axis
11. Main direction of flow
12. Earth fill dam

Figure 10. The new spillway inlet viewed from upstream (Vattenfall, 2012b).

Figure 11. Layout of the new spillway with tunnel, excavated material and highway bridge viewed from downstream (Bergeforsfisket, 2012).

Figure 12. Layout of the area after the construction viewed from the north (Sundsvalls tidning, 2012).

4 Numerical hydraulic modeling

4.1 One-, two- and three-dimensional models

In order to investigate the flow conditions in a water body one can utilize numerical hydraulic models. When choosing a model for solving a specific problem it is important to recognize what category of models that best suits the problem. More sophisticated models can perform more advanced computations and simulations but they also often require a higher quantity and quality of data in order to function properly. One main thing to consider is if the problem requires a one-, two- or three-dimensional model.

In a study made by Bechara et al. (1995), the instream flow incremental methodology was investigated with one- and two-dimensional hydraulic models. It was concluded that in this case, the two-dimensional approach had several advantages. Since the two-dimensional model used the finite element approach, the simulation points were separate from the measuring points which allowed a greater flexibility when choosing the calculation points. By using interpolation among the nodes, good estimations of velocity and water depths at any surface or point were obtained. This gave more freedom to construct detailed bathymetric and riverbed maps which could reduce the error of the model output. It was also noted that during the grid discretization, the spatial scale of the model could be changed and adapted with the objectives of the study which created an advantage. As opposed to one-dimensional models, the two-dimensional models treated the river as a spatial continuum rather than a number of independent cross sections which gave a lower mean error in the results. The two-dimensional models also provided more enhanced accuracy in estimating the physical variables due to a better representation of the field data and greater reliability in calibrating with the Manning's coefficient. However, due to that two-dimensional models do not usually consider a change in the sediment composition and the Manning's coefficient with reduced discharge, these models was not recommended for very shallow rivers and smaller streams with discharges less than 50 m^3/s.

Another study made by Bradbrook et al. (1999) compared the performance of two- and three-dimensional hydraulic models. The latter one was concluded to have improved predictive ability, especially when the former one did not try to correct for the effects of secondary circulation on the depth-averaged flow field. The two-dimensional model was found to be less sensitive to topographic variations but more sensitive to roughness parameterization. However, this was possible to improve by using a higher roughness value than was measured in the field. It was observed that the three-dimensional model was better at estimate the correct bed shear stress and mixing processes. Nevertheless, the three-dimensional models had fundamental limitations of the predictive ability due to higher needs for detailed boundary specifications, higher requirements in computer resources and an increased need of understanding the fundamental assumptions behind the model development.

Considering the conclusions related to these discussions, the optimal way to accomplish the objectives of this project is by employing a two-dimensional hydraulic model.

4.2 Two-dimensional model structure

One category of models which are particularly useful when investigating local details of velocity and depth distribution are the two-dimensional depth-averaged hydraulic models. These models normally focus on a relatively limited extent of the channel, typically less than ten channel widths in length. They also often give transient solutions where the steady state solution is obtained as an asymptotic

transient solution after a longer time period. To compute the flow conditions, two-dimensional models solve the basic mass conservation equation and two horizontal components of momentum conservation. The outputs are two horizontal velocity components and a water depth at each point. The vertical velocity distributions are assumed to be uniform and the pressure is assumed to be hydrostatic (Blackburn & Steffler, 2002).

For input data, the models often needs channel bed topography data, eddy viscosity distributions, bed roughness values, boundary conditions and initial flow conditions together with a designed mesh or grid. The bed roughness, in form of the Manning's coefficient, is often a non-critical parameter as the two-dimensional resistance term only accounts for the direct bed shear stress and a reasonable value can usually be found through the calibration process. This regularly also applies to the eddy viscosity but can somewhat vary from model to model. The boundary conditions are often a total discharge at the inflow sections and a fixed water surface elevation at the outflow sections. It is important to define the boundaries some distance from areas of specific interest to minimize the effect uncertainties in the boundary conditions. Regarding the mesh, the challenge is in distributing the nodes in such a way that the most accurate solution is obtained. This can be done by spacing the nodes closely together at areas of higher interest and have regularity in the shapes of the elements. As a rule of thumb, a minimum of ten elements in each direction are required to resolve the local flow field features satisfactorily (Blackburn & Steffler, 2002). Additionally, information about dams, weirs and bridges included has to be specified before any computations can be performed (Lysne et al., 2003).

During the simulations, verification of the computer model against observed data obtained either from measurements in the physical model or in the prototype needs to be made continuously. The Manning's coefficient and the eddy viscosity are not constants or fluid properties but depend on the flow situation. Therefore, they become the main tuning parameters when calibrating the model. (Lysne et al., 2003).

As mentioned above, two-dimensional models are based on the principles of conservation of mass and momentum. Ultimately all hydraulic model formulations are derived from the Navier-Stokes equations of motion for an incompressible non-turbulent fluid of constant density together with the equation of mass continuity. These equations in cartesian vector notation are described by Bates & Anderson (1993) as shown below:

Motion equation

$$\rho \frac{Du}{Dt} = -\nabla p + \mu \nabla^2 \mathrm{u} + \mathrm{F} \qquad \text{(eq. 1)}$$

where

ρ = fluid density (kg/m^3)
u = velocity (m/s)
t = time (s)
p = pressure (Pa)
μ = viscosity (Pa*s)
F = a set of terms, e.g. gravity, to be included in the particular problem

Mass continuity equation

$$\nabla \cdot u = 0 \qquad \text{(eq. 2)}$$

where

u = velocity (m/s)

In order to discretize the partial differential equations, the models can use various methods which transform the equations into a finite number of equations and mesh points in space and time. These methods include the finite element, the finite volume and the finite difference approach where all have advantages and disadvantages. The most commonly used approach is the finite element method which gives a large geometric flexibility and allows the elements to change size and shape in order to refine the mesh in important and rapidly varying areas. To solve the non-linear algebraic expressions received from the finite element method, the model can use either explicit or implicit solver methods. Explicit methods solves for new variable values at any node based on the values of the surrounding nodes at the previous time step. In the implicit methods all the variable values at a new time step are considered to depend on each other as well as the values of the previous time step (Blackburn & Steffler, 2002).

4.3 Surfacewater Modeling System (SMS)

One program environment that utilizes multidimensional numerical hydraulic models is Surfacewater Modeling System, or SMS. SMS was developed by Engineering Computer Graphics Laboratory at Brigham Young University in cooperation with the U.S. Army Corps of Engineers Waterways Experiment Station (WES) and the U.S. Federal Highway Administration (FHWA) and is marketed by Aquaveo. This program employs both pre- and post-processing for surface water modeling and analysis and includes two-dimensional finite element, two-dimensional finite difference, three-dimensional finite element and one-dimensional backwater modeling programs. The hydrodynamic modeling programs within SMS can calculate and simulate water surface elevations, flow velocities, contaminant migration, salinity intrusion, wave energy dispersion and wave properties for shallow water flow problems where both steady-state and dynamic situations are supported. SMS supports a number of modules that utilize these programs through specifically designed interfaces (BOSS International, 1999).

4.3.1 Scatter module

The scatter point module is used to interpolate scatter data points to meshes and grids using either linear, natural neighbor or inverse distance weighted interpolation. Usually, the scatter point data is collected from surveys of the bottom elevation and contains information about location (x- and y-coordinates) and elevation (z-coordinate) of the different points. However, the points are typically not distributed evenly across the area. Therefore, the data is interpolated in order to use it as background information when creating a finite element mesh (BOSS International, 1999).

4.3.2 Map module

The map module is used to define conceptual models in a GIS format, adding explanations to a plot as well as displaying digital background maps and CAD drawings. The use of feature objects in the map module is to provide the program with GIS capabilities and includes points, arcs and polygons. These objects can be grouped into coverages and several coverages can be constructed in the same project. SMS then uses this conceptual model based on feature objects to build a mesh (BOSS International, 1999).

4.3.3 Mesh module and GFGEN

The mesh module is used for pre- and post- processing of the finite element meshes. In this module, a mesh can be generated from for example the polygons made in the map module using a program called GFGEN. GFGEN stands for Geometry File GENeration program and is developed by the U.S. Army Corps of Engineers Waterways Experiment Station and Hydraulics Laboratory. In SMS, it is used for generating one- and two dimensional finite element mesh files for input to the model of choice. Among other things, the program can identify potential errors and renumber the constructed mesh as well as fit curved element sides to land boundaries and optimize the solution order. There are several kinds of mesh structures that can lead to computational errors and should be avoided. This includes:

- Elements with poor aspect ratio and interior angles
- Elements with ambiguous gradients forming a saddle point
- Concave quadrilateral elements
- Elements with a steep slope
- Erroneous element connections
- Large area change between two adjacent elements

4.3.4 RMA2

The SMS modeling program utilized to generate a solution in this project is called RMA2. RMA2 is a two-dimensional depth averaged finite element hydrodynamic model that supports subcritical flow analysis, including wetting and drying. It is mainly used for calculating water depths, flow distributions and flow velocities in rivers, reservoirs and estuaries and is one of the programs that can function both in steady state and dynamic situations. Friction is calculated using the Manning or Chezy equation and eddy viscosity is used to define turbulence conditions (King, 2005).

4.3.4.1 Assumptions and limitations

RMA2 is two-dimensional in the horizontal plane and vertical accelerations are neglected in the calculations. Instead, the velocity is assumed constant over the whole depth of the water column at any given time and the fluid is assumed to be vertically homogenous with a free flow surface. RMA2 is best used in far-field problems over larger areas as when studying near-field areas vortices, vibrations and vertical accelerations are of higher interest. As mentioned above, the program can only handle problems concerning subcritical flow and may become numerically unstable if the Froude's number surpasses 0,6 (King, 2005).

The version of RMA2 used in this project is v4.35 and is dimensioned as followed:

- Maximum number of nodes: 30 000
- Maximum number of elements: 10 000
- Maximum number of equations: 90 000
- Maximum front width: 700
- Maximum number of continuity check lines: 100
- Maximum buffer size: 1 000 000

If any of these dimensions are exceeded, the program cannot perform the simulation.

4.3.4.2 Governing equations

The program computes the calculations by solving the depth-averaged Reynolds equations. These equations are derived from the Navier-Stokes equations 1 and 2 described above by integrating them over depth and including a number of modifications to account for turbulent flow, external tractive forces of coriolis effects, boundary friction and wind stress at the free surface. The received second order partial differential equations are described in the two horizontal directions *x* and *y* by King (2005).

Force momentum equations

$$h\frac{\partial u}{\partial t} + hu\frac{\partial u}{\partial x} + hv\frac{\partial u}{\partial y} - \frac{h}{\rho}\left[E_{xx}\frac{\partial^2 u}{\partial x^2} + E_{xy}\frac{\partial^2 u}{\partial y^2}\right] + gh\left[\frac{\partial \alpha}{\partial x} + \frac{\partial h}{\partial x}\right]$$

$$+\frac{gun^2}{\left(1{,}486h^{1/6}\right)^2}(u^2+v^2)^{1/2} - \varsigma V_\alpha^2 \cos\psi - 2hv\omega\sin\Phi = 0 \qquad \text{(eq. 3)}$$

$$h\frac{\partial v}{\partial t} + hu\frac{\partial v}{\partial x} + hv\frac{\partial v}{\partial y} - \frac{h}{\rho}\left[E_{yx}\frac{\partial^2 v}{\partial x^2} + E_{yy}\frac{\partial^2 v}{\partial y^2}\right] + gh\left[\frac{\partial \alpha}{\partial y} + \frac{\partial h}{\partial y}\right]$$

$$+\frac{gvn^2}{\left(1{,}486h^{1/6}\right)^2}(u^2+v^2)^{1/2} - \varsigma V_\alpha^2 \sin\psi + 2hu\omega\sin\Phi = 0 \qquad \text{(eq. 4)}$$

Continuity equation

$$\frac{\partial h}{\partial t} + h\left(\frac{\partial u}{\partial x} + \frac{\partial v}{\partial y}\right) + u\frac{\partial h}{\partial x} + \frac{\partial h}{\partial y} = 0 \qquad \text{(eq. 5)}$$

where

h = water depth
u,v = velocities in the x and y direction
x,y,t = cartesian coordinates and time
ρ = density of fluid
E = eddy viscosity coefficient,
for xx = normal direction on x-axis surface
for yy = normal direction on y-axis surface
for xy and yx = shear direction on each surface
g = acceleration due to gravity
α = bottom elevation
n = manning's roughness coefficient
ς = empirical wind shear coefficient

V_α = wind speed
ψ = wind direction
ω = rate of earth's angular rotation
Φ = local latitude

In this project, the coriolis effects and wind stress at the free surfaces are neglected. Equation 3 to 5 are solved for each element in the mesh using the Galerkin finite element method of weighted residuals. This method assumes that the dependent variables vary in a set behavior over each element, quadratically for velocity and linear for depth. This results in the development of a single equation for each node in the mesh, representing the sum of contributions from all adjacent elements. The local equations are then collected in a global matrix which is solved using Gaussian integration. Derivates in time are substituted by a nonlinear finite differentiation approximation and variables are assumed to vary over each time step as equation 6 below (King, 2005):

$$f(t) = f(t)_0 + at + bt^c \qquad t_0 \leq t < t_0 + \Delta t \qquad \text{(eq. 6)}$$

where *a,b,c* are constants and *t* is time.

The solution received is implicit and the set of equations are solved by the Newton-Raphson non linear iteration scheme (King, 2005).

4.3.4.3 Steady state and dynamic solutions

RMA2 can solve for both steady state and dynamic situations. As mentioned in section 4.2, a steady state solution removes all time derivates from the used equations. The solution can therefore be said to be the result of a number of dynamical simulations where the solution does no longer changes from one time step to the next. On the other hand, a dynamic solution includes all time derivates and changes in response to long-wave propagation characteristics. In order to decide what type of solution that is best suited for the situation one can utilize the table 1 below:

Table 1. Common methods of handling steady state/dynamic simulation strategies for combinations of river and tide (King, 2005).

	Tidal forcings	
River inflows	None	Yes
None	Why run the model?	Dynamic only
Minor constant flows	Steady state only	Steady state + Dynamic
Strong constant flows	Steady state only	Steady state + Dynamic
Hydrograph of flows	Steady state + Dynamic	Steady state + Dynamic

5 Physical hydraulic modeling

5.1 Model structure and governing equations

A physical hydraulic model is a small-scale version of the area where flow and pressure is to be analyzed and includes both topography and structures. The reasons for using these kinds of models are, first of all, due to the fact that natural flowing water is complicated to analyze by theory as it includes irregular boundaries such as variable slope, expansions, constrictions etc. Secondly, the hydraulic structures often need to function for a number of flow situations and conditions which cannot be investigated by analyzing a full-scale prototype. Therefore, by constructing a topographical model of a river reach one can investigate the flow through weirs, spillways, bridges, in river channels, the performance of pumps and turbines, erosion and sediment transport (Hamill, 2001).

The degree of accuracy and reliability of the model depends on certain factors such as the applied model law, the choice of scale and the model boundaries. Since there are many laws and the model cannot comply with all of them simultaneously, the model will never completely reflect the prototype performance. Basically, there are three types of hydraulic similarities between a model and a prototype to consider. First is the geometric similarity which gives that a model length must be related to the same prototype length by a scale factor. Second is the kinematic similarity, the similarity of motion, which says that at any given time, the model must reproduce the scale of velocity and flow direction of the prototype. Third is the dynamic similarity which is the similarity of forces. This relationship says that at similar points, the model must reproduce the scale of the forces of the prototype (Hamill, 2001).

In the case of the Bergeforsen dam, the flow is turbulent (Reynold's number > 2000) and consequently driven by gravity as the most important force. Therefore, the most important parameters to represent in such a model is geometry and water flow along with friction. Viscosity and surface tension can often be neglected in these conditions. In this situation, the scale ratios are obtained from Froude's model law (Lysne et al., 2003). This model law is derived, as described by Hamill (2001), from comparing the model and the prototype version of Froude's number and can be seen in equation 7 to 13 below:

$$Fr = \frac{V}{\sqrt{gL}} \qquad \text{(eq. 7)}$$

$$Fr_p = Fr_m \rightarrow \frac{V_p}{\sqrt{gL_p}} = \frac{V_M}{\sqrt{gL_M}} \rightarrow \frac{V_M}{V_p} = \left(\frac{L_M}{L_P}\right)^{1/2}$$

This gives the following relationships

Geometric scale

$$\frac{L_M}{L_P} = \frac{1}{X} \qquad \text{(eq. 8)}$$

Velocity scale

$$\frac{V_M}{V_P} = \frac{1}{X^{1/2}} \qquad \text{(eq. 9)}$$

Time scale

$$\frac{T_M}{T_P} = \frac{1}{X^{1/2}} \quad \text{(eq. 10)}$$

Flow scale

$$\frac{Q_M}{Q_P} = \frac{1}{X^{5/2}} \quad \text{(eq. 11)}$$

By introducing the Manning equation (eq. 12), the surface roughness scale between the prototype and the model can be determined

$$V = \left(\frac{1}{n}\right) R^{2/3} S_0^{1/2} \quad \text{(eq. 12)}$$

Combining equation 9 and 12

Surface roughness scale

$$\frac{n_M}{n_P} = \frac{1}{X^{1/6}} \quad \text{(eq. 13)}$$

where

Fr = Froude's number
g = gravity
X = scale factor
V = velocity
for *M* = in the model
for *P* = in the prototype
L = length
for *M* = in the model
for *P* = in the prototype
T = time
for *M* = in the model
for *P* = in the prototype
Q = flow
for *M* = in the model
for *P* = in the prototype
R = hydraulic radius
S_0 = bottom slope
n = Manning's roughness coefficient
for *M* = in the model
for *P* = in the prototype

In order to obtain a good physical model it has to be calibrated against observed data from the prototype. This will include adjustments of boundary conditions such as surface roughness and downstream water depths (Lysne et al., 2003).

5.2 Bergeforsen hydraulic model

Throughout the years, two different set of physical hydraulic models of the Bergeforsen dam has been set-up in the laboratory at Vattenfall R&D in Älvkarleby, one based on the old situation before construction of the new spillway and one after. Both are based on Froude's model law and have a scale factor of 50. The bed topography is determined by high resolution sonar. The models are not intended to be used for determination of pressure and force on constructions and objects as the artificial slopes of the flow are not correctly recreated. Detailed designs will instead be primarily based on empirical studies from laboratory and field observations (Wänn & Yang, 2010).

5.2.1 Pre-construction

The pre-construction model was constructed in 1997 and was in operation from 1998 to 2000. It was used to investigate the spillway capacity and erosion potential downstream of the dam during high flows. It included a stretch of 350 meters upstream to 875 meters downstream of the dam with the power station and the gated spillway. It was 7-12 meters wide and 25 meters long and the spillway chutes were constructed in plastic, the power station inlets in sheet metal and the riverbed in concrete (Yang, 2000). The velocities used in this project was measured in 2000 along the water surface in seven stretches across the river width downstream of the existing spillway (see section 7.6). The model can be seen in figure 13 to 15 below.

Figure 13. The model viewed from upstream (Yang, 1998).

Figure 14. The power station and the spillway with viewed from downstream (Wänn & Yang, 2010).

Figure 15. The spillway with chutes viewed from upstream (Yang, 1998).

5.2.2 Post-construction

The post-construction model has been in operation since 2009. Its primary function is to aid in the optimization and configuration of the new spillway that is to be constructed on the left riverside as well as in the investigation of the erosion potential. It includes a stretch of 100 meters upstream and 700 meters downstream of the dam with the power station, the existing spillway with chutes and the new spillway with tunnel. The spillways and the power station inlets are constructed in sheet metal and the river bed in concrete (Wänn & Yang, 2010). The velocities used in this project was measured in 2010 along the water surface in two stretches across the river width, 250 and 450 meters downstream of the existing spillway (see section 7.6). The model can be seen in figure 16 to 19 below.

Figure 16. The model viewed from above (Wänn & Yang, 2010).

Figure 17. The power station and existing spillway viewed from downstream (Wänn & Yang, 2010).

Figure 18. The power station and existing spillway viewed from the side (Wänn & Yang, 2010).

Figure 19. The new spillway viewed from downstream (Wänn & Yang, 2010).

6 River bed transport processes

6.1 Erosion

In a normal topography, there are usually four typical processes present that will characterize the river course from source from outlet; erosion, sediment transport, sediment deposition and delta development. Erosion takes place when a river transports more material out from an area than the watershed can supply. General erosion is the gradual degradation of the soil over large areas due to rain, flow and wind and is the main source for sediment transport in rivers. Local erosion is typically taken place downstream of dams and sills, in reaches with loose bed materials located downstream of reaches with protected bed or solid rock and next to local constrictions such as bridge pillars and road embankments (Lysne et al., 2003).

Due to turbulence, the particles will have a probability of moving which decreases with particle size. This leads to sorting of the sediment at the surface of the riverbed where the coarser material will remain in place and thereby change the well-graded composition. Due to an orderly arrangement of the stones in an armoring interlocking pattern, the riverbed might have a much steeper slope than would otherwise be possible with the existing grain size distribution. This bed may also resist a higher stress than normal. However, extreme flood events might break up local parts of this established armored layer (Lysne et al., 2003).

A hydropower dam will trap some of the sediment and consequently the water that passes through the spillway and bottom sluices will therefore not be in equilibrium with the sediment situation downstream. This may in many cases cause erosion downstream of the dam, where the original bed consisted of sediments in equilibrium, due to that a stable transport situation has not been obtained. The bed reacts to the erosion by degradation of the bed in order to add the transport towards the capacity and to reduce the slope until the actual sediment transport is in equilibrium with the transport capacity of the new slope (Lysne et al., 2003).

The exact particle size distribution of the river bed material downstream of Bergeforsen dam is unknown. However, the channel bed can be assumed to follow certain characteristics of a bed located downstream of a hydropower dam in Northern Sweden. This includes deeper mid sections with fractured bedrock, boulders and stones with finer sediment in between the coarser material and shallow side sections with erosion protection material or shorelines with somewhat finer material (Yang, 2012).

6.2 Sediment transport

Transport of river material is a natural process which occurs when eroded fragments are carried by water in motion. The material can be of both mineral and organic origin and the sediment mixture is commonly described in terms of percent finer by weights of particles. Mixtures with a wide spread are referred to as “well-graded” and mixtures with a narrow spread as “uniform”. The particle size is denoted d with the amount of finer material in percent as sub index. The diameter d_{50} is thereby the mean diameter of the sediment mixture (Lysne et al., 2003).

As mentioned above, sediment transport can only occur if the destabilizing forces of the water, promoting movement of the sediment particle, are greater than the stabilizing forces (Lysne et al., 2003). A force balance on a particle placed in a sloping channel illustrated by Coufal (1997) can be seen in figure 20 below:

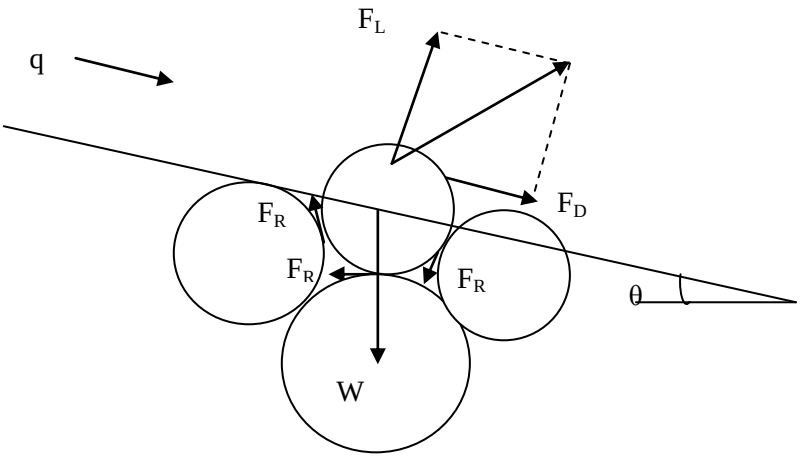

Figure 20. Forces acting on a particle placed on a sloping channel (Coufal, 1997).

Equation 14 to 16 below shows drag, lift and gravity as described by Coufal (1997):

*Drag force (kg*m/s^2)*

$$F_D = C_D A \rho_w \frac{u^2}{2} \quad \text{(eq. 14)}$$

*Lift force (kg*m/s^2)*

$$F_L = C_L A \rho_w \frac{u^2}{2} \quad \text{(eq. 15)}$$

*Gravity force (kg*m/s^2)*

$$W = \rho_s V g \quad \text{(eq. 16)}$$

where

q = flow per unit width (m^2/s)
θ = bottom slope (degrees)
F_R = cohesive forces (kg*m/s^2)
C_D = drag coefficient
C_L = lift coefficient
A = area of exposure (m^2)
u = velocity (m/s)
ρ_s = density of particle (kg/m^3)
ρ_w = density of water (kg/m^3)
g = gravity (m/s^2)
V = volume of particle (m^3)

In figure 20, it can be seen that the drag force works in the main direction of the flow and the lift force works perpendicular to the flow. These forces represent the destabilizing forces i.e. the flow turbulence and are countered by the gravity and cohesive forces, the stabilizing forces (Coufal, 1997). The total sediment load transported by water can be divided into bed load and suspended load. Bed load is a mode of transport where the particles rolls, slides or jumps along the bed and is the dominant form of transport for low flow rates and large particles. Suspended load is when the particles are carried in suspension at the same speed as the current and occurs when the settling velocity is smaller than the upward turbulent velocity (Lysne et al., 2003).

When dealing with sediment transport and erosion it is impossible to analyze each single particle. Therefore, factors such as shear stress and turbulence are introduced. Shear stress is the average force per unit area exerted by the water turbulence on the bed and in natural waters depends on the change in velocity from the bed upwards to the free flow. Turbulence is the irregular flow resulting from eddies. Eddies are constantly formed by the shear stress inside the flow and on the bed and dissipate due to viscous and boundary friction. The turbulence makes the flow velocity and bed shear stress fluctuate around the average value. This is important when investigating bed stability and erosion as it is the flow velocity and bed shear stress that determine whether a particle may be moved or not (Lysne et al., 2003). Just before the particles at the river bed begin to move one speaks of the threshold of motion, critical shear stress $\tau_{cr} = \tau$ and critical particle diameter $d_{50,cr} = d_{50}$. These parameters can be calculated by a number of different methods. In Soulsby (1997) the bed shear stress is defined as:

Bed shear stress (N/m^2)

$$\tau = \rho_w C_f \bar{U}^2 \quad \text{(eq. 17)}$$

The friction coefficient C_f depends on the Manning's roughness coefficient and the water depth:

$$C_f = \frac{gn^2}{h^{1/3}} \quad \text{(eq. 18)}$$

combining equation 17 and 18 gives:

Bed shear stress (N/m^2)

$$\tau = \frac{\rho_w g n^2 \bar{U}^2}{h^{1/3}} \quad \text{(eq. 19)}$$

where

ρ_w = density of water (kg/m^3)
g = gravity (m/s^2)
n = Manning's roughness coefficient
$\bar{U}$ = depth-averaged velocity (m/s)
h = water depth (m)

In 1997, Soulsby and Whitehouse developed an algebraic expression of the Shields curve, describing how the Shields parameter θ, used to calculate the initiation of motion of sediment in a fluid flow, changed with threshold of motion. The derived equation 20 and the definition of the critical Shields parameter 21 found in Soulsby (1997) are shown below:

Critical Shields parameter

$$\theta_{cr} = \frac{\tau_{cr}}{g(\rho_s - \rho_w)d_{50}} \qquad \text{(eq. 20)}$$

Critical Shields parameter developed by Soulsby and Whitehouse

$$\theta_{cr} = \frac{0{,}3}{1+1{,}2D_*} + 0{,}055[1 - exp(-0{,}02D_*)] \qquad \text{(eq. 21)}$$

where

τ_{cr} = critical bed shear stress
D_* = dimensionless grain size
d_{50} = average particle diameter (m)
g = gravity (m/s^2)
ρ_s = density of particle (kg/m^3)
ρ_w = density of water (kg/m^3)

For larger grain sizes corresponding to $D_* > 100$, giving $d_{50} > 4$ mm , equation 21 can be approximated to $\theta_{cr} \approx 0{,}055$ (Soulsby, 1997) as can be seen in figure 21 below.

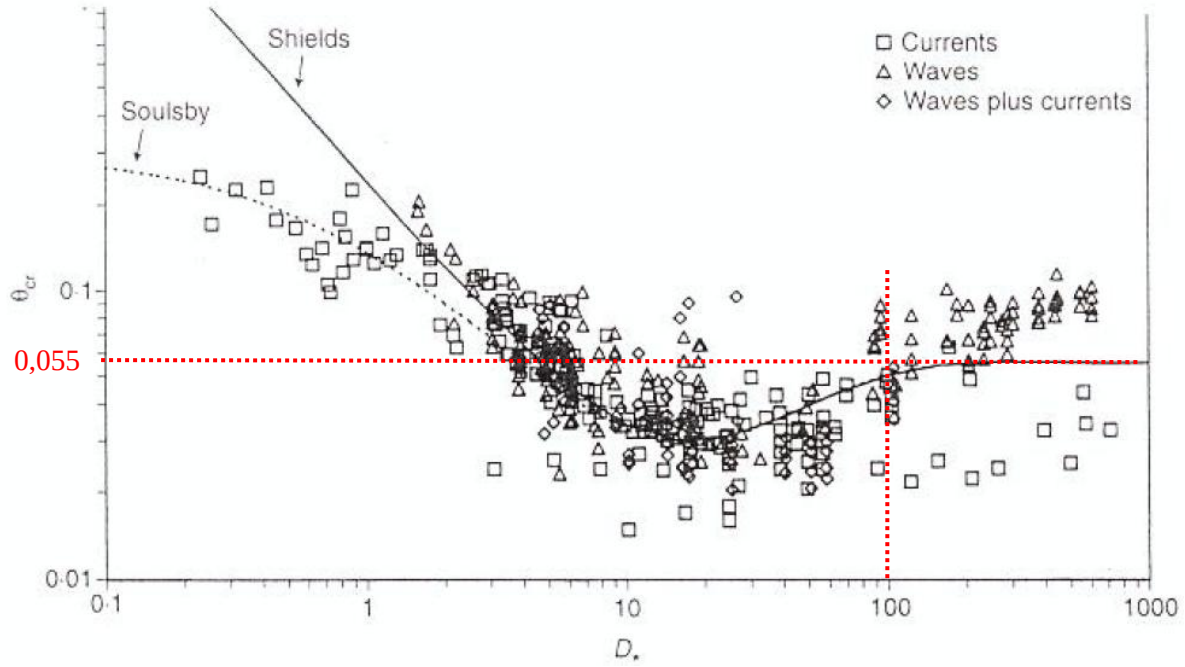

Figure 21. Threshold of motion of sediments beneath waves and/or currents (Soulsby, 1997).

From this, a formula can be derived for the critical particle diameter $d_{50,cr}$ meaning the grain diameter that will stay immobile for given flow conditions. In theory, all grains smaller than this value will be moved. For immobile and mobile beds, the following friction law can be obtained using measured values (Soulsby, 1997):

$$\frac{u_*}{\bar{U}} = \frac{1}{7}\left(\frac{d_{50}}{h}\right)^{\frac{1}{7}} \quad \text{(eq. 22)}$$

where

u_* = friction velocity (m/s)
$\bar{U}$ = depth averaged velocity (m/s)
d_{50} = average particle diameter (m)
h = water depth (m)

By combining equation 21 and equation 22 with the assumption of $\theta_{cr} \approx 0{,}055$ the following formula for steady flow is obtained:

Critical particle diameter (m)

$$d_{50,cr} = \frac{0{,}25\bar{U}^{2.8}}{h^{0.4}(g(s-1))^{1.4}} \quad \text{(eq. 23) valid for } d_{50,cr} > 4 \text{ mm}$$

where

$\bar{U}$ = depth averaged velocity (m/s)
d_{50} = average particle diameter (m)
h = water depth (m)
g = gravity (m/s^2)
$s = \rho_s / \rho_w$ = density of particle / density of water

7 Model set-up

The two models that will be used to simulate the different flow conditions both include an area of 700 meters downstream of the hydropower dam as well as the whole river width, which is equidistant to the physical model at Vattenfall R&D in Älvkarleby. The numerical hydraulic modeling program SMS is used in order to simulate and analyze the different discharge combinations. Two sets of models, prior and subsequent to the construction of the new spillway are created. The flow situations and erosion are then simulated using the RMA2 model. As the majority of the flows are strong and constant and since the boundaries are not connected to the ocean (providing none, or very small, tidal forcings) all solutions are in steady state in accordance with table 1 in section 4.3.4.3. The outputs received are flow velocities in two dimensions and water depth in each point. The high flow situations will be simulated with a total flow rate from 1500 to 4000 m^3/s and the normal situations at 840 m^3/s.

7.1 Topography

In order to create a numerical model, information about the topography in the study area is needed. The topography for the area downstream of Bergeforsen dam was surveyed in advance with high resolution sonar by Vattenfall R&D. From this survey, around 134 000 scatter points were received with x-, y- and z-coordinates. For the pre-construction situation, these points are simply converted into contour lines by using the scatter module within SMS as can be seen in figure 22 below.

Figure 22. Contour lines for the pre-construction situation from +80,9 meters to +111,5 meters.

For the post-construction situation, manufactured topographical data regarding the new spillway and the excavated material zone is added to the pre-construction topography. This data is then converted into contour lines as shown in figure 23 below.

Figure 23. Contour lines for the post-construction situation from +80,5 meters to +123,7 meters.

As can be seen from the two figures above, there are some shallow areas and islets in the middle right and upper left riverside where the velocities and shear stresses could be become high during high flow.

7.2 Mesh model

7.2.1 Arcs, vertices and polygons

When constructing a finite element mesh, the first thing to address is the definition of the outer borders. In this project the borders are located at the spillways, above the water edge along the shores and 700 meters downstream of the dam.

The fixed water depth at the downstream end for different flow rates have previously been established by Wänn & Yang (2010) and can be seen in figure 24 below. For the flow rate 4000 m^3/s (the highest used in this model) the water depth at the downstream end is around +103,4 meters. This is thereby the maximum water depth that will occur in the simulations.

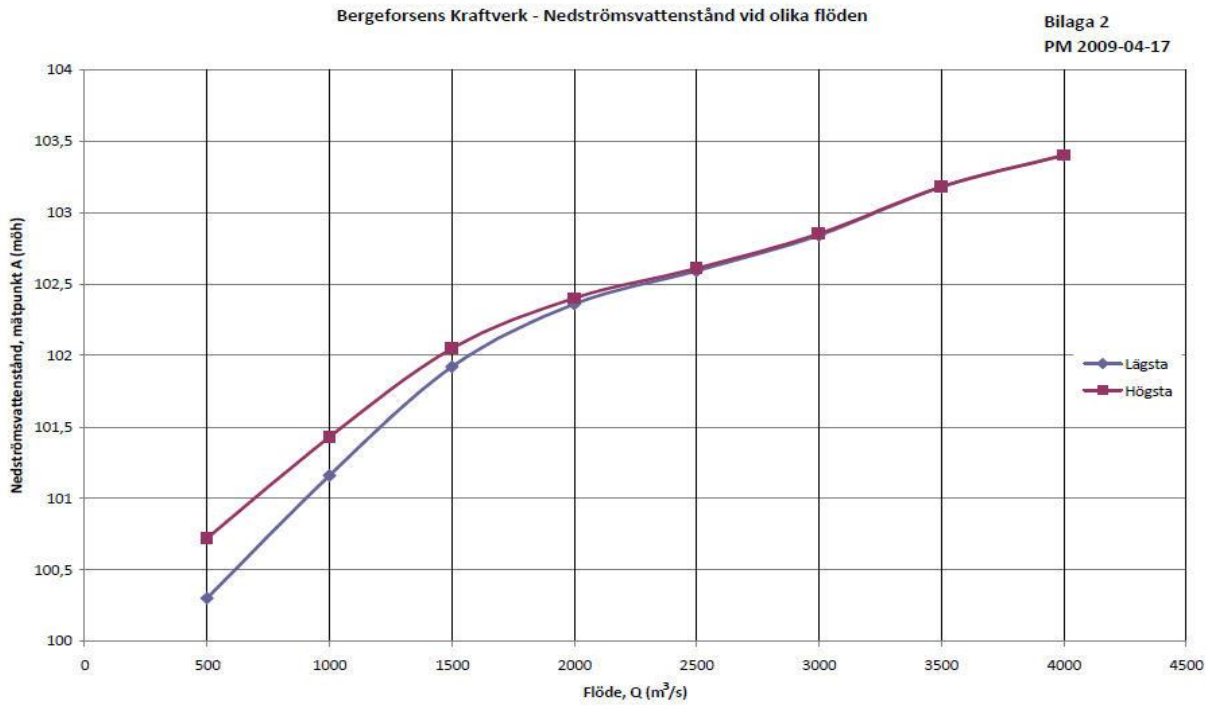

Figure 24. Water depth (meters above sea level plus 100 meters) 700 meters downstream of the dam in relation to flow rate (m^3/s) (Wänn & Yang, 2010).

In order to have some margin, the outer borders are defined at +103,5 meters. The deeper, central part of the riverbed is defined at around +97 meters and is separated from the areas closer to the shore by arcs. The model is thereby divided into areas with separate material zones with different roughness properties; the deep and rougher central channel and the shallow and finer shorelines. Next, the rest of the model is divided into smaller polygons in order to promote a higher amount of quadratic elements when the mesh is generated.

The alignment and the density of the vertices on the arcs are important since it determines how the elements in the mesh will be arranged. The alignment of the vertices of two opposite arcs determines the angles of the elements and they should therefore be faced as straight to each other as possible. The density of the vertices determines the detail of the element mesh in that area. The vertices should therefore be positioned closer together in areas of particular interest such as downstream the spillways and around the excavated material zone. As a result, these areas will have a finer grid with more points meaning that a higher number of calculations will be performed. This in turn promotes a more detailed image of the flow conditions in these areas. The final distribution of the arcs and material zones in the pre- and post-construction models can be seen in figure 25 and 26 below.

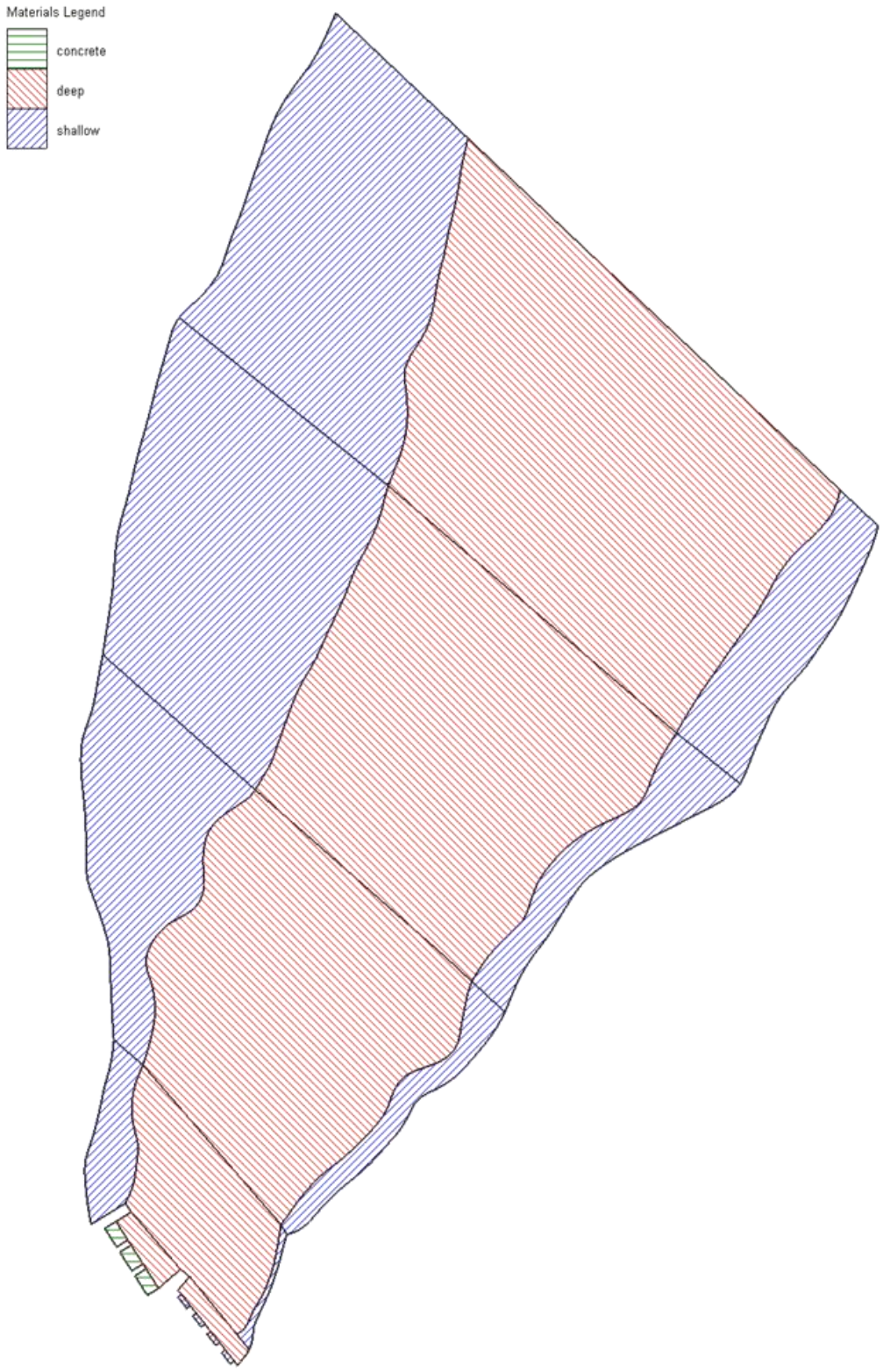

Figure 25. Arcs and material zones in the pre-construction model.

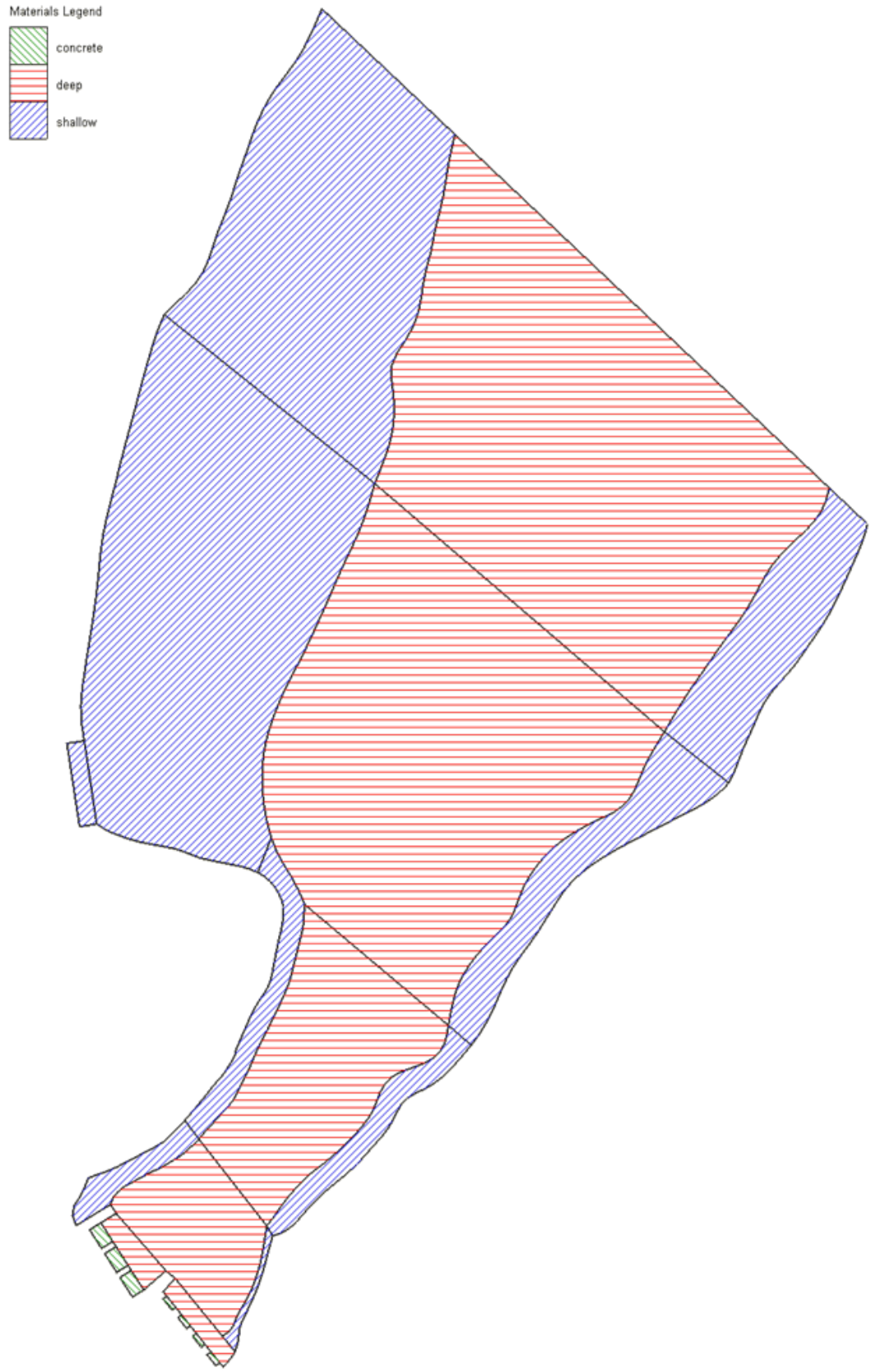

Figure 26. Arcs and material zones in the post-construction model.

7.2.2 Finite element mesh

Besides that a finer mesh will increase the accuracy of the calculations it will also consume more computational power. Generating a finite element mesh is therefore always an issue about accuracy versus calculation load. In this project, the areas of particular interest mentioned above will have an average element resolution of 3x3 meters and the remaining areas a resolution of 6x6 to 8x8 meters. When all the vertices and nodes are distributed the mesh is then generated and the topography is interpolated to the mesh nodes by linear interpolation. The mesh structure is then revised and refined in order to minimize the amount of elements that can disrupt the computational process as described in section 4.3.3. Generally, the more quadratic and less triangular elements there are, the better the mesh is generated. After editing the mesh, the number of elements in the pre-construction model becomes 5683 elements whereof 58 triangular and 5625 rectangular, and in the post-construction model 5211 elements whereof 58 triangular and 5153 rectangular.

7.2.2.1 Inflow boundary mesh

When using linear interpolation from scatter points in the areas around the inlets, for example in a chute where the geometry and the bathymetry changes abruptly, the sections can be difficult to reproduce in a finite element mesh. Therefore, the elevation of the mesh nodes might need to be evened out manually for a better representation of the reality as shown in figure 27 below:

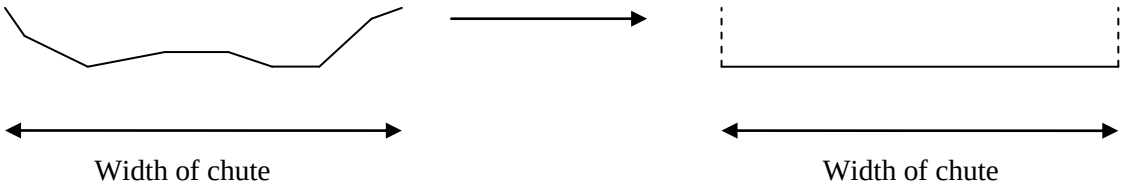

Figure 27. Example of mesh node elevations of a chute (seen from a cross-sectional perspective) after interpolation (to the left) and after a manually correction (to the right).

Another problem that arises at the inlets is the high Froude's numbers. Froude's number is a dimensionless parameter which can be used to describe the type of flow that will occur in a channel. It depends on the gravitational forces, the velocity and the water depths as follows:

$$Fr = \frac{V}{\sqrt{gh}} \qquad \text{(eq. 24)}$$

where

V = velocity (m/s)
g = gravity (m/s^2)
h = water depth (m)

A Froude's number > 1 means supercritical flow, a relatively shallow and fast flow where the upstream flow conditions govern the flow and water depth.
A Froude's number < 1 means subcritical flow, a relatively deep and slow flow where the downstream

flow conditions govern the flow and water depth.
A Froude's number = 1 means transitional flow, which often occurs at for example a hydraulic jump where the flow transits from supercritical to subcritical.

RMA2 is very sensitive to supercritical flow and high Froude's numbers and the model can become numerically unstable if it surpasses 0,6. As can be seen from equation 24 above, the Froude's number increases if the velocity increases or if the water depth decreases. The relatively steep slopes at the spillways together with high flows and a high bathymetry (meaning a low water depth) will create these high Froude's numbers. In order to avoid this problem, the full lengths of the spillways are not included in the model and the upstream boundaries are set to after the elevation of the chutes have reached the surrounding bottom elevation. However, it should be mentioned that this simplification might have an impact on the initial velocity and the velocity magnitude and profiles of the whole model as it reduces the initial momentum of the flow down the inlets. The scale and importance of this change is however hard to estimate and is believed to be most prominent at the first 100 meters from the spillway inlets.

In order to determine at what level the bottom elevation of the inlet mesh nodes can be positioned, equation 24 above is combined with the continuity equation. In this way, the minimum required water depth (and thereby the maximum mesh node elevation) at the three inlet sections can be calculated as follows:

Continuity equation

$$Q = VA = VhL \rightarrow V = \frac{Q}{hL} \qquad \text{(eq. 25)} \qquad \text{for rectangular cross-sections}$$

where

Q = flow (m^3/s)
V= velocity (m/s)
h = water depth (m)
L = width of inlet (m)

Combining with equation 23 gives

$$Fr = \frac{V}{\sqrt{gh}} = \frac{\frac{Q}{hL}}{\sqrt{gh}} \qquad \text{(eq. 26)}$$

In order to have some margin, the highest acceptable Froude's number is set to 0,55. For each inlet section, the flow which causes the highest inlet Froude's number together with the downstream water depth is then used in order to determine the maximum allowed mesh node elevation for that specific inlet flow and width:

Existing spillway

Flow in one chute (Q) = 1000 m^3/s
Downstream water depth = +102,8 meters
Width of one chute (L) = 15 meters

$$Fr = \frac{\frac{Q}{hL}}{\sqrt{gh}} \rightarrow 0{,}55 = \frac{\frac{1000}{h * 15}}{\sqrt{gh}} \rightarrow h = 11{,}45\ meters$$

Maximum mesh node elevation = 102,8 – 11,45 = 91,35 meters

New spillway

Flow in chute (Q) = 1500 m^3/s
Downstream water depth = +102 meters
Width of spillway (L) = 56 meters

$$Fr = \frac{\frac{Q}{hL}}{\sqrt{gh}} \rightarrow 0{,}55 = \frac{\frac{1500}{h * 56}}{\sqrt{gh}} \rightarrow h = 6{,}23 meters$$

Maximum mesh node elevation = 102 – 6,23 = 95,77 meters

Power station

Flow in one turbine (Q) = 210 m^3/s
Downstream water depth = +101 meters
Width of one chute (L) = 9,45 meters

$$Fr = \frac{\frac{Q}{hL}}{\sqrt{gh}} \rightarrow 0{,}55 = \frac{\frac{210}{h * 9{,}45}}{\sqrt{gh}} \rightarrow h = 5{,}5\ meters$$

Maximum mesh node elevation = 101 – 5,5 = 95,5 meters

The inlet meshes before and after executing the changes above can be seen in figure 28 to 31 below.

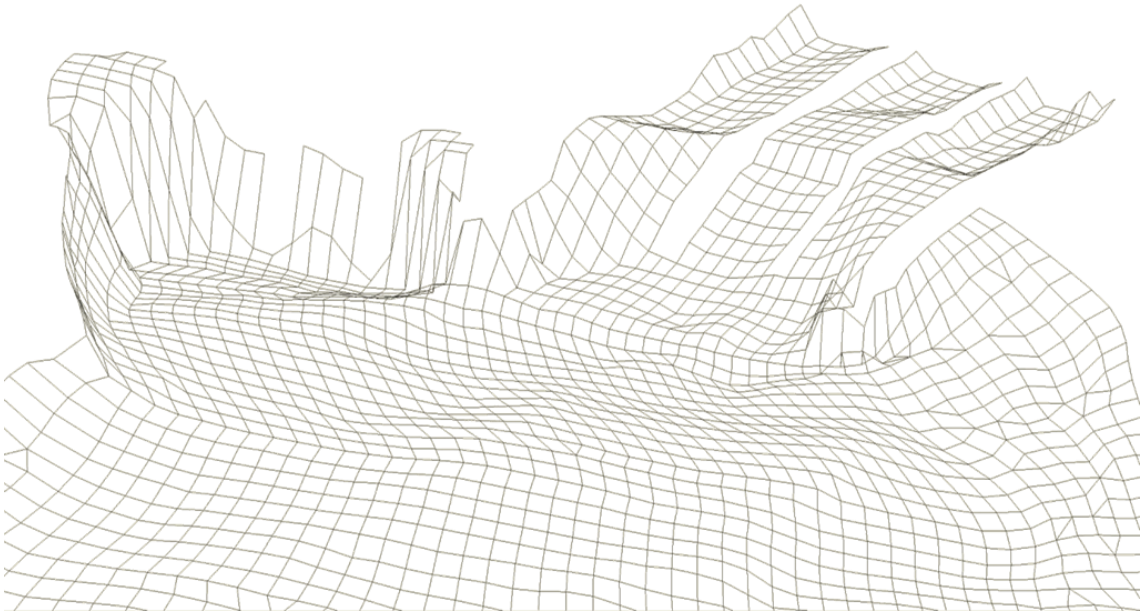

Figure 28. The existing spillway (to the right) and the power station outlet (to the left) before modification of the mesh nodes.

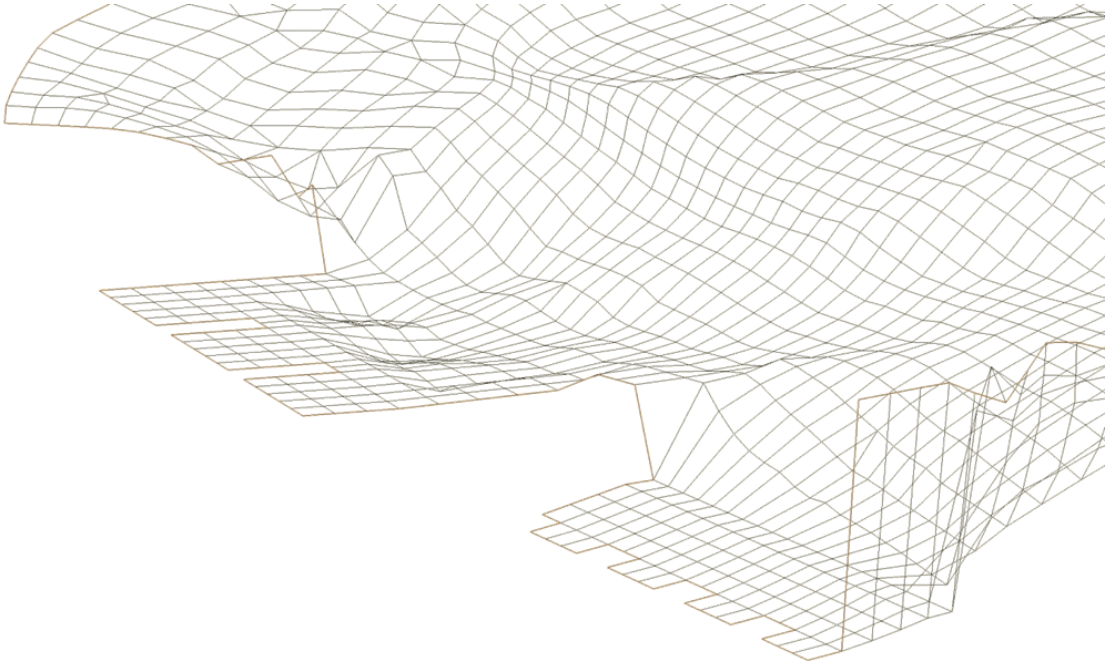

Figure 29. The existing spillway (to the left) and the power station outlet (to the right) after modification of the mesh nodes.

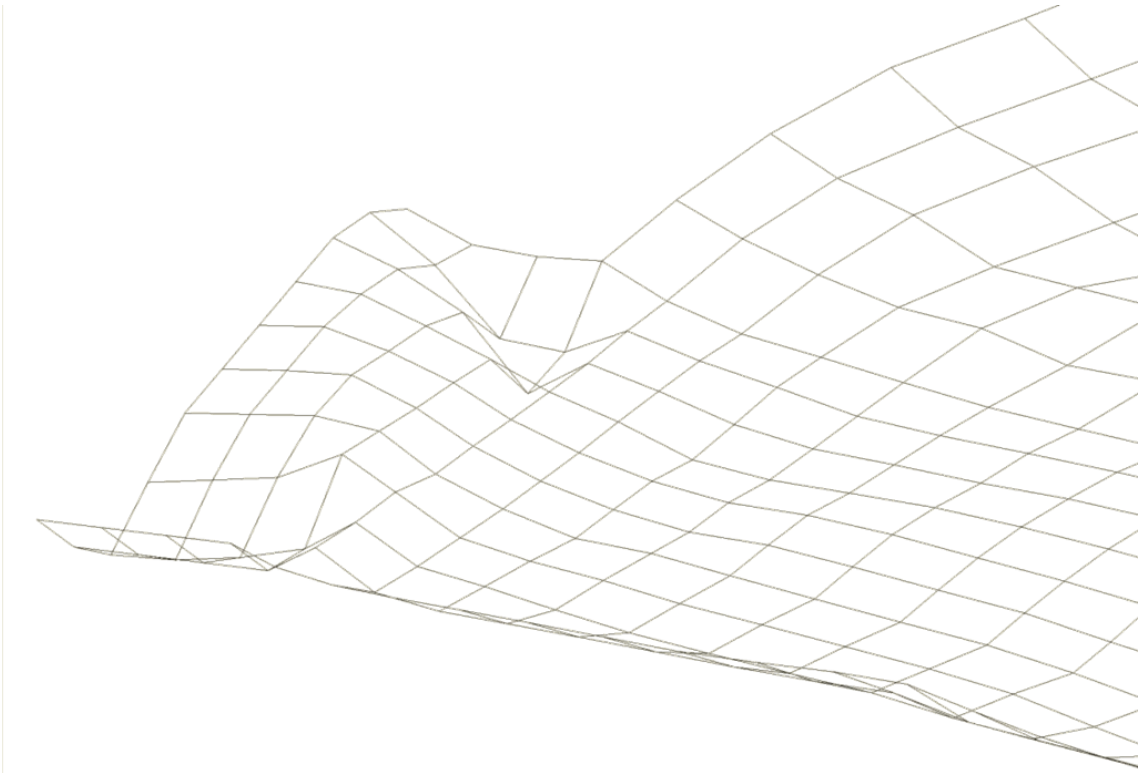

Figure 30. The new spillway outlet before modification of the mesh nodes.

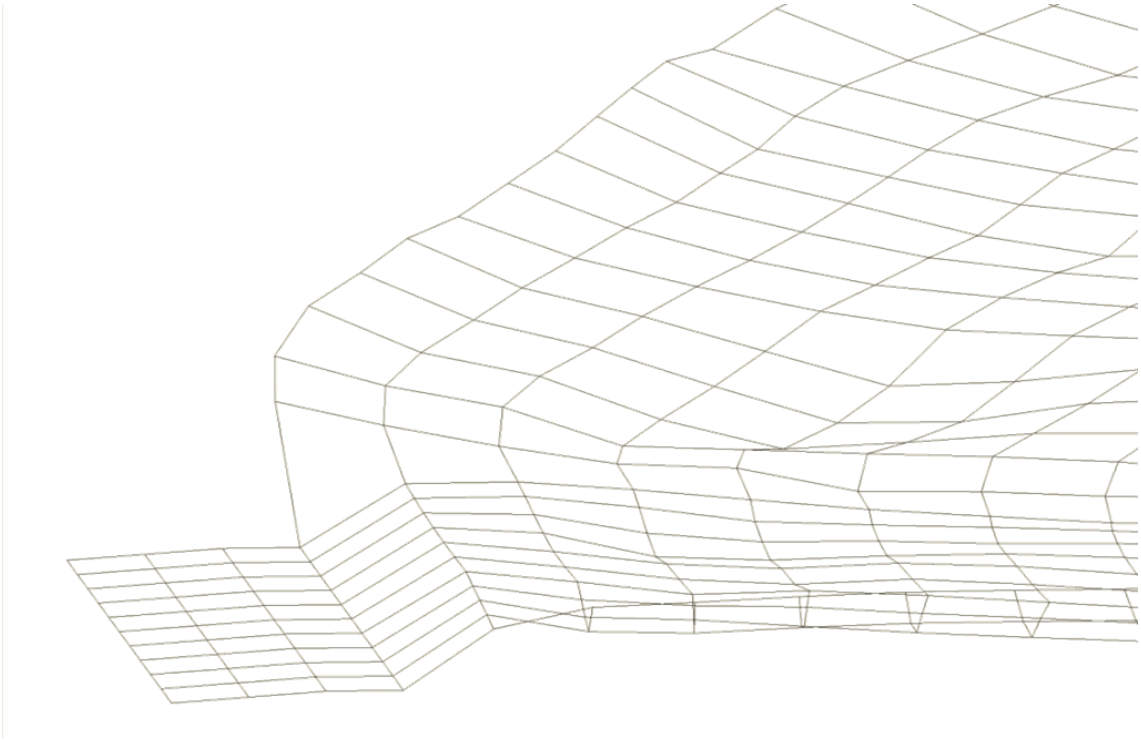

Figure 31. The new spillway outlet after modification of the mesh nodes.

The final version of the finite element mesh in the pre- and post-construction models can be seen in figure 32 and 33 below.

Figure 32. The finite element mesh in the pre-construction model.

Figure 33. The finite element mesh in the post-construction model.

7.3 Input parameters and boundary conditions

In order to receive reliable results from the RMA2 computations, the input parameter values have to be properly assigned. The input parameters in this model includes the upstream boundary conditions (flow from the hydropower station, flow from the existing spillway and flow from the new spillway), the downstream boundary condition (water depth at 700 meters from the dam), the Manning's roughness coefficient *n* and the eddy viscosity *E*. As mentioned in section 4.2, the Manning's coefficient and the eddy viscosity are used as tuning parameters in the calibration process and these values are found in table 5 and 6, section 7.6.3 instead.

A summary of the boundary conditions are shown in table 2 and 3 below. The downstream water levels for the different flow rates are determined from figure 24 in section 7.2.1.

Table 2. Upstream and downstream boundary conditions for the different discharge combinations in the pre-construction model.

Discharge combination	*Flow rate from hydropower station (m^3/s)*	*Flow rate from existing spillway (m^3/s)*	*Downstream water depth (m)*
DC1	840	0	+101,3
DC2	0	2300	+102,5
DC3 (flooding)	0	3000	+102,9

Table 3. Upstream and downstream boundary conditions for the different discharge combinations in the post-construction model (lowest value used).

Discharge combination	*Flow rate from hydropower station (m^3/s)*	*Flow rate from existing spillway (m^3/s)*	*Flow rate from new spillway (m^3/s)*	*Total flow rate (m^3/s)*	*Downstream water depth (m)*
DC4	840	0	0	840	+101,3
DC5	0	2300	0	2300	+102,5
DC6	0	0	1500	1500	+102
DC7	0	1800	1500	3300	+103,1
DC8 (flooding)	0	2300	1700	4000	+103,4

7.4 Model control

While simulating the flow conditions using RMA2 there is also a number of model control parameters to take into account. These includes the maximum number of iterations for one simulation, the

required nodal steady state depth for convergence, the depth below which a node is defined as dry, the depth above which a node is defined as wet, the latitude for the coriolis forces, the impact of wind, rainfall and evaporation. Depending on the wanted accuracy of the results, some parameters can be more roughly estimated or even neglected in order to get the model to converge. For example, the required depth convergence can be increased which allows a higher difference between the nodal water depths. In table 4 below, these parameters and the assigned values for the simulations are shown.

Table 4. Model control parameters

Parameter	*Value*
Iterations	20
Depth convergence	0,05 meters
Dry depth	0,084 meters (default)
Wet depth	0,183 meters (default)
Latitude	Neglected
Wind speed	Neglected
Rainfall/Evaporation	Neglected

The depth convergence parameter determines the maximum depth difference in a node from the fixed water depth for the specific simulation, which can have a slight impact on the end result. For example, choosing a low value of 1 cm provides a more accurate solution than 10 cm. However, the former parameter value might prove much more difficult or impossible for the model to converge to. In this project, a value of 5 cm has been estimated to be good enough to provide a correct solution.

7.5 RMA2 spin-down

The iterative solution received from the nonlinear flow equations needs to be started from some initial guessed values. However, since these guessed values might differ a lot from the desired boundary conditions it might be impossible to reach convergence using the cold start conditions. Therefore, a solution is often obtained using a method called spin-down. Here, initial conditions are defined that are often very different from the desired boundary conditions but are easier for the model to handle. By starting with a completely wet model i.e. the downstream water depth is higher than the highest mesh node elevation and a low flow, there is no initial wetting or drying problems. The model can then from this initial run gradually steer the water elevation down and the flow up to the desired values by using the conditions received from the previous result file. Starting the model from a preceding solution is called hot starting. The model has converged in the specific run when it reaches either the maximum number of iterations and the maximum depth change is less than one or the convergence

depth mentioned in section 7.4 above. A spin-down for the flow 2300 m^3/s and the water elevation +102,5 meters is shown in figure 34 and 35 below.

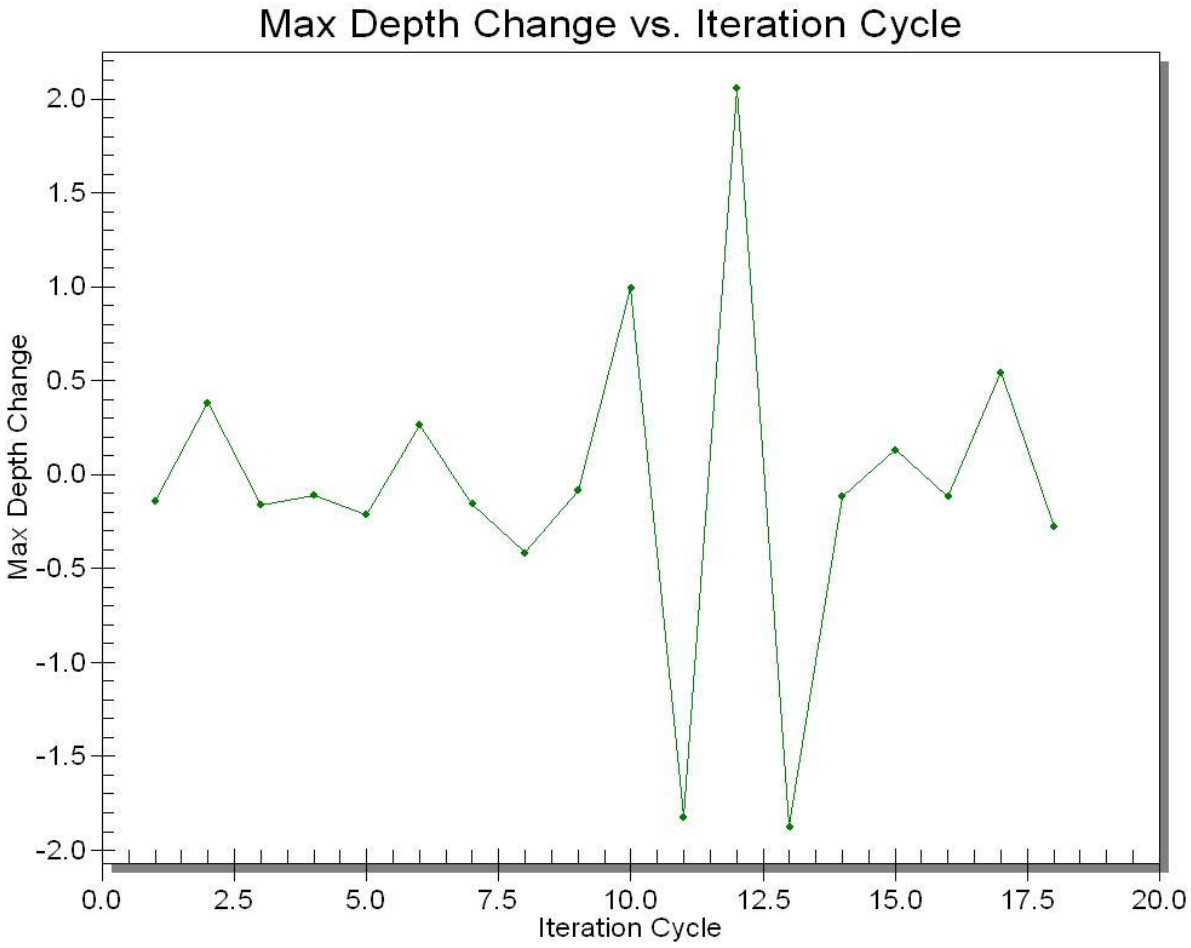

Figure 34. One spin-down run where the maximum depth change has not yet reached below 0,05 meters.

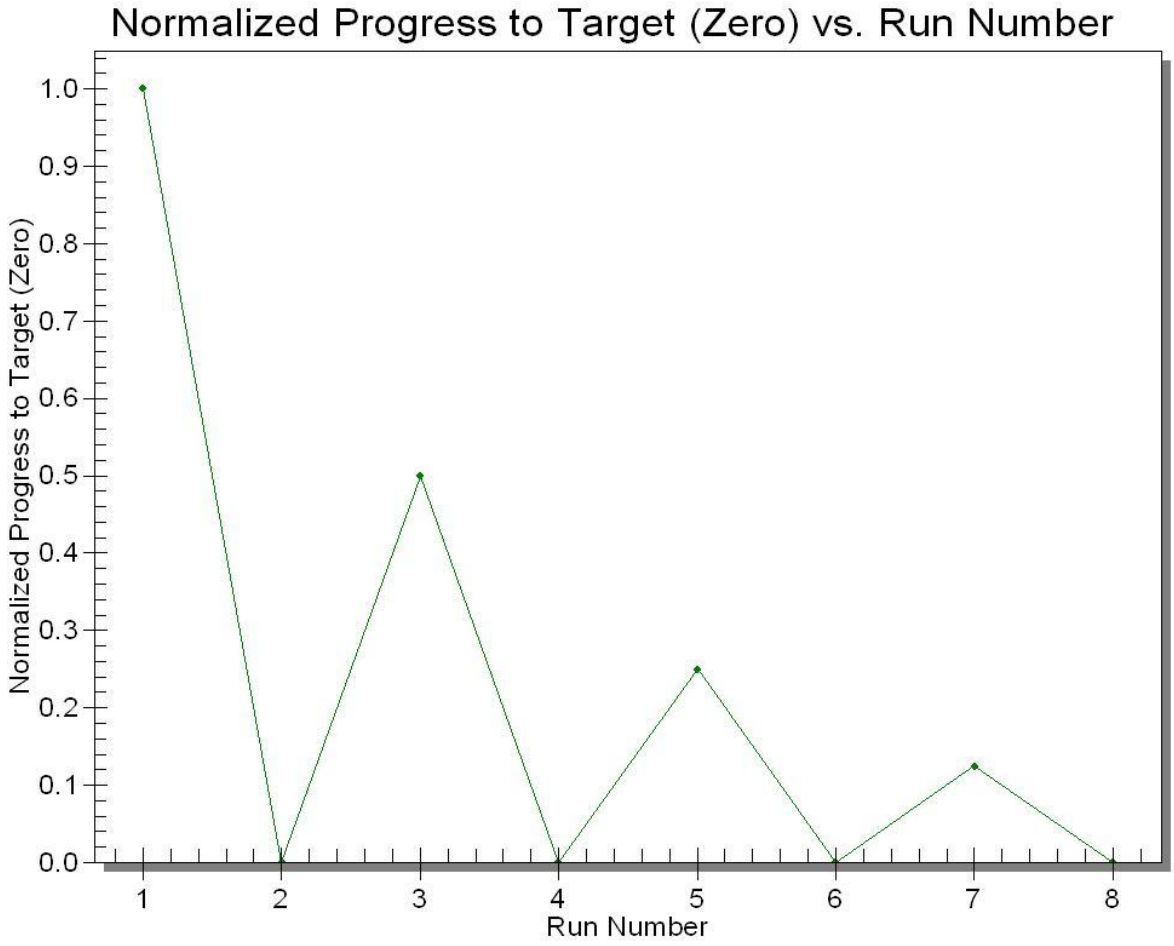

Figure 35. Normalized progress to target vs. run number. Here, it took nine runs before the model converged to a flow of 2300 m^3/s and a water depth of +102,5 meters.

For these two models, a complete run takes between 15 and 45 minutes, depending on the flow situation that is to be simulated.

7.6 Verification

In order for the results of the numerical simulations to have any reliability, the models have to be verified i.e. calibrated and validated against existing observed data. Calibration is the process of varying the model parameters until the solution reflects the observed data from a certain flow situation within a specified level of accuracy. The model is then said to be validated if the solution in the same way matches a different set of observed data with unchanged model parameter values. There are a number of factors which affect the verification results; the overall geometry design, the choice of model, the boundary conditions, the Manning's roughness coefficient and the eddy viscosity. As mentioned in section 4.2, the latter two are the parameters used for fine-tuning of two-dimensional models. The relative importance of the different aspects to the verification process can be seen in figure 36 below.

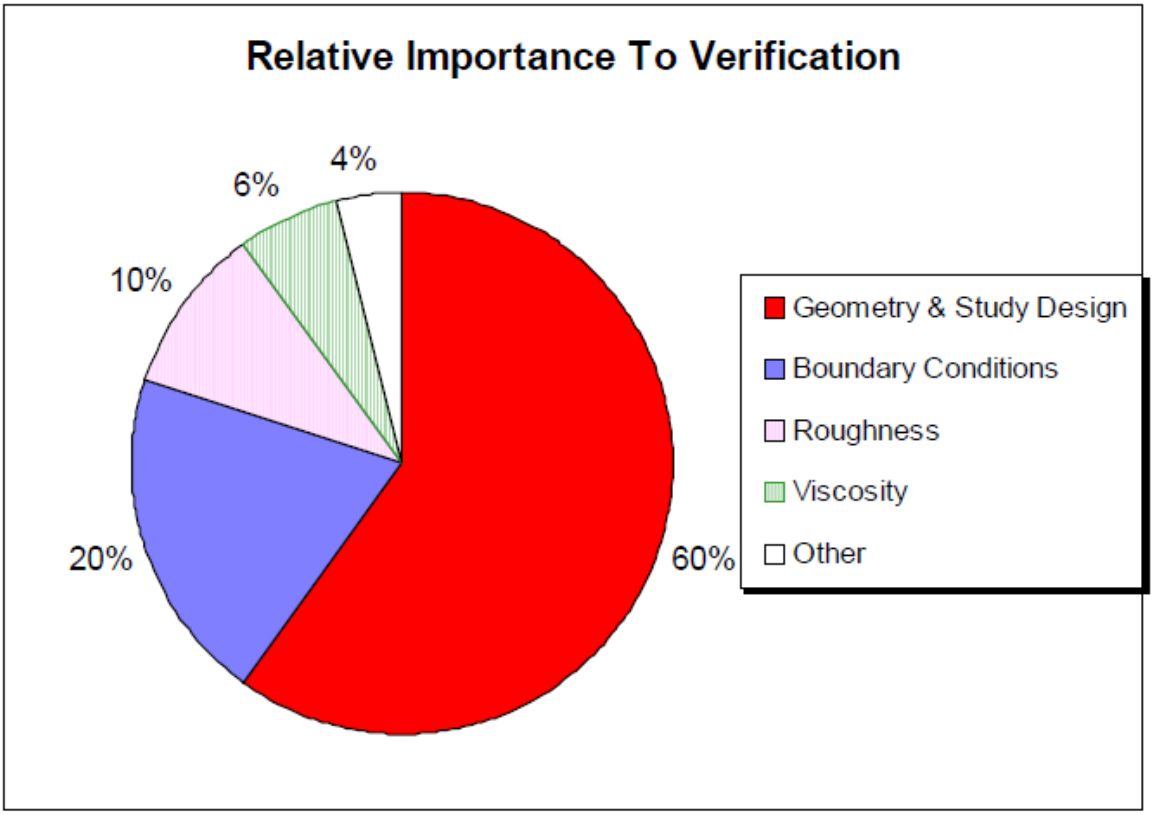

Figure 36. The quantitative percentages of the parameters used to receive a successful simulation (King, 2005).

In SMS, the model is verified by creating a coverage with observation points or arcs that matches the points or lines of measurements in the physical model. The points can then be evaluated against the observed data with an accuracy interval. An accuracy of for example 1 m/s means that if the difference of the data from the numerical and the physical model is ± 1 m/s or less in each point, the model is said to be calibrated. The higher accuracy that is used, the higher reliability the model results will have. This relationship between the computed and the observed values can be illustrated by using verification bars or a graph. The verification bar is illustrated in figure 37 below where the center corresponds to the observed value, the top to the observed value plus the accuracy, the bottom to the observed value minus the accuracy and the colored bar the error. If the error lies within the target interval the bar becomes green, if it is outside the target interval but within 200% it becomes yellow and if it is more than 200% it becomes red.

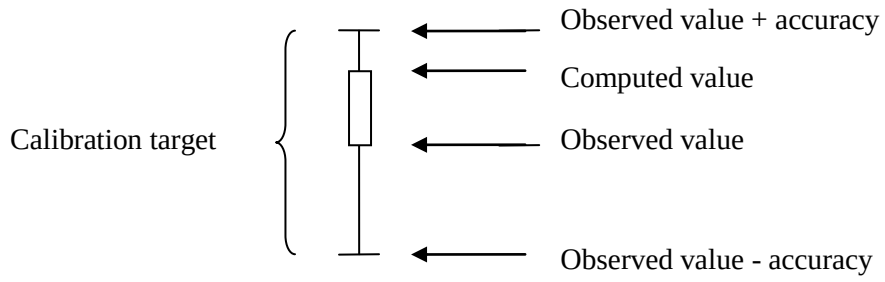

Figure 37. Verification bar.

The observation arcs are lines that run across the river stretch and can be used for investigating the velocity profile. If the observed data consists of velocity profile graphs rather than points, these observation arcs can be useful to apply.

In this project, the observed data for the pre- and the post-construction situations consists of surface velocities measured across specific stretches in the two physical hydraulic models present at Vattenfall R&D in Älvkarleby. The measurements for the pre-construction situation were made in the old model in the year 2000 before the addition of the new spillway and the measurements for the post-construction situation were made in the new model in the year 2010 after the addition. These velocity profiles and the location of the measurements can be seen in figure 38 to 42. There a two sets of data for each situation, one used for calibration and one for validation.

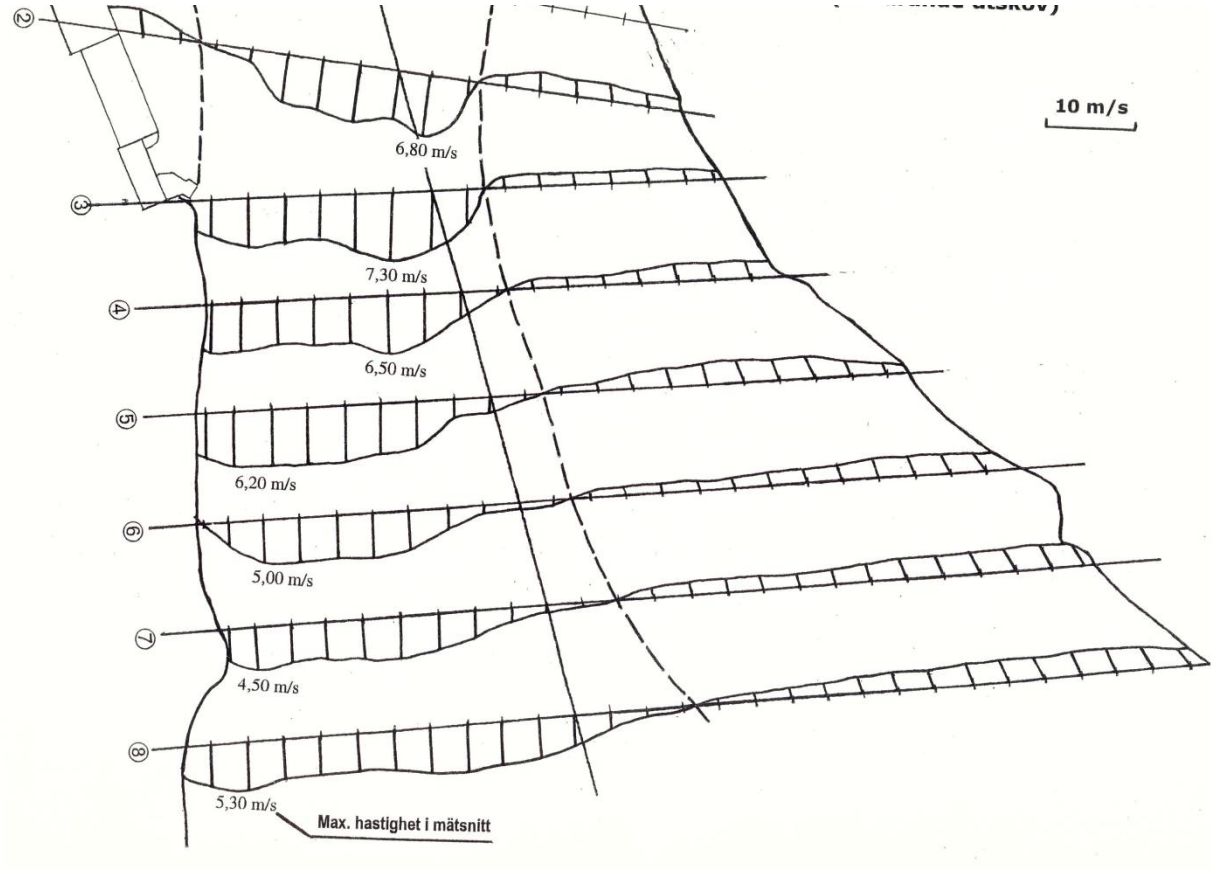

Figure 38. Location of the measurements and the surface velocities for the flow 2300 m^3/s in the pre-construction physical hydraulic model (Yang, 2000).

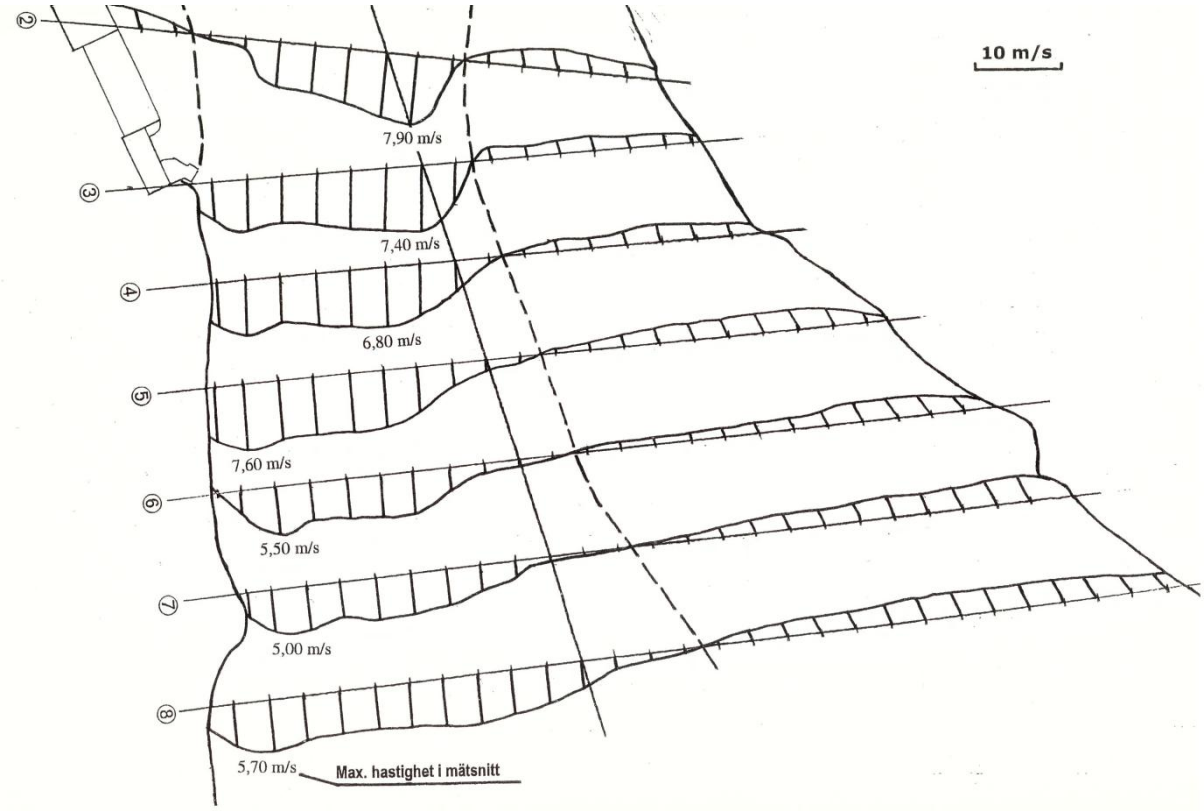

Figure 39. Location of the measurements and the surface velocities for the flow 2715 m^3/s in the pre-construction physical hydraulic model (Yang, 2000).

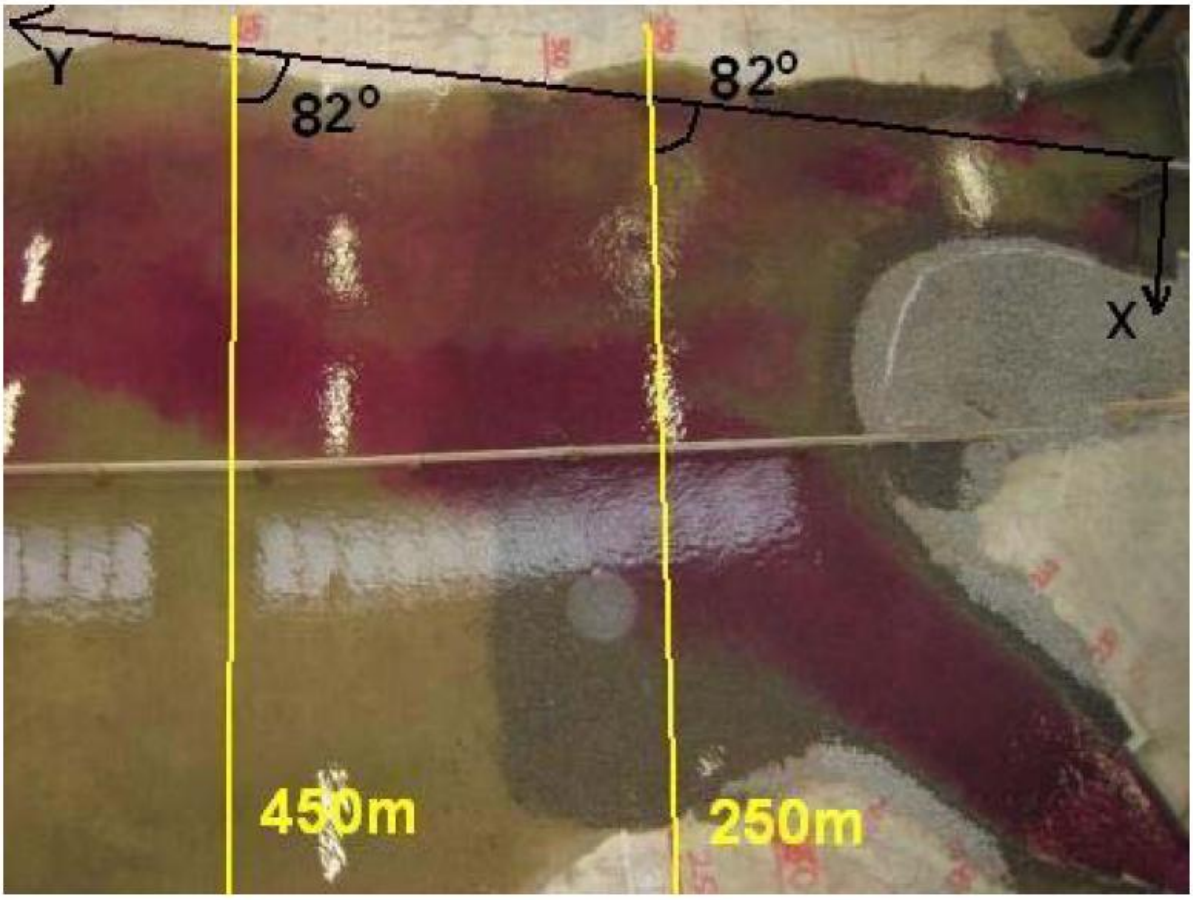

Figure 40. Location of the measurements in the post-construction physical hydraulic model measured from the end of the existing spillway chutes (Frisk et al., 2010).

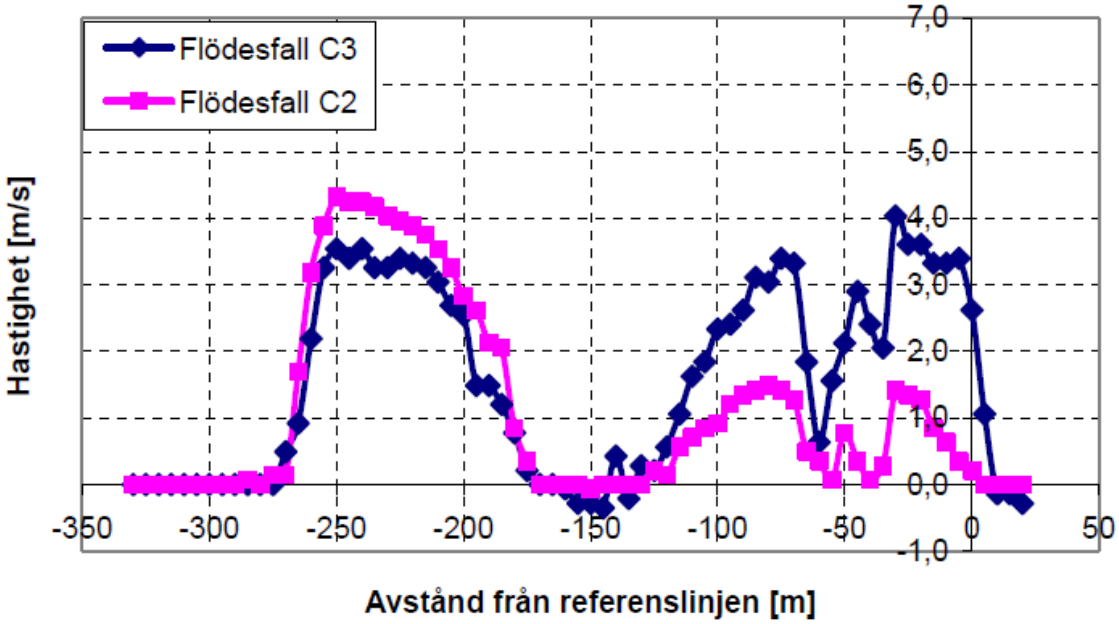

Figure 41. Surface velocities in the post-construction physical hydraulic model 250 meters from the end of the existing spillway. Flow situation C3 corresponds to 1500 m^3/s from the new spillway and 1800 m^3/s from the existing spillway and flow situation C2 corresponds to 1500 m^3/s from the new spillway and 840 m^3/s from the power station (Frisk et al., 2010).

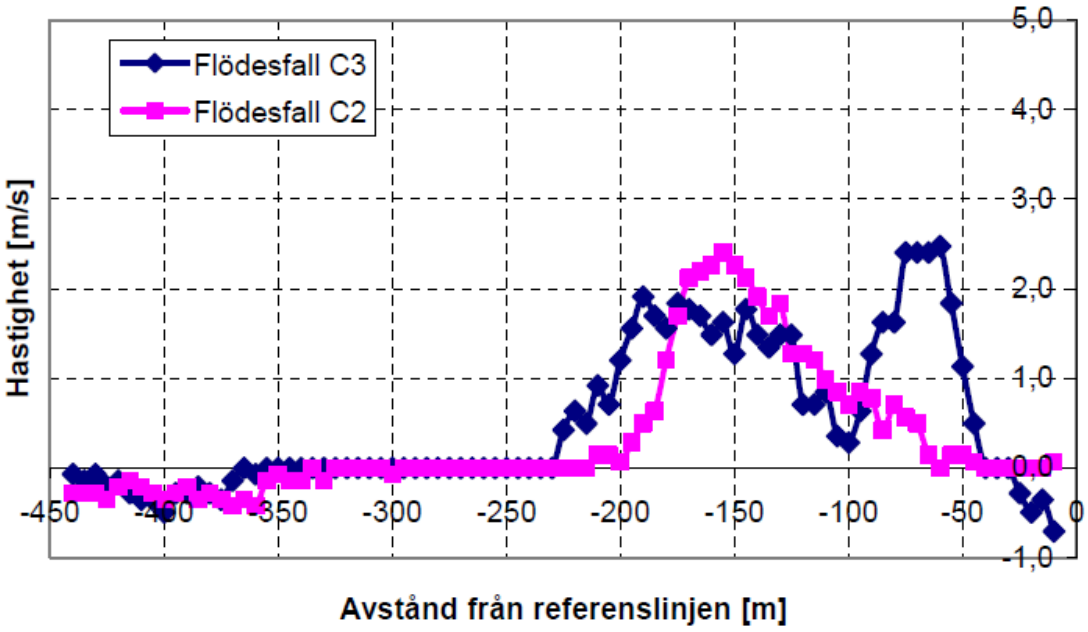

Figure 42. Surface velocities in the post-construction physical hydraulic model 450 meters from the end of the existing spillway. Flow situation C3 corresponds to 1500 m^3/s from the new spillway and 1800 m3/s from the existing spillway and flow situation C2 corresponds to 1500 m^3/s from the new spillway and 840 m^3/s from the power station (Frisk et al., 2010).

However, these observed data cannot directly be used for calibration and validation as the velocities received from the numerical RMA2 simulations are depth averaged. Usually, the velocity in a river channel decreases with depth and the average velocity is lower than the surface velocity as can be seen in figure 43 below.

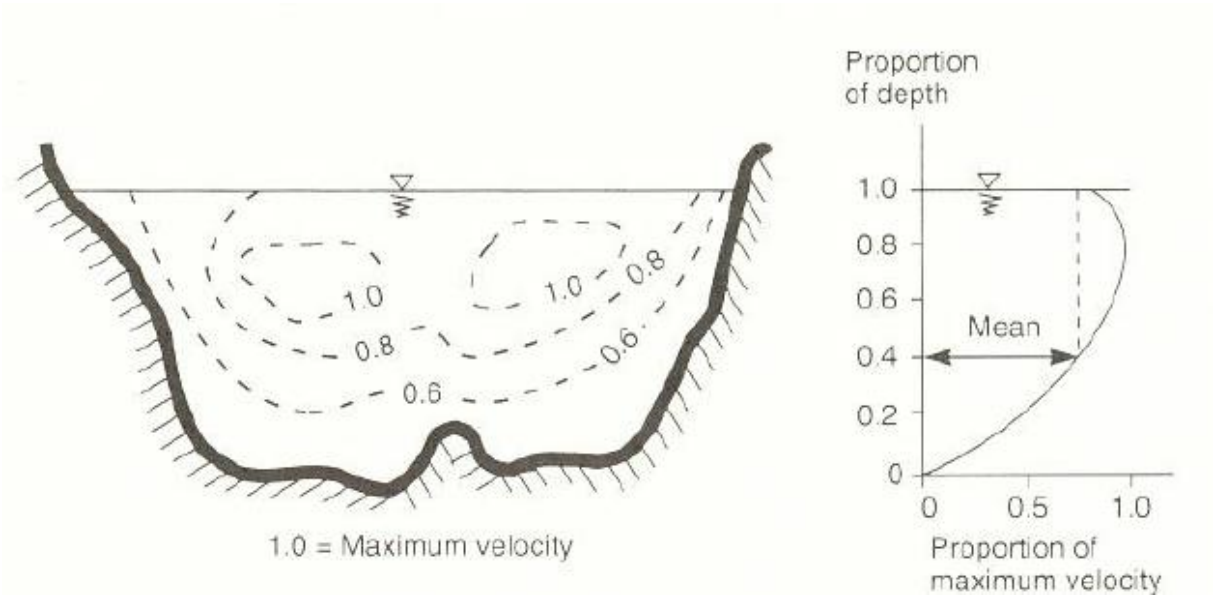

Figure 43. Variation of relative velocity in a river channel shown by a cross-section and a vertical profile (Hamill, 2001).

Determining the average velocity from surface velocity is not easy task as the relationship depends both on the water depth and the bed roughness. Usually it is sufficient to assume a standard value. According to Hamill (2001), Hudson (1993) and USBR (2001) the ratio between the surface velocity and the average velocity can vary from 70% to 80%, depending on the water depth and flow rate. From these guidelines, a value of 70% is assumed for all flows in this project and the measured values are therefore multiplied with 0,7 before being used in the verification process.

The location of the observation lines seen in figure 38, 39 and 40 above are then translated to the numerical model. The location of the observation points and observation arcs in the pre- and post-construction model can be seen in figure 44 and 45 below. Since it is difficult to determine any exact velocities from figure 38 and 39 except for the maximum, the observation points in the pre-construction model are placed only at the observed maximum velocities in the pre-construction physical hydraulic model. These locations are the same both for the flow 2300 m^3/s and 2715 m^3/s.

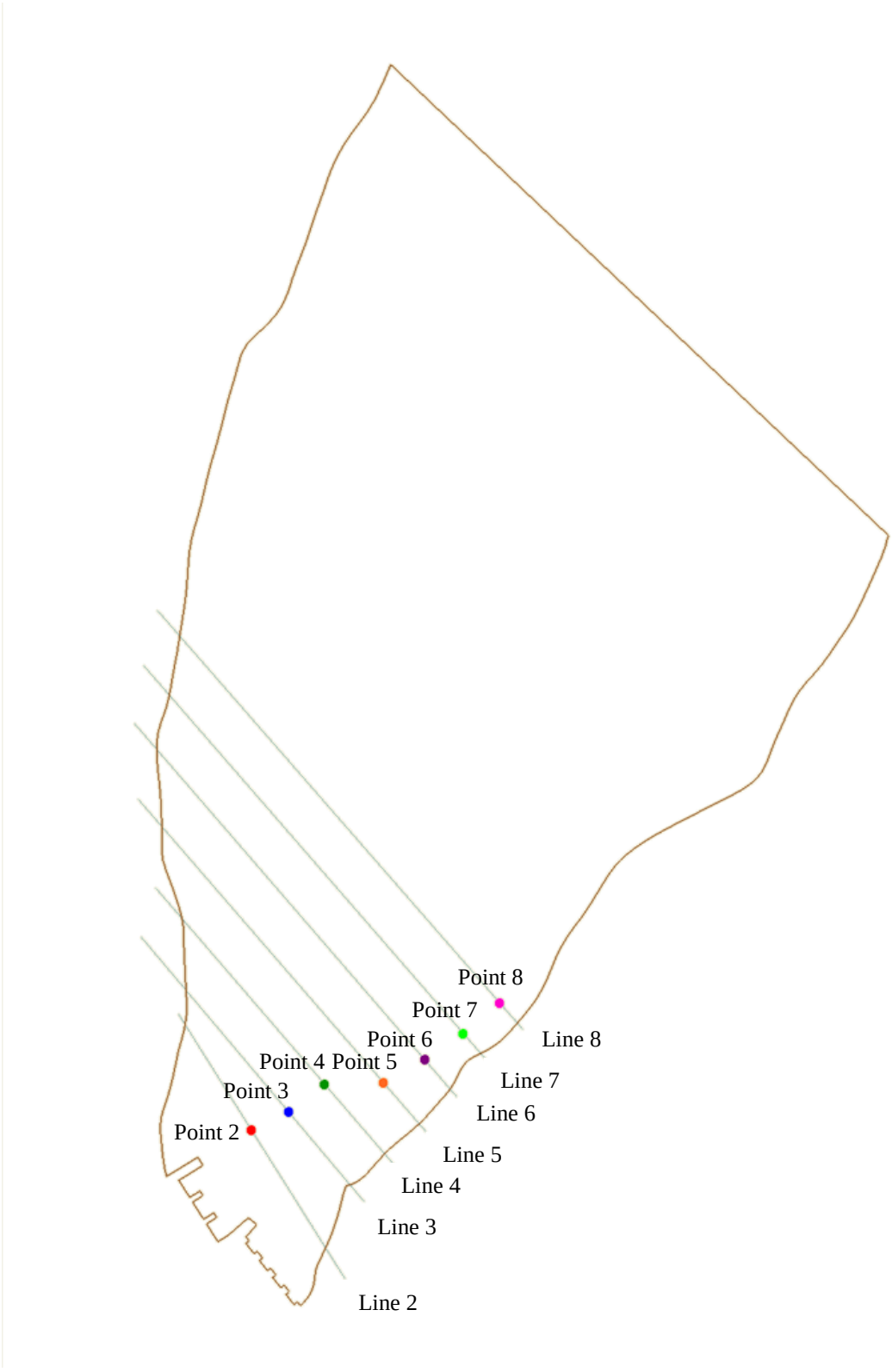

Figure 44. Location of the observation points and observation arcs in the pre-construction model.

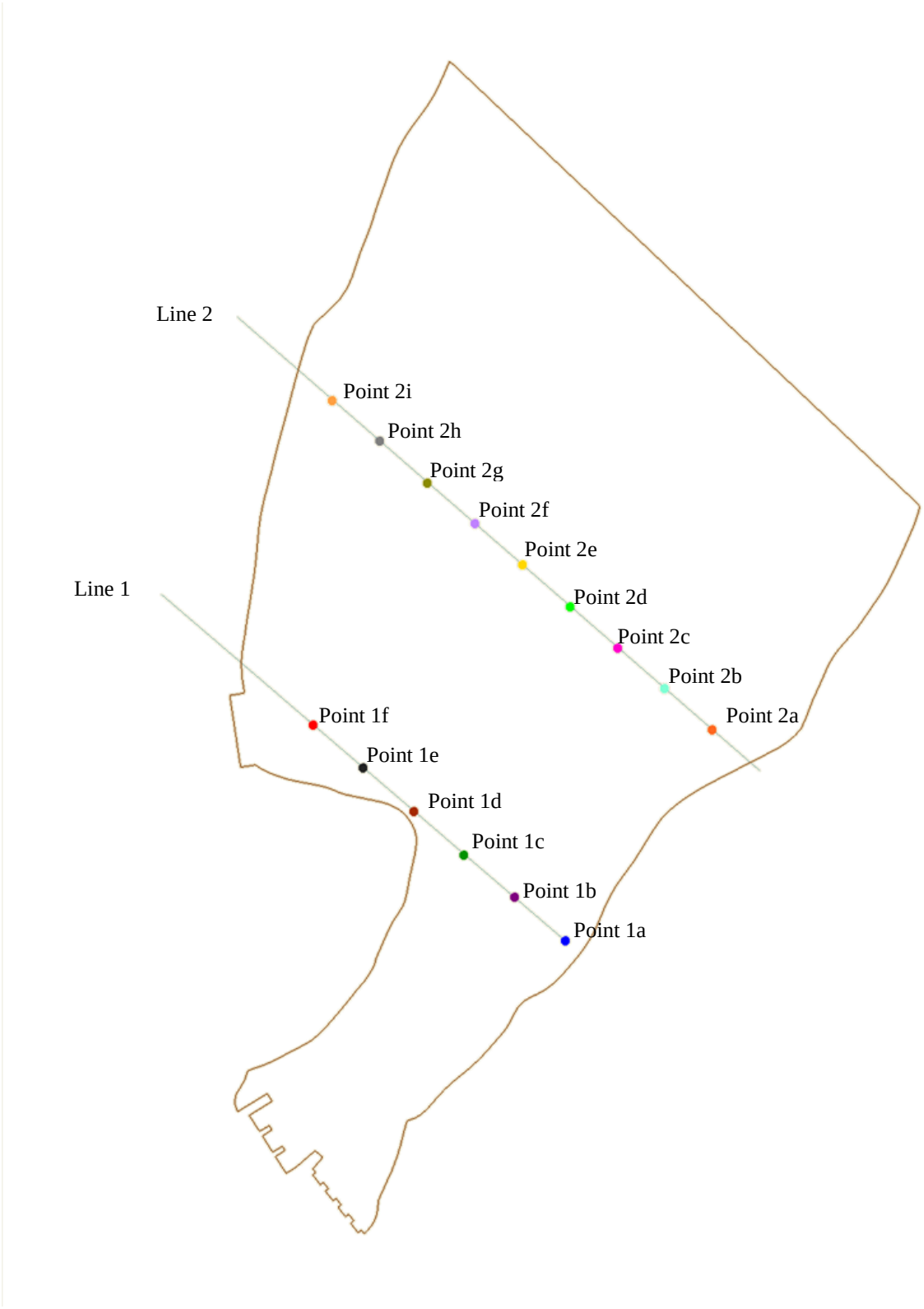

Figure 45. Location of the observation points and observation arcs in the post-construction model.

As mentioned above, the verification process also requires an accuracy interval based on the reliability of the observed values and the assumptions made in the simulations. In this project, there are a number of factors determining this accuracy for the calibration and validation:

- A hydraulic numerical model can never completely reflect the complex physical relationships and their interactions, despite of sophisticated formulas as the ones presented in section 4 above. The results can therefore never fully comply from the ones received from a physical hydraulic model or field observations.
- The measurements in the laboratory are made over several hours while the results from the simulations are steady state and thereby time-averaged.
- When measuring the velocity in a physical model, the results are never 100% accurate. While laboratory measurements are more precise than field measurements, one can expect an error of around 10-15% in some sections. This error can also increase with increasing flow.
- The transformation of the data from the physical model to the reality using the equations and the transformation factors presented in section 5 might also contribute to a small error in the results.
- As mentioned above, the supercritical sections at the inflows are neglected. This might lead to a reduction in the initial momentum of the flow down the inlets and a change in the velocity profiles. The scale and importance of this change is however hard to estimate and is believed to be most prominent at the first 100 meters.
- Throughout the model area, complex three-dimensional effects which RMA2 does not incorporate will affect the flow pattern and the velocities. This could include for example upward going jets at the spillways as well as backward currents in sections where the channel bed rapidly varies between deep and shallow sections as described in figure 46 below:

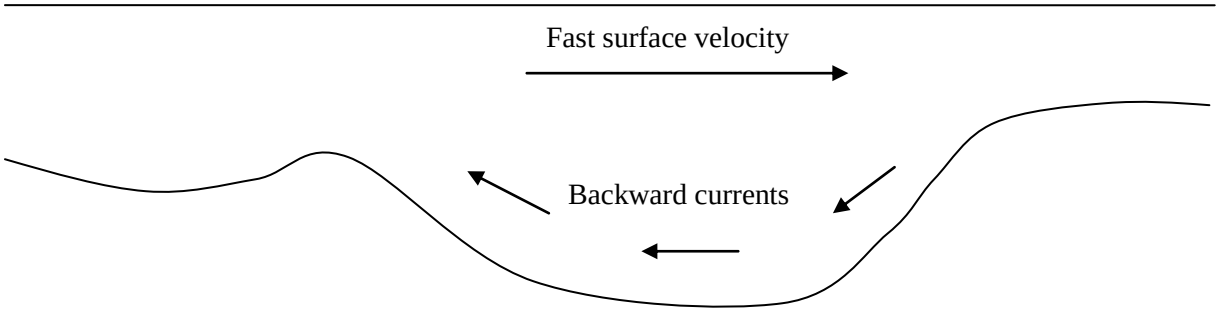

Figure 46. Formation of backward currents.

Normally, an uncertainty of around ±0,5 m/s to 1 m/s would be acceptable (BOSS International, 1999). However, due to the various factors described above the uncertainty increases. When including all the factors an increase of up 100% is estimated to be realistic, giving a new uncertainty of ± 2 m/s for all flows in this project.

7.6.1 Pre-construction model

7.6.1.1 Calibration

The pre-construction model is calibrated against a flow of 2300 m^3/s from the existing spillway. The verification bars, a plot of the computed vs. the observed values as well as a plot of the velocity

profiles (note that the velocities in the profile plots are not surface velocities) received from the simulations can be seen in figure 47 to 49 below.

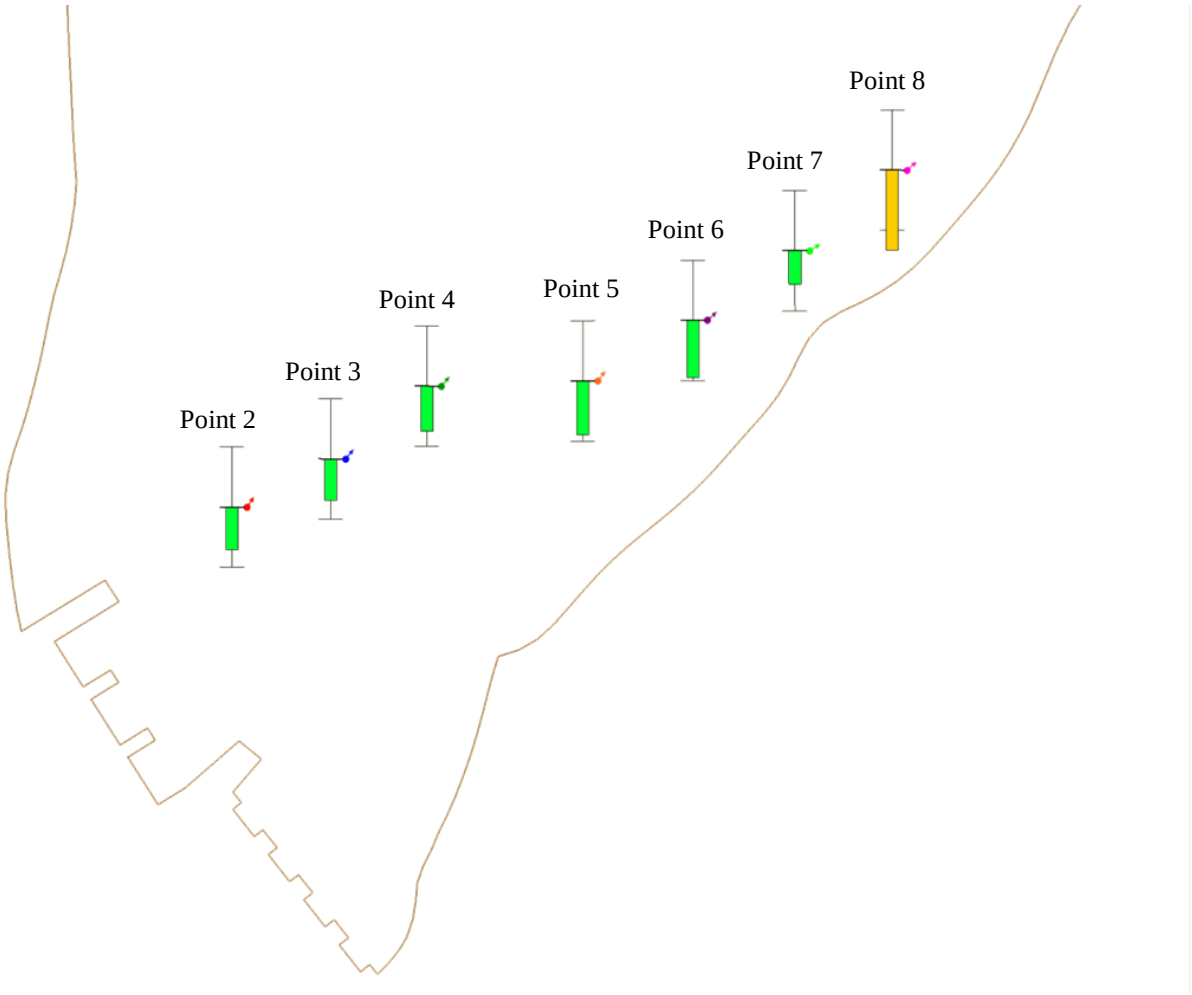

Figure 47. Calibration bars in the pre-construction model.

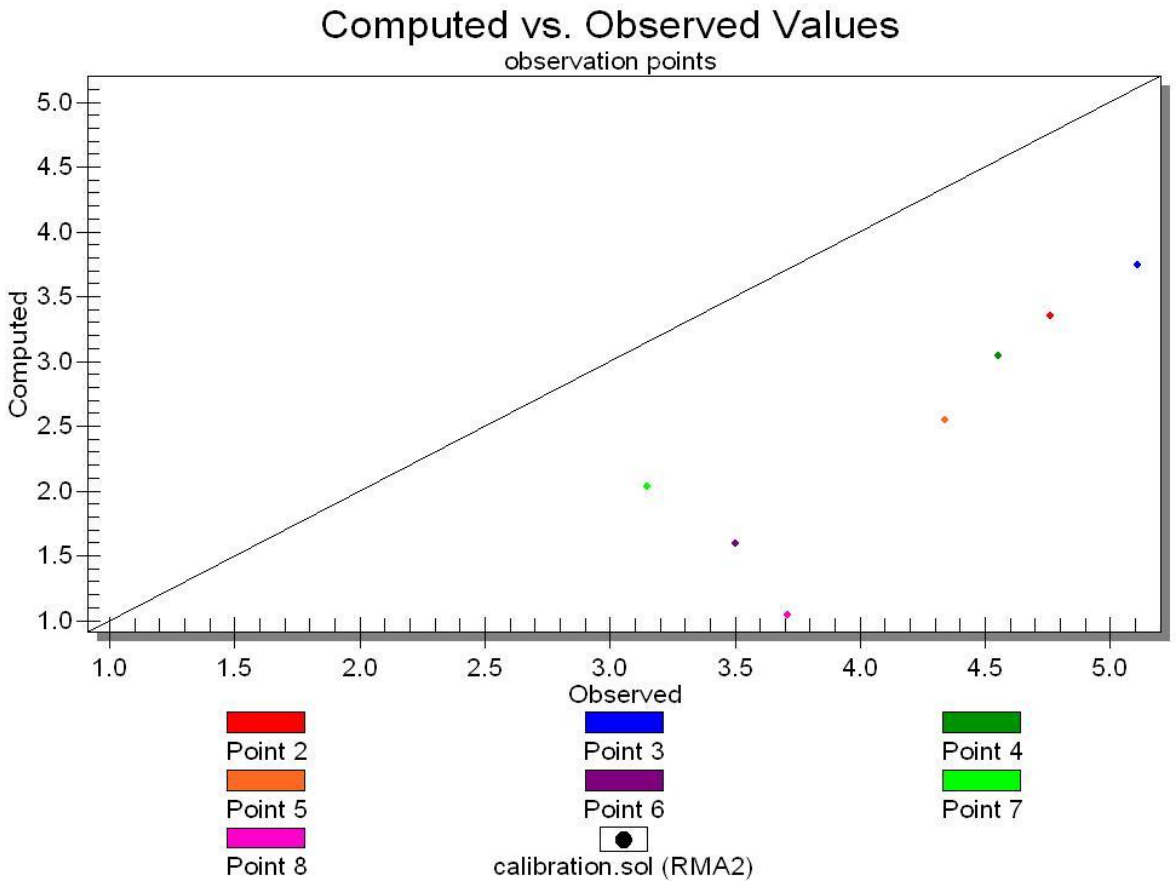

Figure 48. Computed vs. observed values in the pre-construction model.

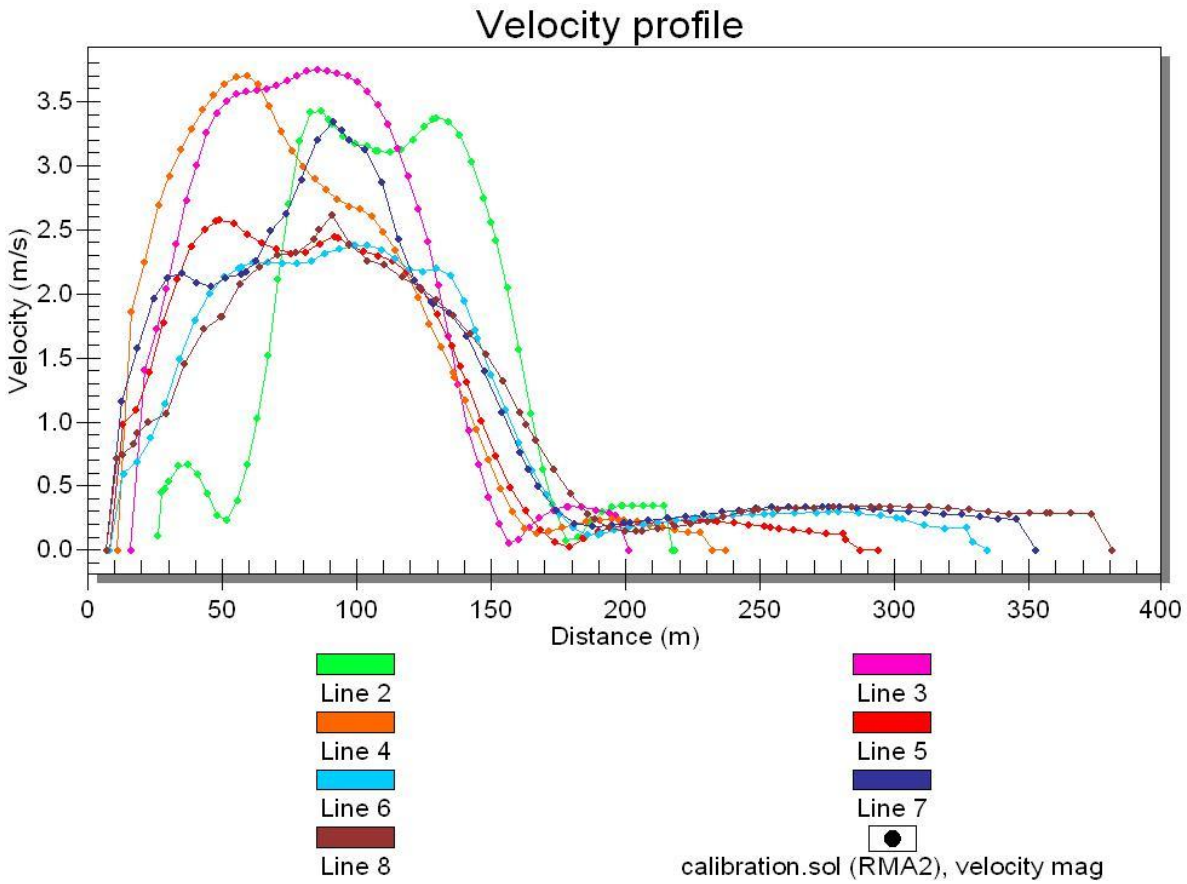

Figure 49. Velocity profile plot in the pre-construction model. The profile goes from right to left in the general flow direction, same as in figure 38 above.

7.6.1.2 Validation

The pre-construction model is validated against a flow of 2700 m^3/s from the existing spillway. The verification bars, a plot of the computed vs. the observed values as well as a plot of the velocity profiles received from the simulations can be seen in figure 50 to 52 below.

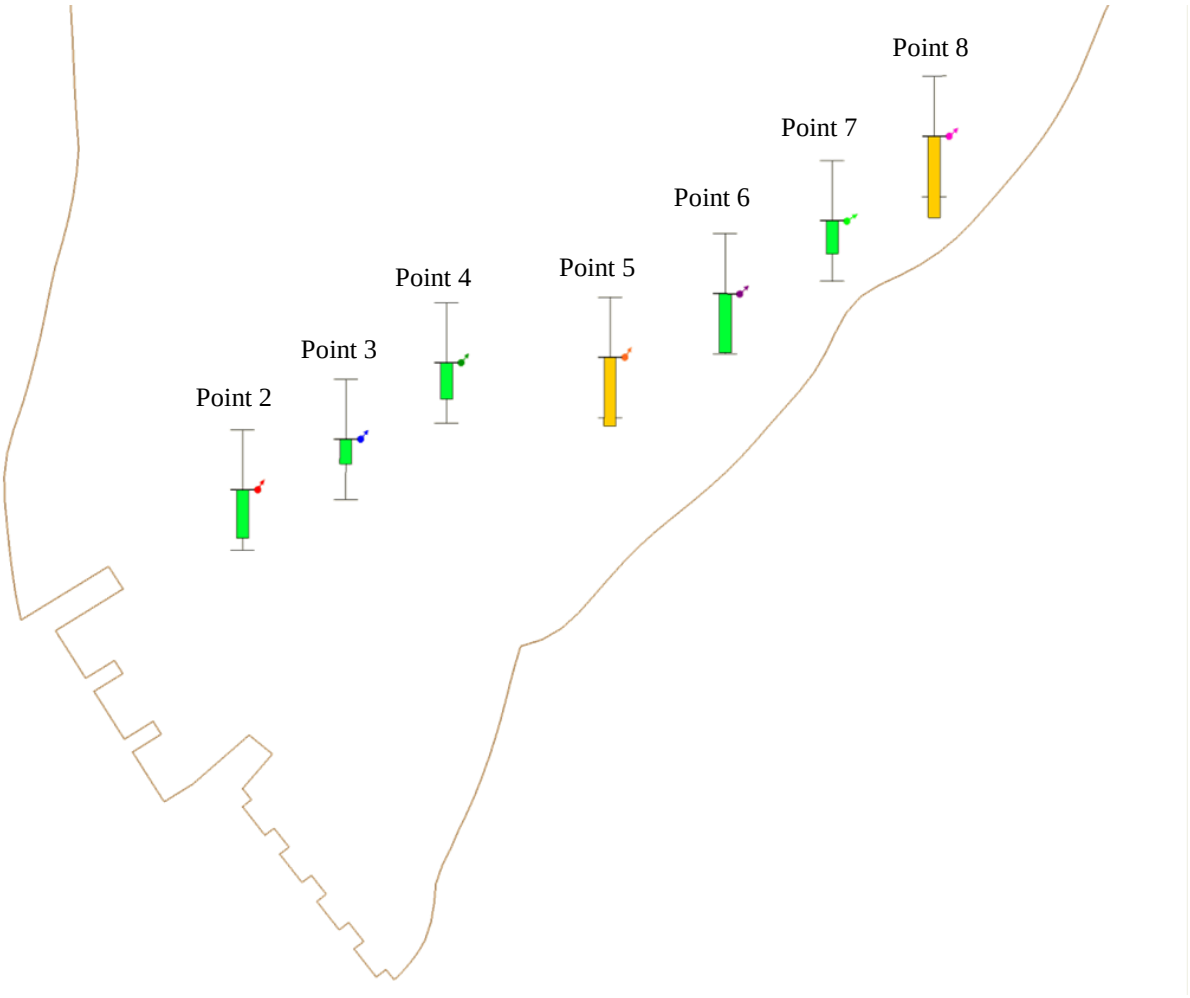

Figure 50. Validation bars in the pre-construction model.

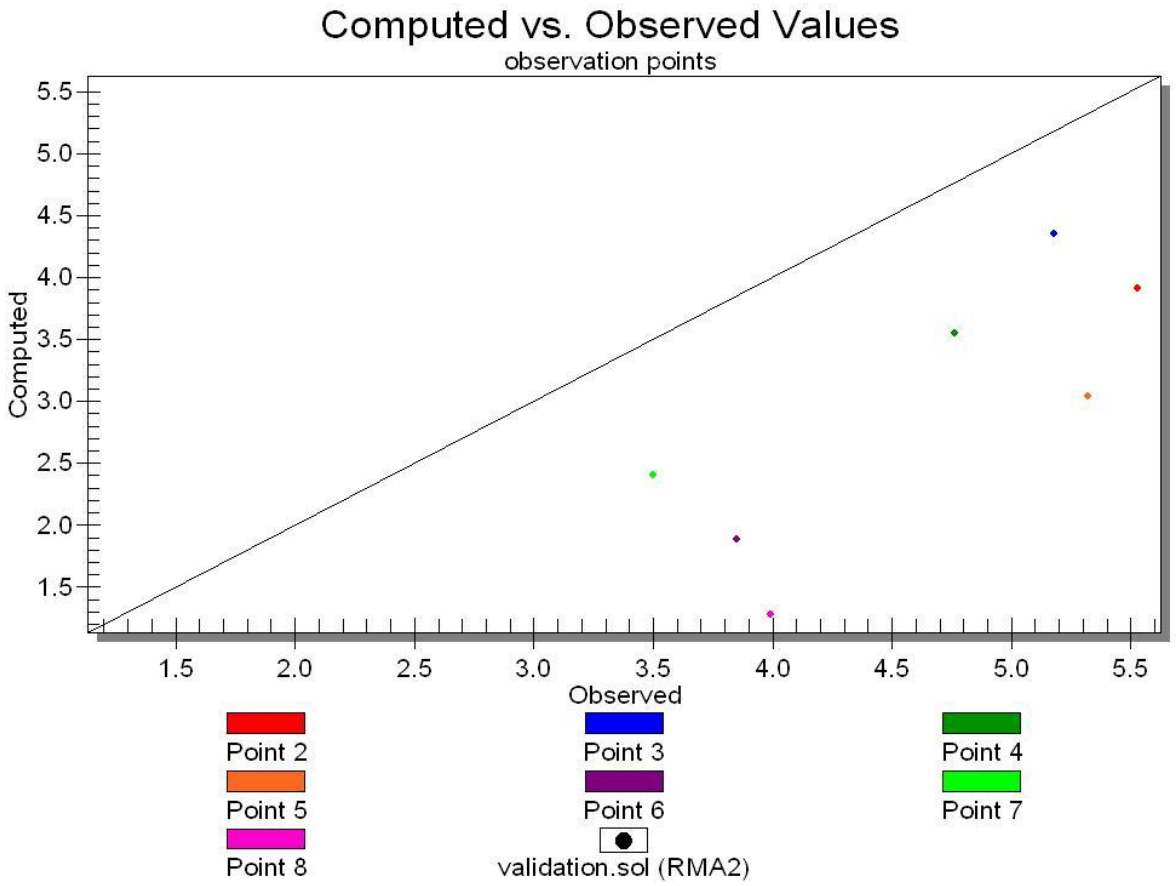

Figure 51. Computed vs. observed values in the pre-construction model.

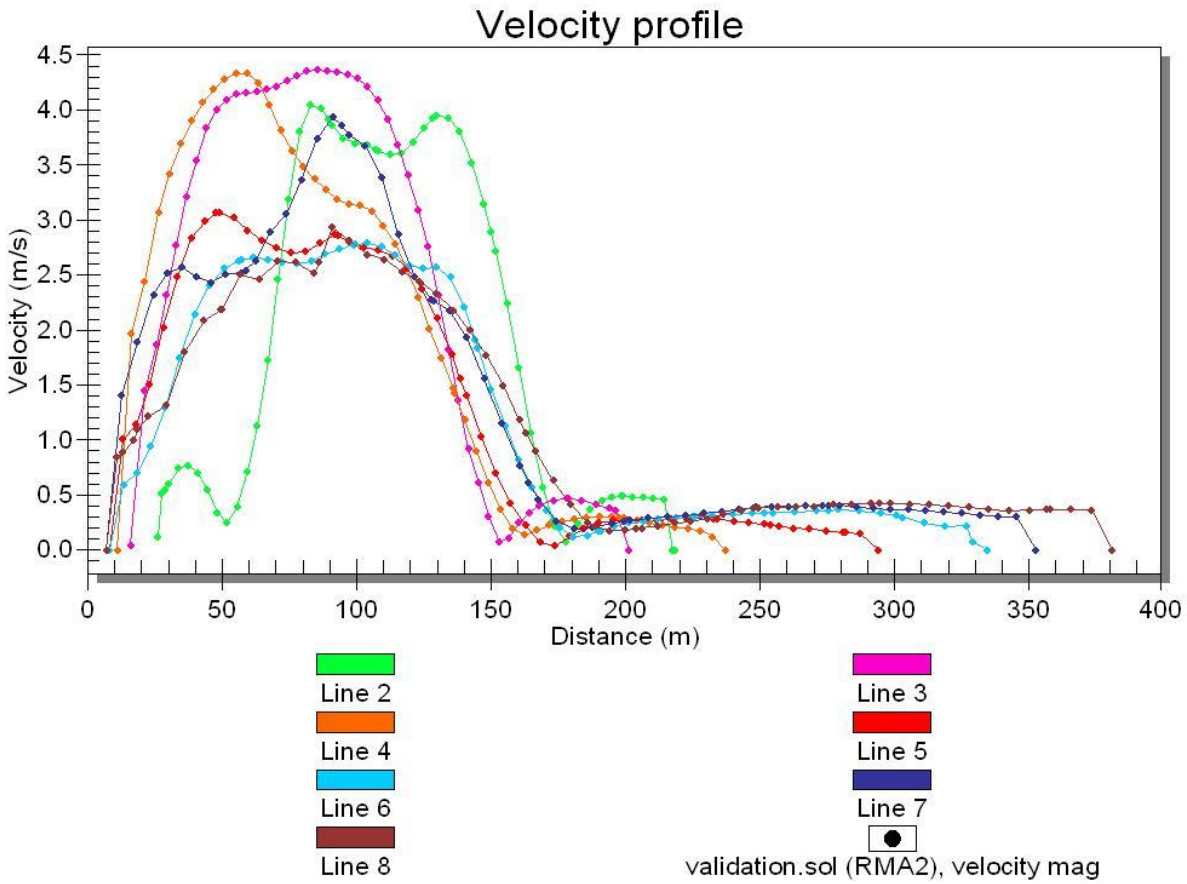

Figure 52. Velocity profile plot in the pre-construction model. The profile goes from right to left in the general flow direction, same as in figure 39 above.

7.6.2 Post-construction model

7.6.2.1 Calibration

The post-construction model is calibrated against a flow of 1500 m^3/s from the new spillway and 840 m^3/s from the power station. The verification bars, a plot of the computed vs. the observed values as well as a plot of the velocity profiles received from the simulations can be seen in figure 53 to 55 below.

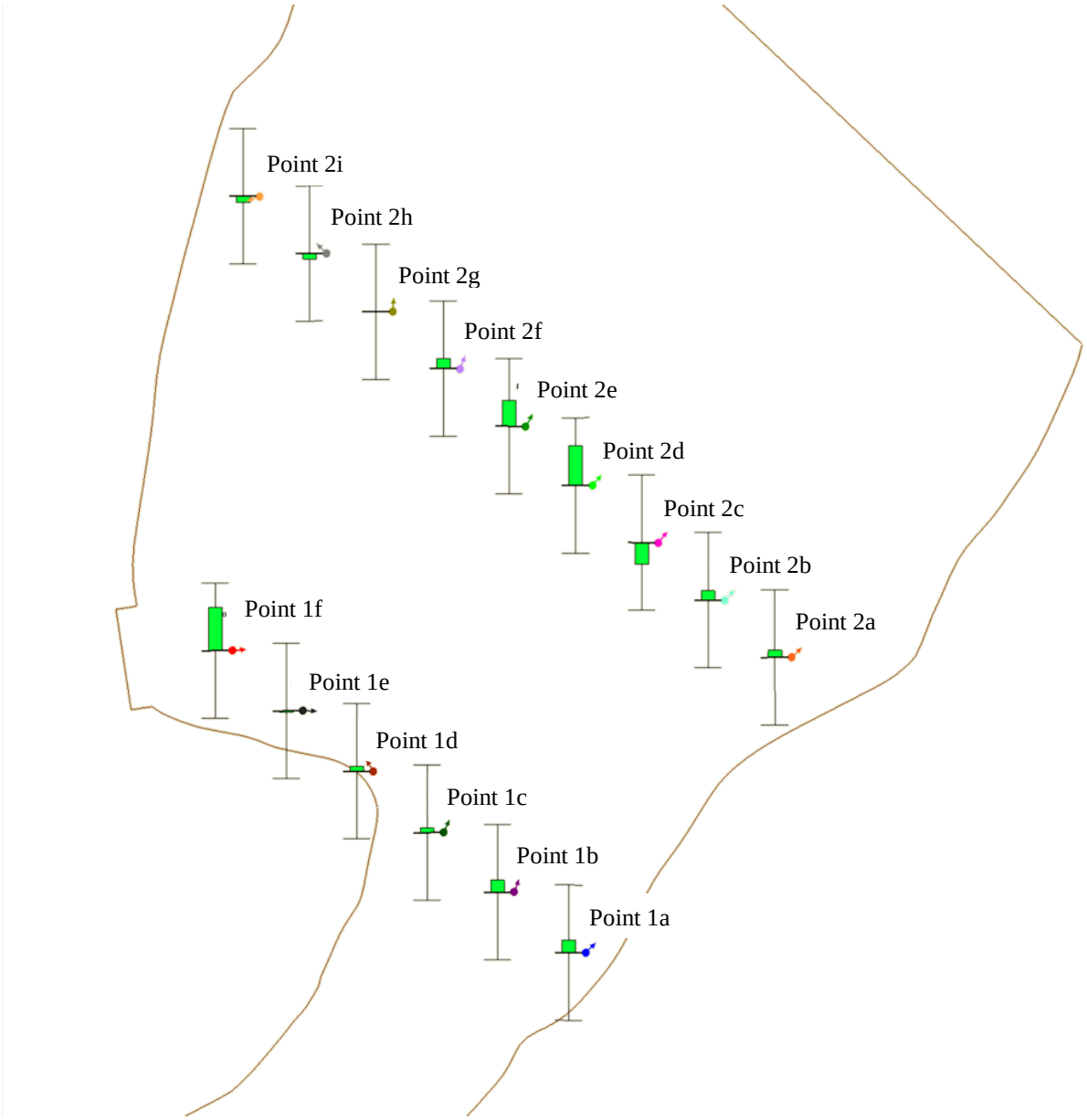

Figure 53. Calibration bars in the post-construction model.

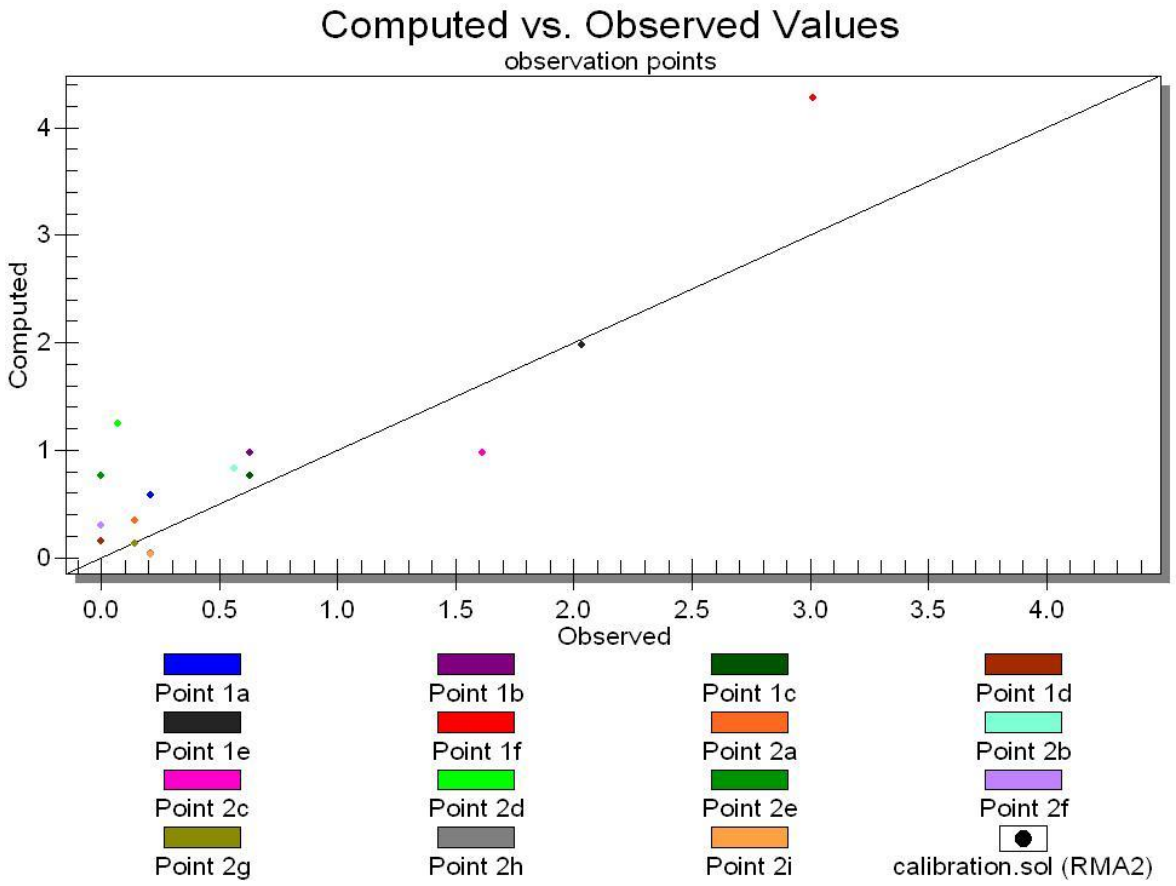

Figure 54. Computed vs. observed values in the post-construction model.

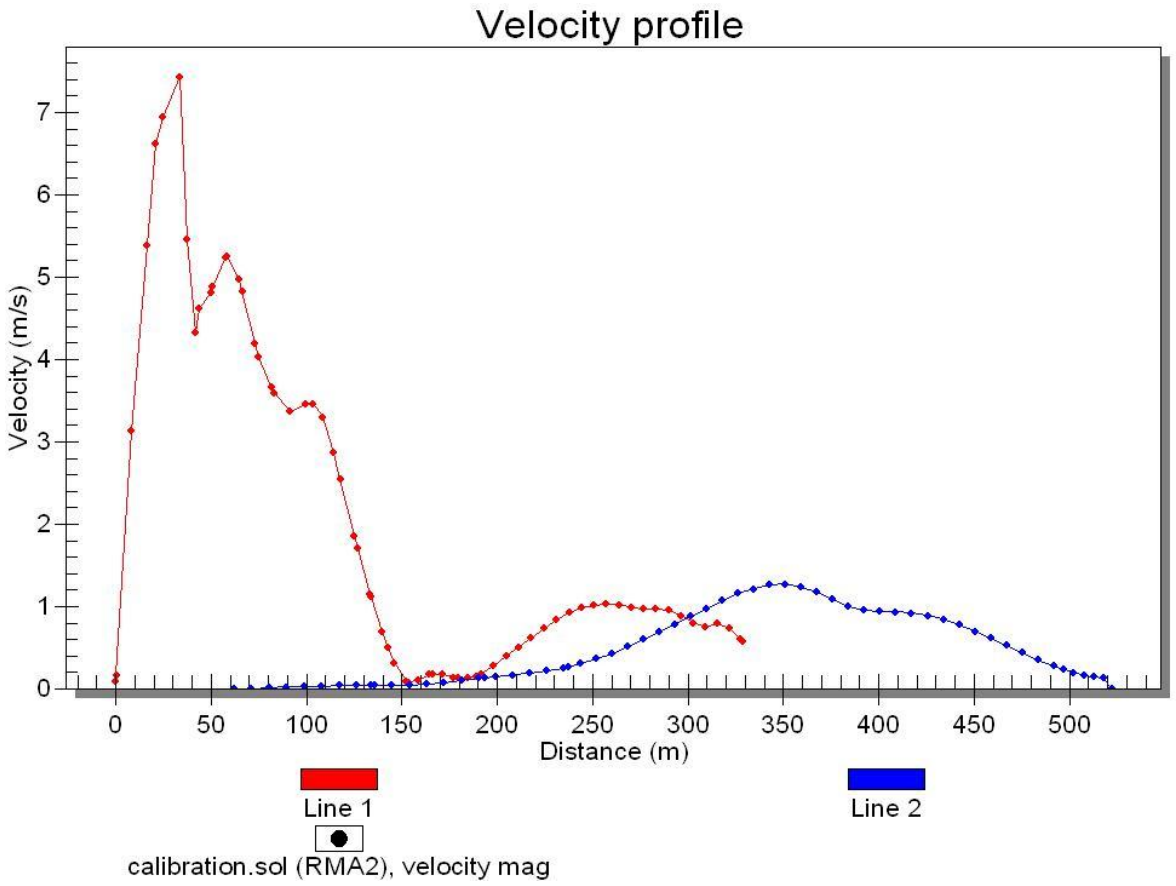

Figure 55. Velocity profile plot in the post-construction model. The profile goes from left to right in the general flow direction, same as in figure 41 and 42 above.

7.6.2.2 Validation

The post-construction model is validated against a flow of 1500 m^3/s from the new spillway and 1800 m^3/s from the existing spillway. The verification bars, a plot of the computed vs. the observed values as well as a plot of the velocity profiles received from the simulations can be seen in figure 56 to 58 below.

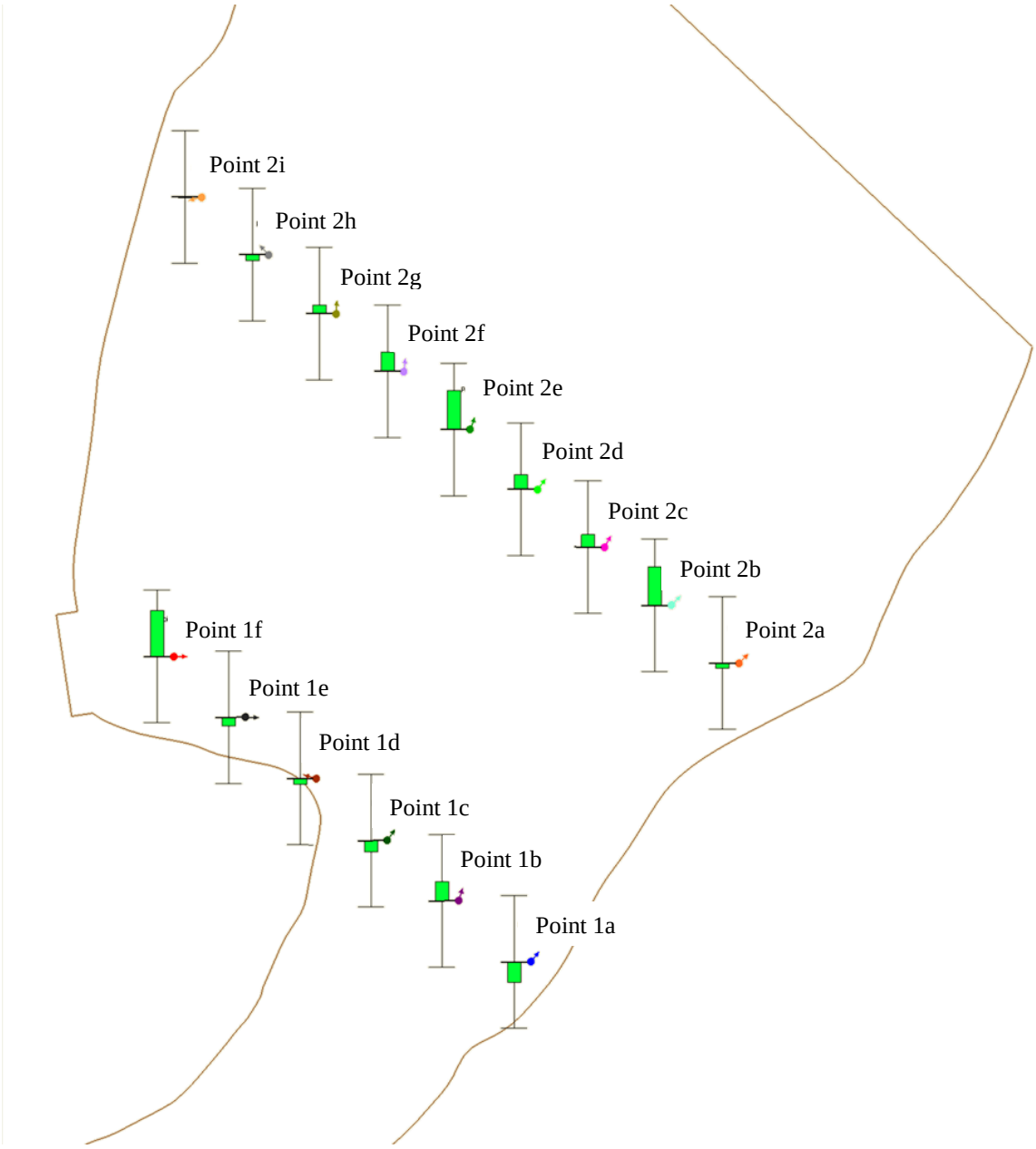

Figure 56. Validation bars in the post-construction model.

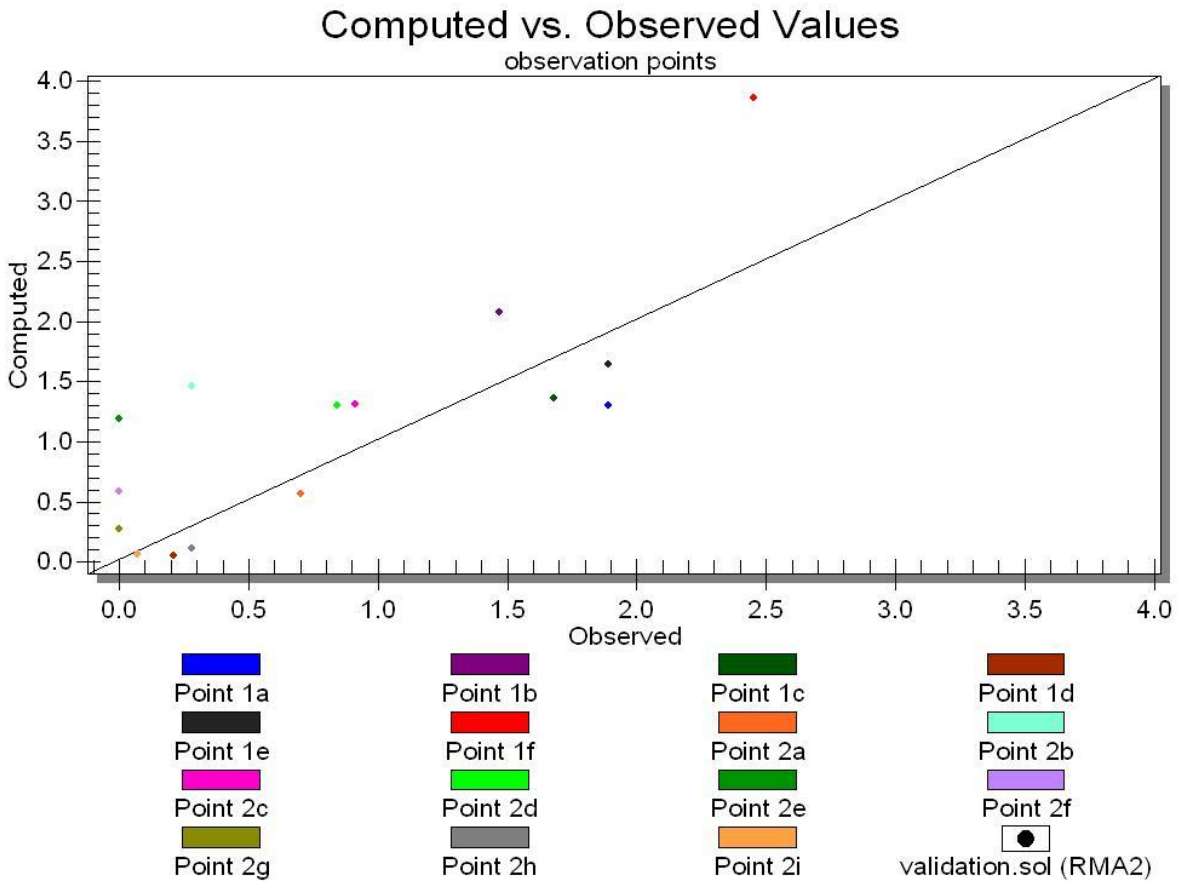

Figure 57. Computed vs. observed values in the post-construction model.

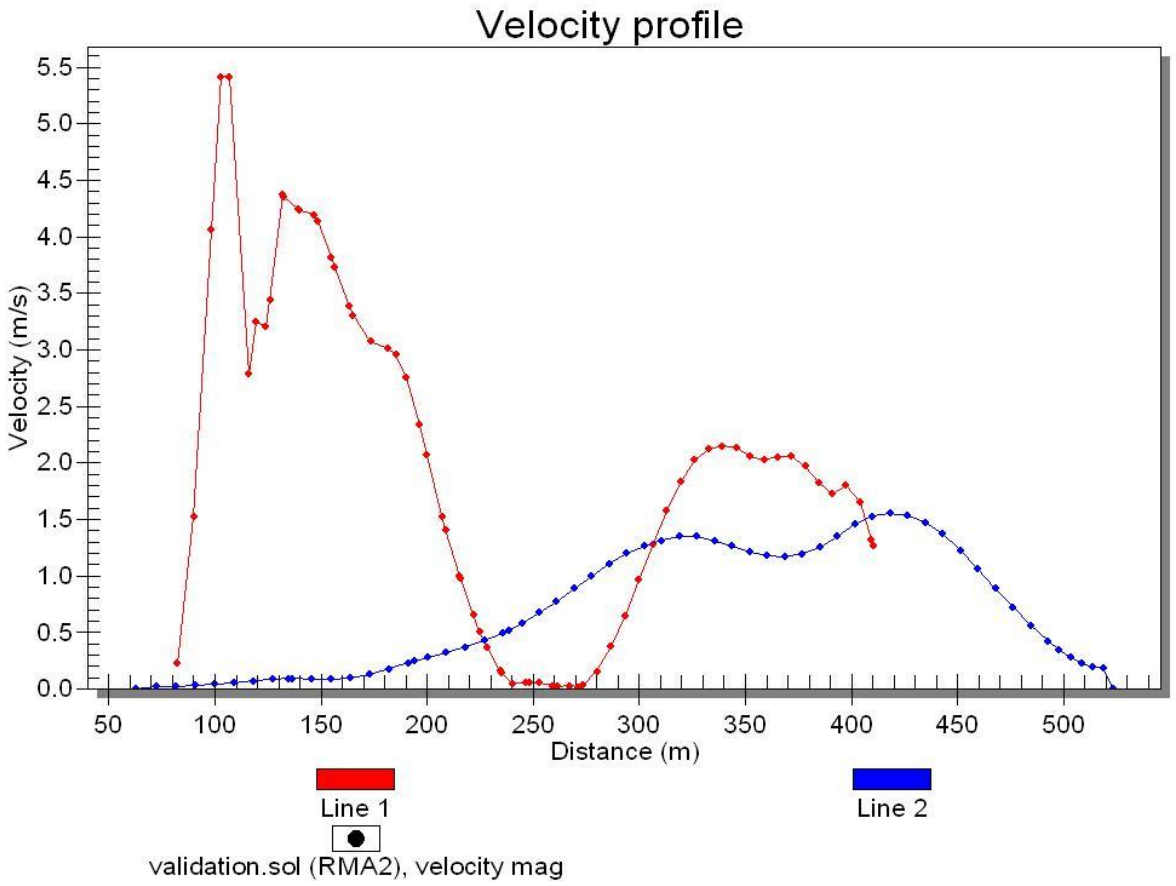

Figure 58. Velocity profile plot in the post-construction model. The profile goes from left to right in the general flow direction, same as in figure 41 and 42 above.

7.6.3 Final tuning parameters

After the verification process, the Manning's roughness coefficient and the eddy viscosity in the different material zones is determined for the two models. The final values are shown in table 5 and 6 below.

Table 5. Final tuning parameter values in the different material zones in the pre-construction model.

	Material zones		
Parameter	Shallow zone	Deep zone	Concrete zone
Manning's roughness coefficient	0,06	0,05	0,01
Eddy viscosity (Pa*s)	2000	2000	2000

Table 6. Final tuning parameter values in the different material zones in the post-construction model.

	Material zones		
Parameter	Shallow zone	Deep zone	Concrete zone
Manning's roughness coefficient	0,07	0,06	0,01
Eddy viscosity (Pa*s)	3000	3000	3000

The values presented in the two tables above are similar to the roughness coefficients for river bed materials downstream of hydropower dams estimated by Chow (1959) and Hamill (2001) and to the eddy viscosities found in the User's Manual to Surfacewater modeling systems v.6 (1999) for homogenous horizontal flow in a river with small islands. It should be noted that the eddy viscosity is assumed to be isotropic i.e. have the same value in all four directions (E_{xx}, E_{xy}, E_{yx} and E_{yy}).

The higher Manning's roughness coefficient in the shallower parts is motivated by that the water depth is lower in those areas and the flow is therefore more affected by the bed roughness than the deeper parts.

7.7 Sensitivity analysis

In addition to the verification process, a sensitivity analysis is performed in order to evaluate the effects of changes in the Manning's roughness coefficients, eddy viscosities and mesh resolution.

7.7.1 Tuning parameters

Generally, if the changes in water depths and the velocities are small while changing the tuning parameters, the model is considered stable and reliable. The analysis is performed by using the water depth profile plot for different simulation runs using the same flow. In table 7 below, an explanation of the simulations is made:

Table 7. Simulation number and the change in tuning parameters relative to the verified values for the pre- and post-construction models.

	Concrete zone		*Shallow zone*		*Deep zone*	
Simulation number	*Manning's roughness coefficient*	*Eddy viscosity*	*Manning's roughness coefficient*	*Eddy viscosity*	*Manning's roughness coefficient*	*Eddy viscosity*
1	100%	100%	100%	100%	100%	100%
2	200%	100%	200%	100%	200%	100%
3	100%	200%	100%	200%	100%	200%
4	100%	400%	100%	400%	100%	400%
5	400%	100%	400%	100%	400%	100%

Unfortunately, a decrease of the tuning parameters is not possible as this would create supercritical flow in several sections. A decrease is however believed to follow the same pattern as an increase. The flow used in the pre-construction model is 2300 m^3/s from the existing spillway and in the post-construction model 1500 m^3/s from the new spillway.

The water depth profile for the five simulation runs in the pre- and post -construction models can be seen in figure 59 and 60 below.

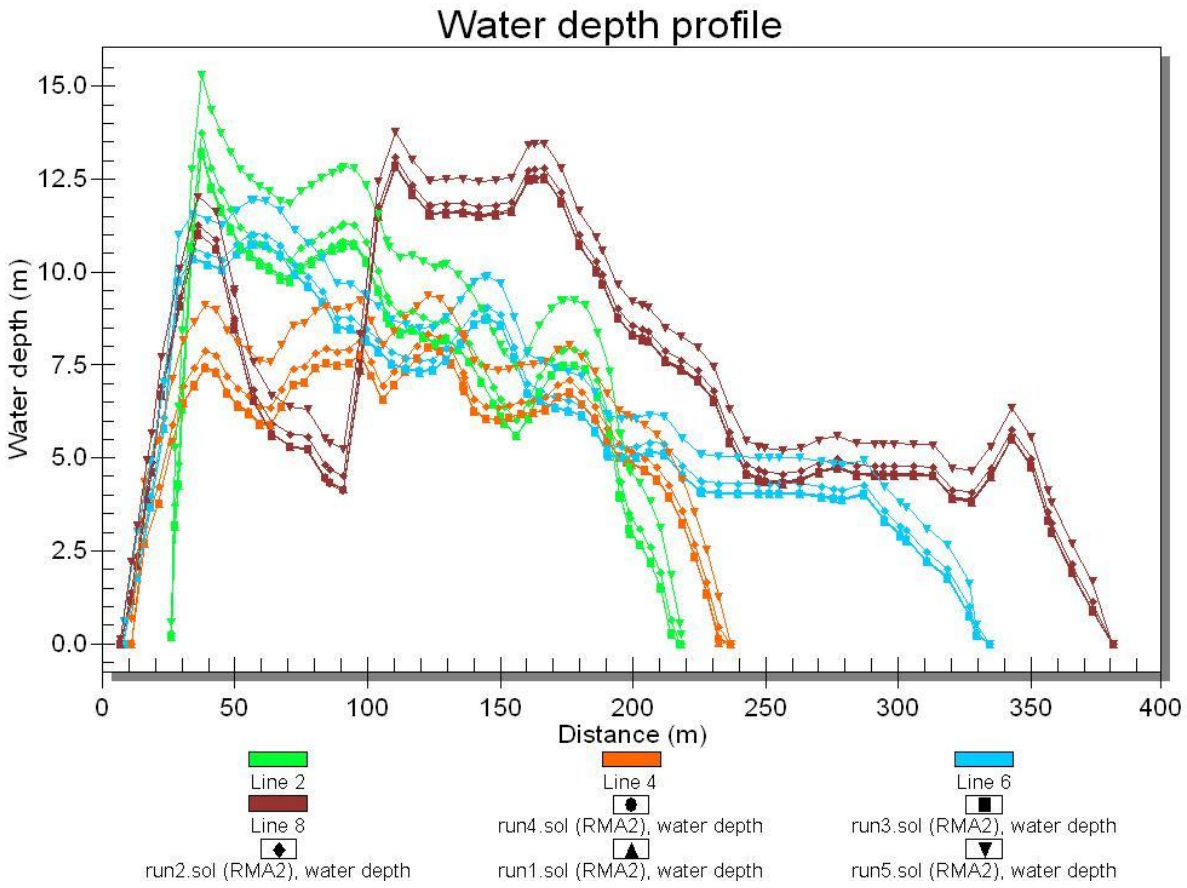

Figure 59. Water depth profile for the pre-construction model. The profile goes from right to left in the general flow direction, same as in figure 38 above.

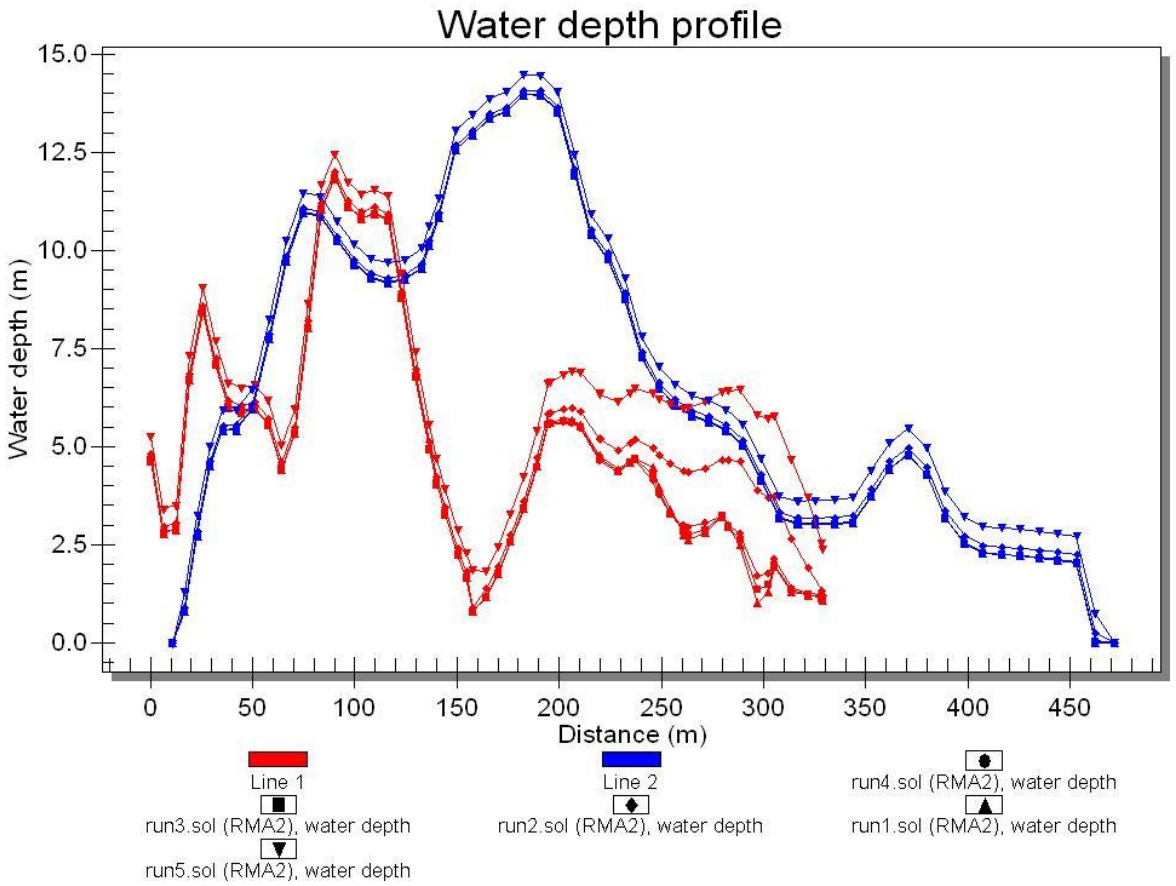

Figure 60. Water depth profile for the post-construction model. The profile goes from left to right in the general flow direction, same as in figure 41 and 42 above.

From figure 59 and 60 above, it can be seen that the water depth hardly changes at all, even when increasing the roughness coefficient or the eddy viscosity with as much as 400%. As mentioned above, this is an indication of a consistent and stable model.

7.7.2 Mesh resolution

Numerical modeling is a compromise of accuracy vs. time where an increase in the number of elements will lead to an increase in simulation time but also an increase in accuracy. In order to investigate at what resolution this increase in accuracy levels off, the number of elements in the pre-construction model is varied for the same flow. The water depth is then investigated in the same points as in the verification process. As mentioned in section 4.3.4.1, the current version of RMA2 is limited to 10 000 elements and the resolution is therefore varied from 500 to 8000 elements. The water depth in the observation points at different resolutions for the flow 2300 m^3/s from the existing spillway can be seen in figure 61 below.

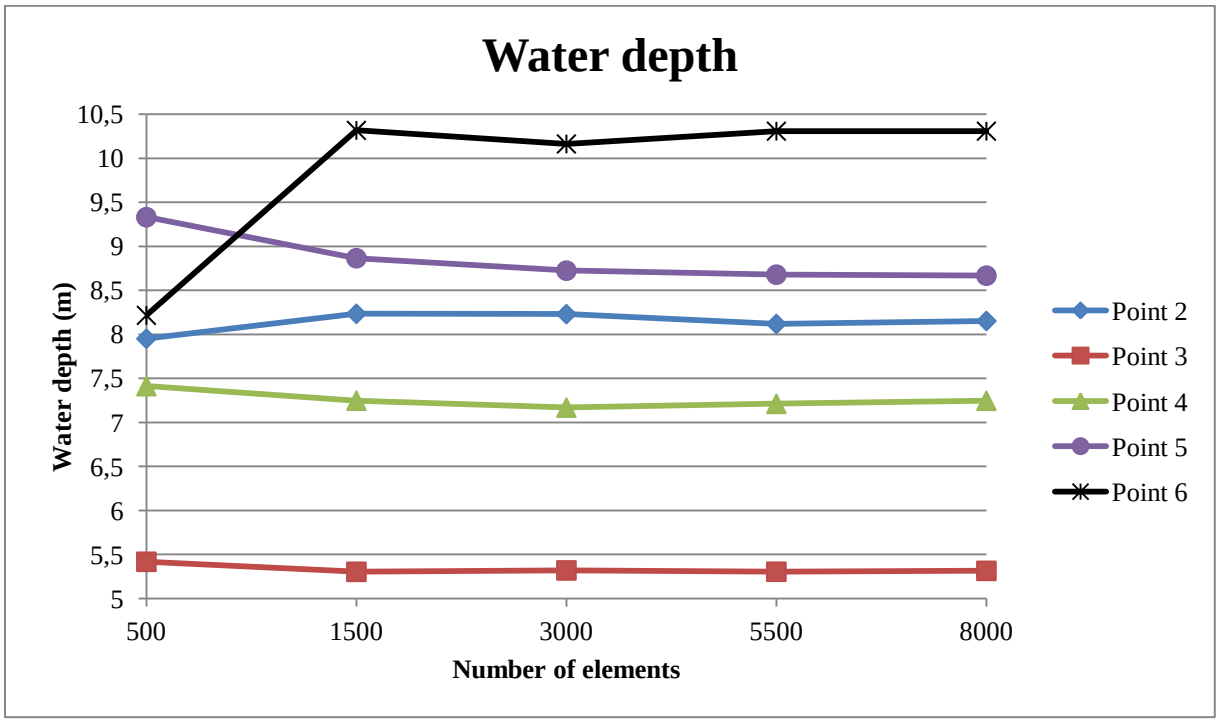

Figure 61. Change in water depth for different number of elements in the pre-construction model.

As can be seen in the figure above, the number of elements has a moderate impact on the results received from the simulations. The changes begin to level off at around 3000-4000 elements. A general observation is that the number of elements in the two models, 5683 and 5122, seems to be sufficient to simulate the flow conditions with a sufficiently high accuracy.

7.8 Erosion calculations

As mentioned in section 6.1, the exact particle size distribution of the river bed material downstream of Bergeforsen dam is unknown. It can be assumed to include a deeper mid section with fractured bedrock, boulders and stones with finer sediment in between the coarser material and shallow side sections with erosion protection material or shorelines with somewhat finer material. Erosion of fractured bedrock is too complex to investigate by only using two-dimensional data about velocities and water depths. However, the erosion potential of the loose material such as stones, cobbles and sand is more easily described and is best estimated using the existing particle size distribution in the area and then related to the results received from the simulations.

However, as no such data is available the only parameters that can be determined correctly are the bed shear stress and the critical particle diameter. These parameters will then be used to estimate the *relative* erosion potential in the different areas. The parameters can be calculated by using the relationships and equations described in section 6.2 above and mapped in SMS by utilizing the depth-averaged velocity $\bar{U}$ and water depth h received from the flow simulations. The bed shear stress is computed from equation 19 and the critical particle diameter from equation 23 in section 6.2.

Since SMS cannot compute with different Manning's roughness coefficients for different material zones when mapping the bed shear stress, an average weighted *n* by the size the material zone represents in the model is calculated (concrete is neglected):

$$n_{pre} = 60\% * 0{,}05 + 40\% * 0{,}06 = 0{,}054$$

$$n_{post} = 50\% * 0{,}06 + 50\% * 0{,}07 = 0{,}065$$

where

n_{pre} = weighted average Manning's roughness coefficient in the pre-construction model
n_{post} = weighted average Manning's roughness coefficient in the post-construction model

The density of the solid particle ρ_s is estimated to 2650 kg/m^3 and the density of the water ρ_w to 999,1 kg/m^3 (water temperature = 15 °C) (Soulsby, 1997).

7.9 Change in water depth downstream

The alterations of the channel due to the construction of the new spillway and the erosion protection bank will lead to an overall change in the wetted area, roughness and slope of the channel. This might in turn lead to a change in water depths downstream which can affect the effectiveness of the power plant as the operational water head is changed. If the water depth decreases i.e. the water head increases, this could lead to a better output from the power plant. On the other hand, if the water depth increases this could lead to a worse output. The power output is calculated from equation 27 below as described by Hamill (2001).

Power output (W)

$$P = \frac{\rho g Q H}{\varepsilon} \qquad \text{(eq. 27)}$$

where

ρ = density of water (kg/m^3)
g = gravitational forces (m/s^2)
Q = flow through turbines (m^3/s)
H = water head (m)
ε = efficiency (%)

In order to investigate this, the change in water depth at the downstream end will be derived from the results of the simulations with a flow of 840 m^3/s from the power station in the pre- and post-construction models. However, since the downstream water surface elevation is a boundary condition which needs to be kept constant, it is assumed that the change in water depth at the power station outlet equals the change in the water depth at the downstream end in the simulations. This is described in figure 62 below.

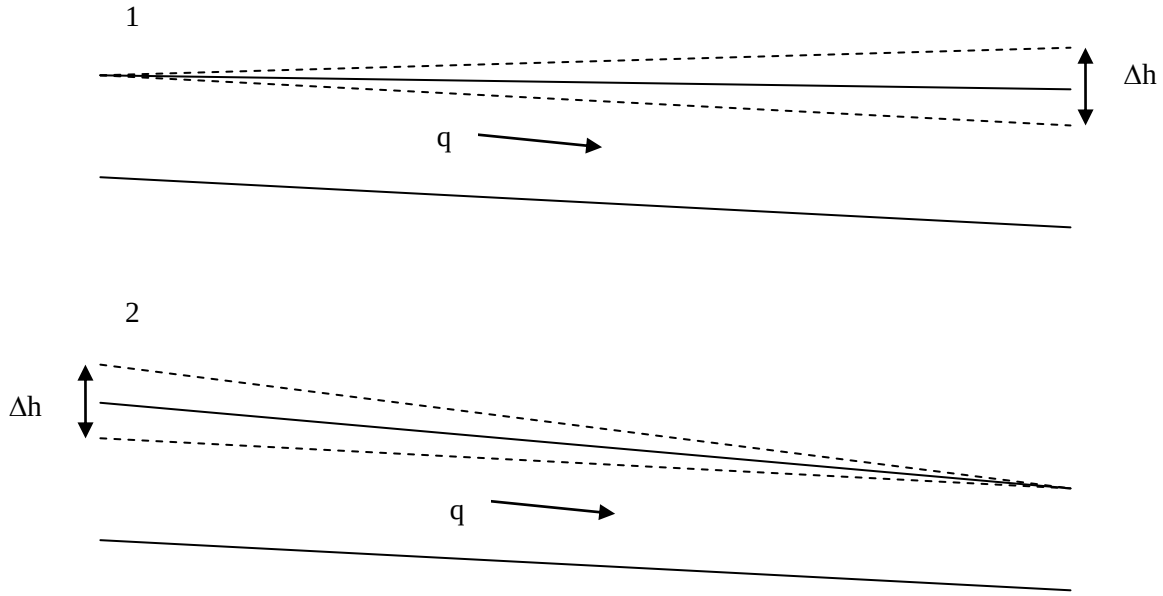

Figure 62. Change in water depth due to the construction. Image 1 describes the real situation and image 2 the model situation.

Since the channel bed roughness and the eddy viscosity directly affect the water depth, both simulations are made using the same parameter values from the post-construction model shown in table 5 above.

8 Results

In the results, the velocities, water depths, shear stresses and critical particle diameters are presented by color contours as well as with arrows which shows the parameter magnitude and the general direction of the flow. For the pre-construction situation, three discharge combinations are investigated and for the post-construction situation five combinations are investigated.

8.1 Pre-construction situation

8.1.1 DC1

This DC includes a flow from power station of 840 m^3/s.

8.1.1.1 Velocity

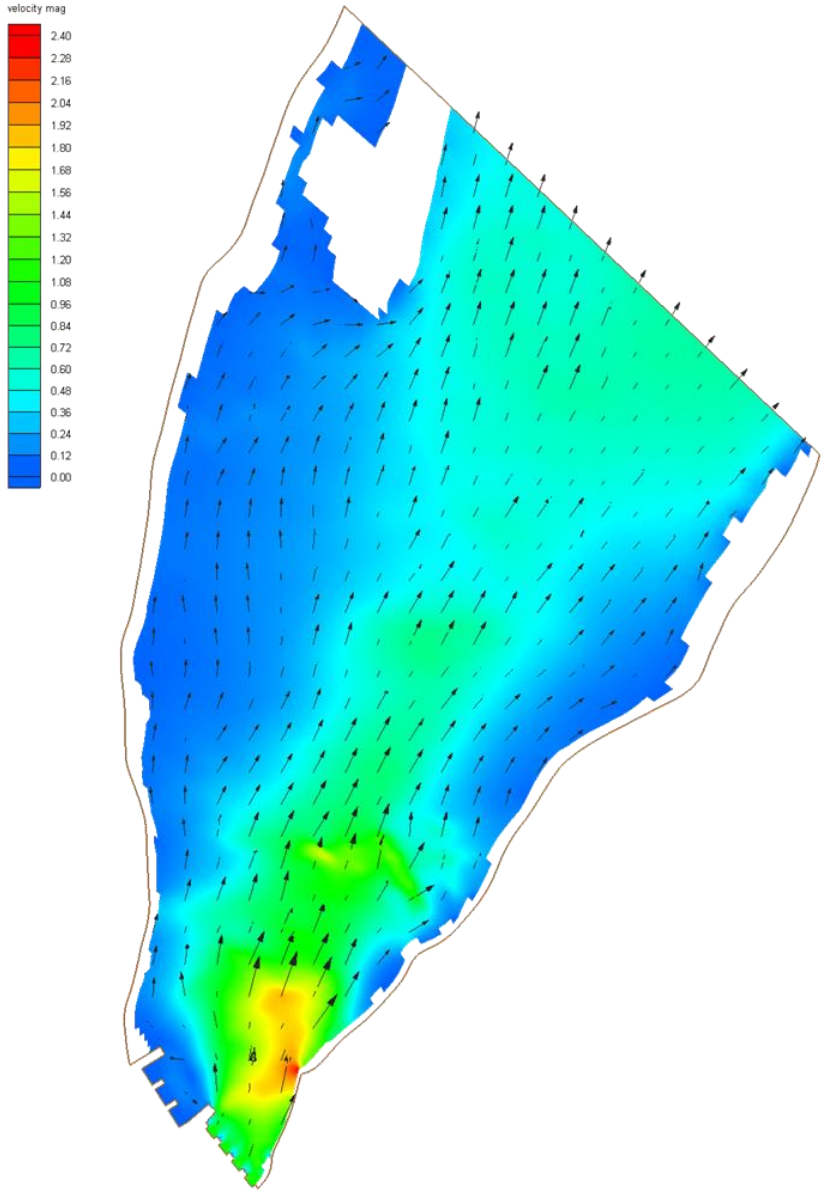

Figure 63. Velocity distribution (m/s) for DC1 in the pre-construction model.

8.1.1.2 Water depth

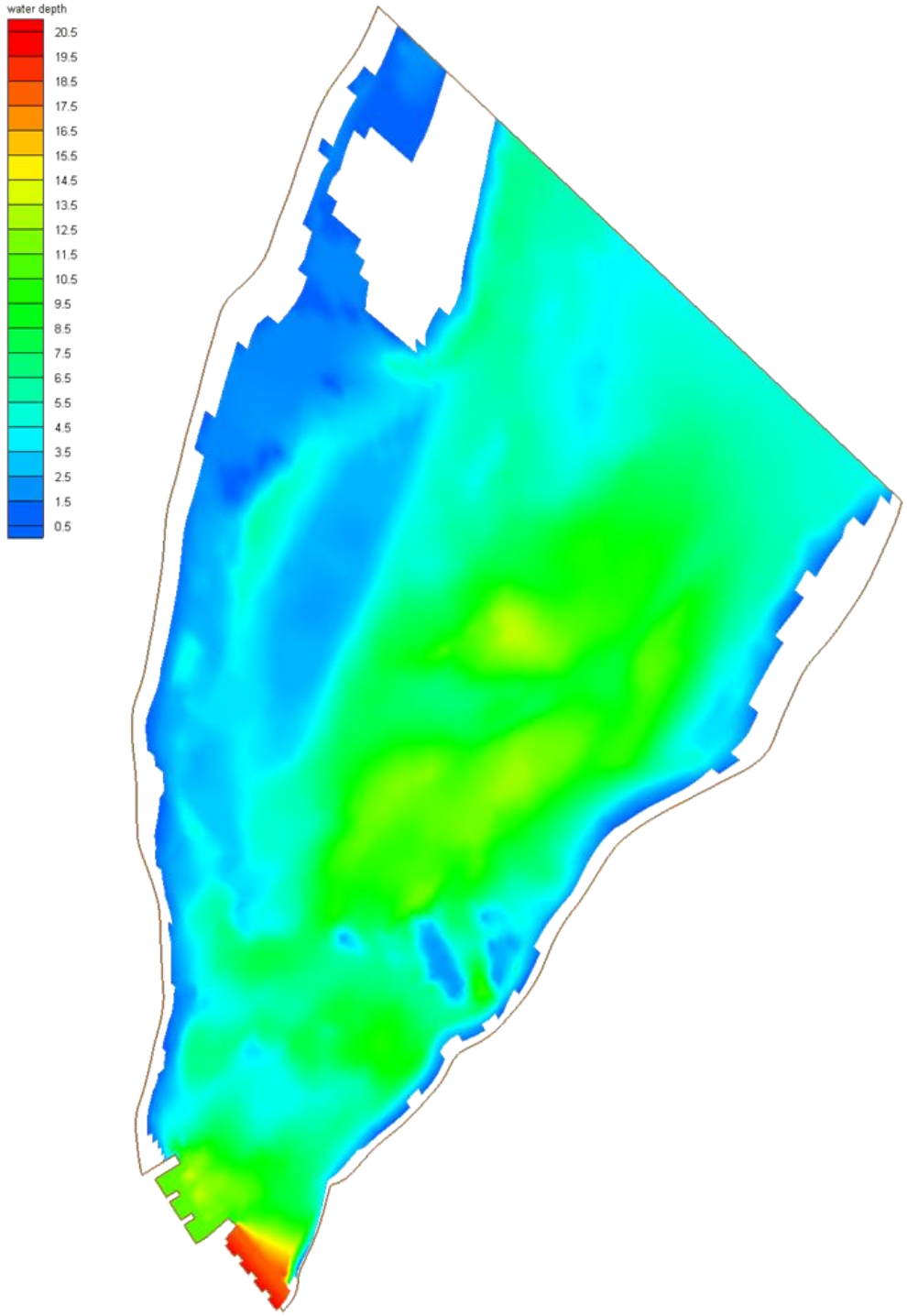

Figure 64. Water depth (m) distribution for DC1 in the pre-construction model.

8.1.1.3 Shear stress

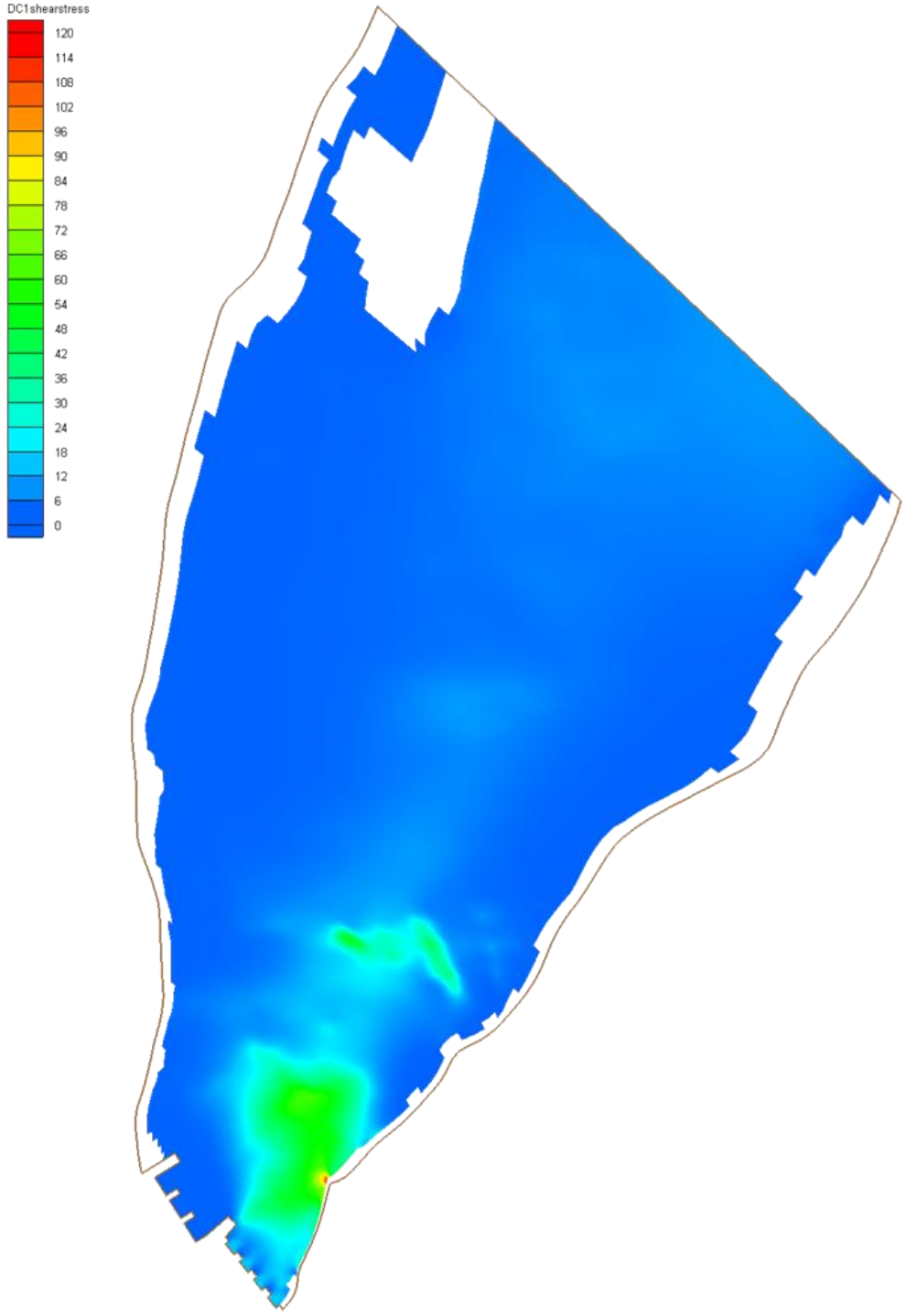

Figure 65. Shear stress (N/m^2) distribution for DC1 in the pre-construction model.

8.1.1.4 Critical particle diameter

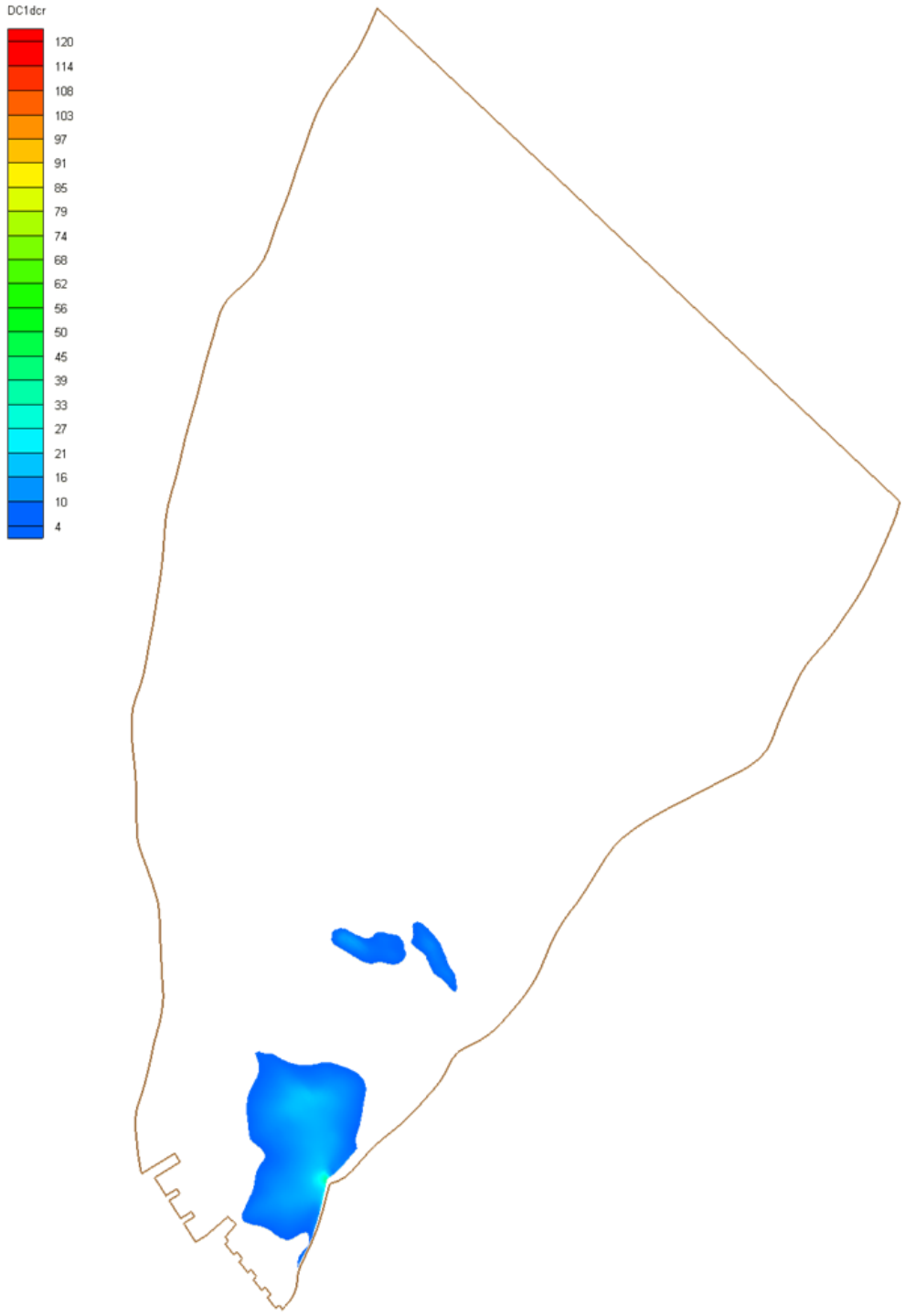

Figure 66. Critical particle diameter (mm) distribution for DC1 in the pre-construction model.

8.1.2 DC2

This DC includes a flow from existing spillway of 2300 m^3/s.

8.1.2.1 Velocity

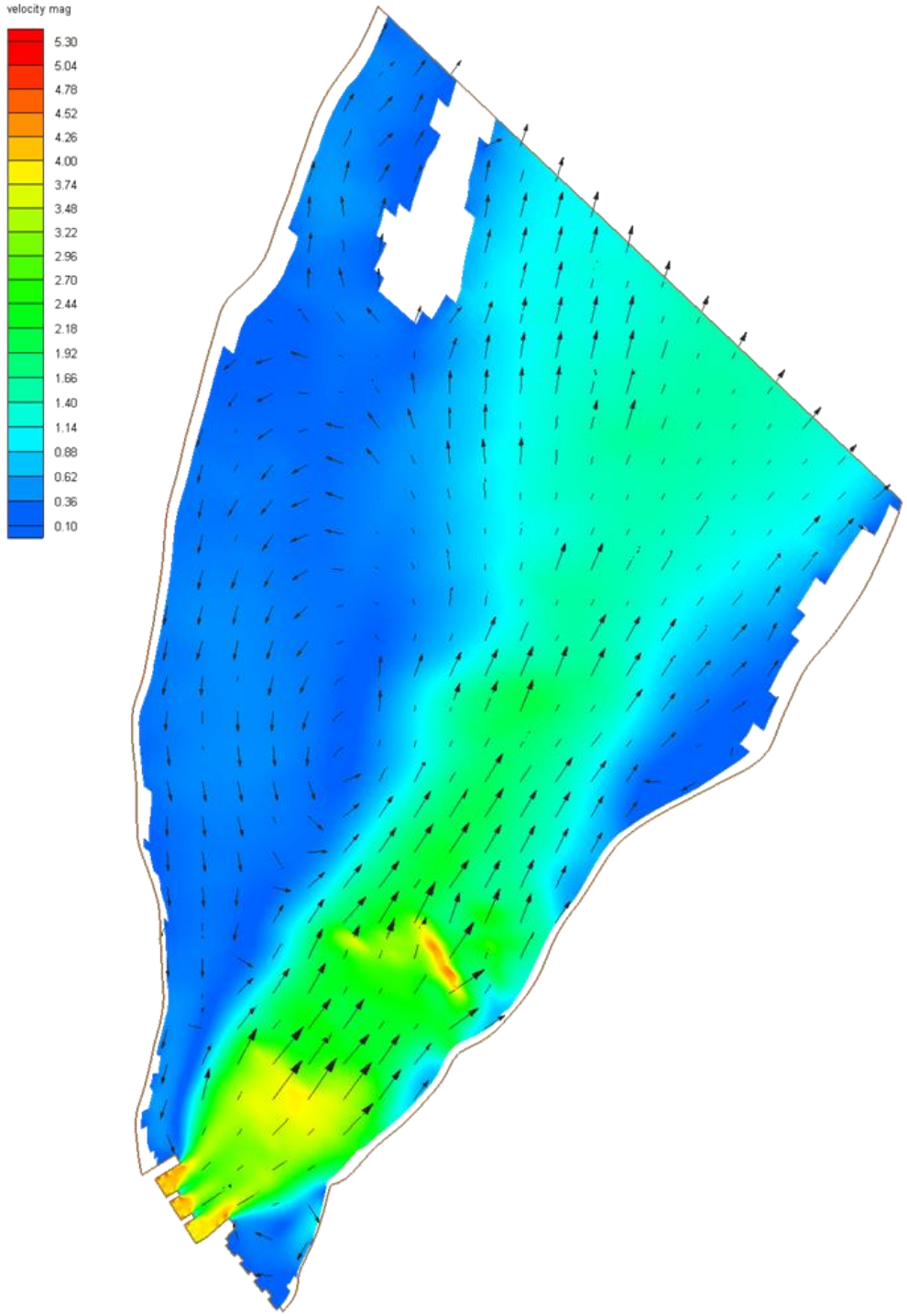

Figure 67. Velocity (m/s) distribution for DC2 in the pre-construction model.

8.1.2.2 Water depth

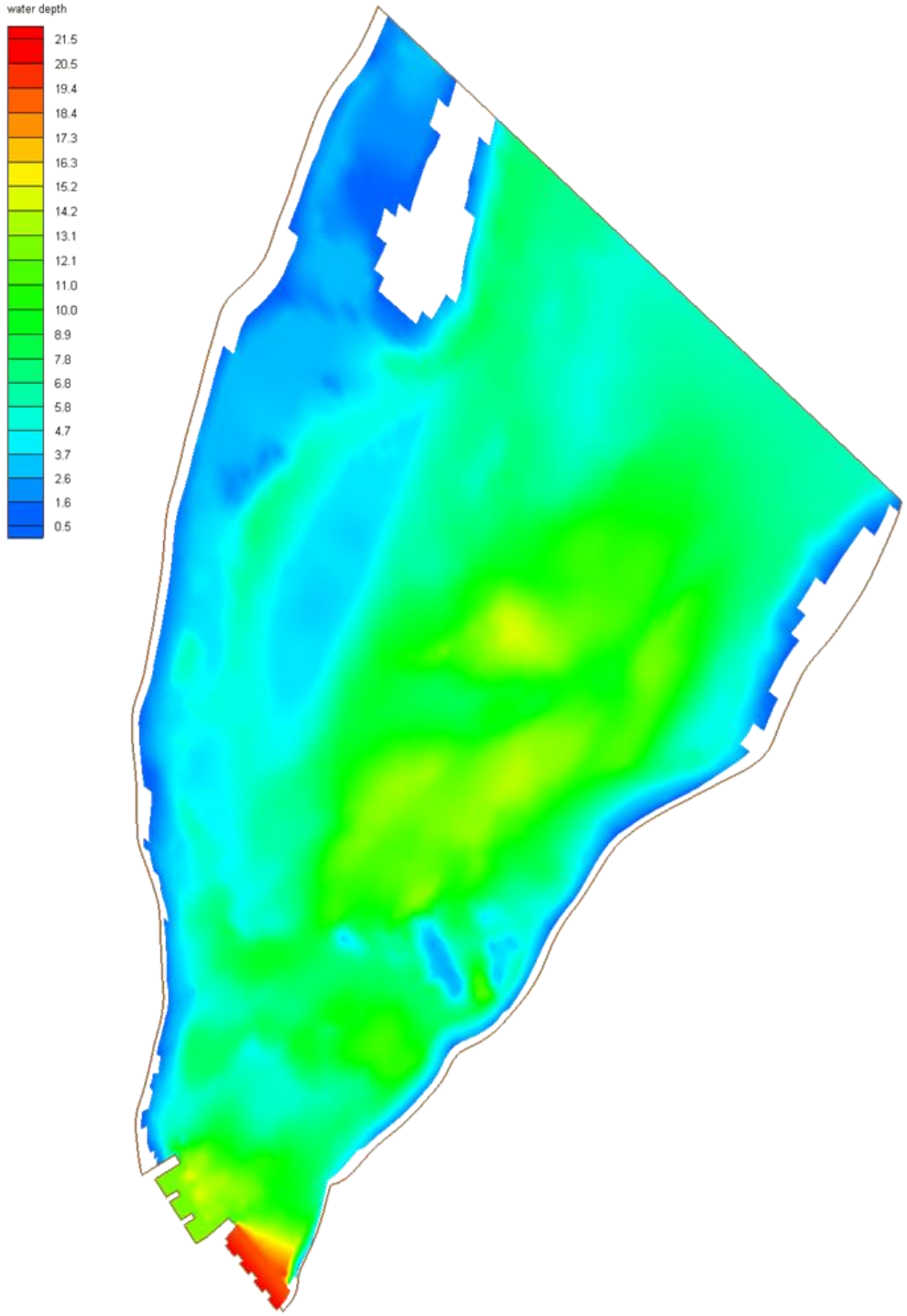

Figure 68. Water depth (m) distribution for DC2 in the pre-construction model.

8.1.2.3 Shear stress

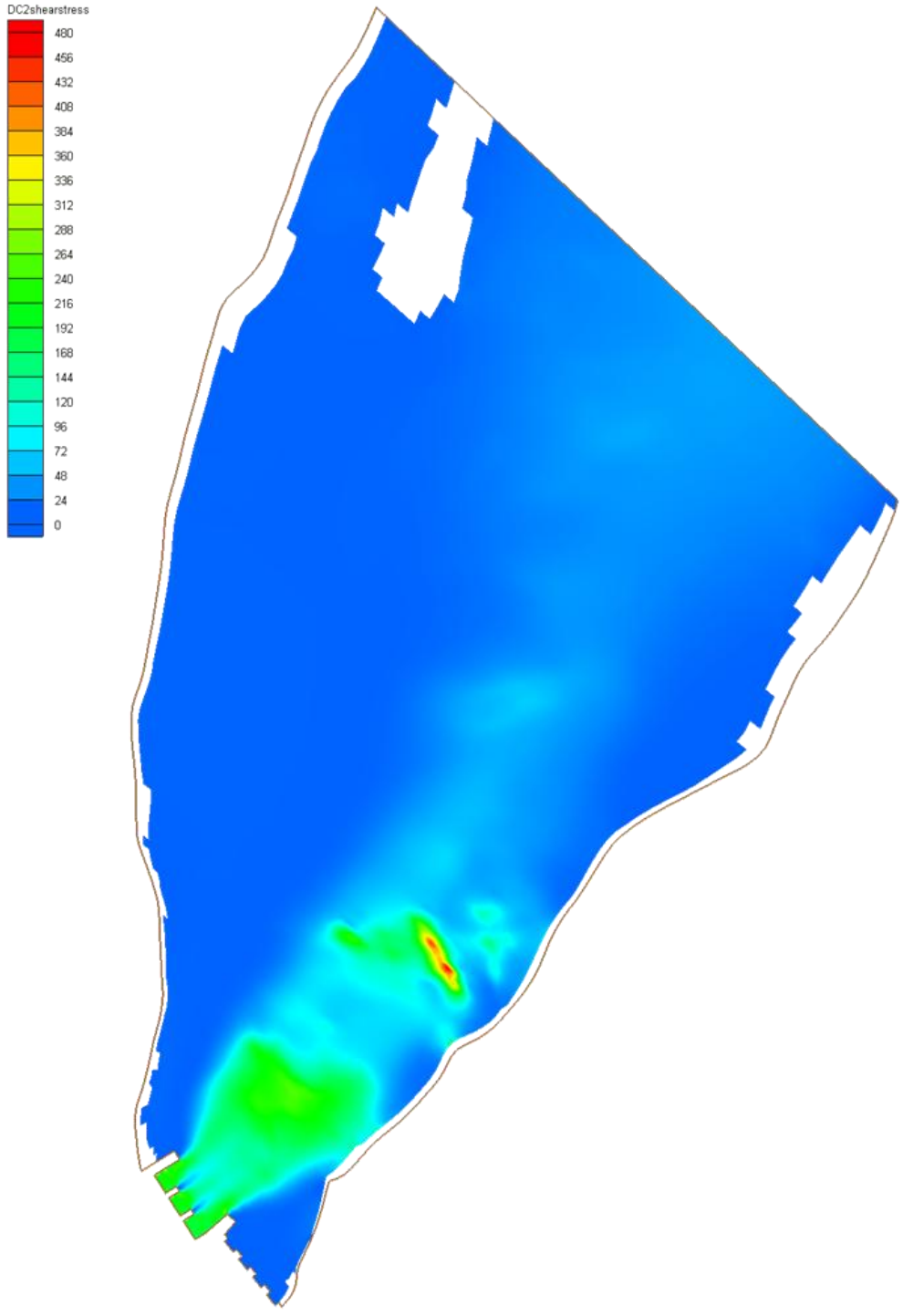

Figure 69. Shear stress (N/m^2) distribution for DC2 in the pre-construction model.

8.1.2.4 Critical particle diameter

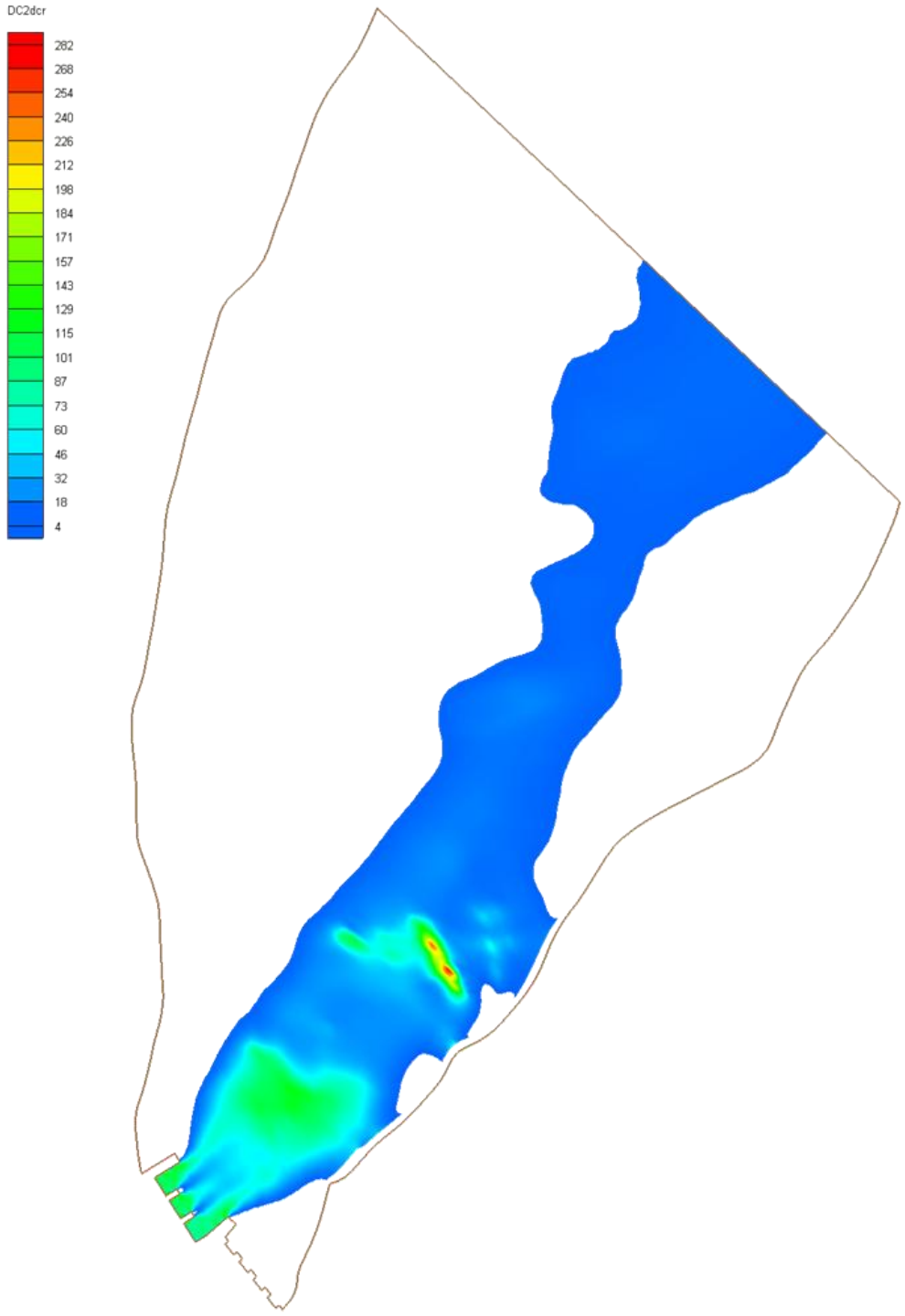

Figure 70. Critical particle diameter (mm) distribution for DC2 in the pre-construction model.

8.1.3 DC3

This DC includes a flow from existing spillway of 3000 m^3/s.

8.1.3.1 Velocity

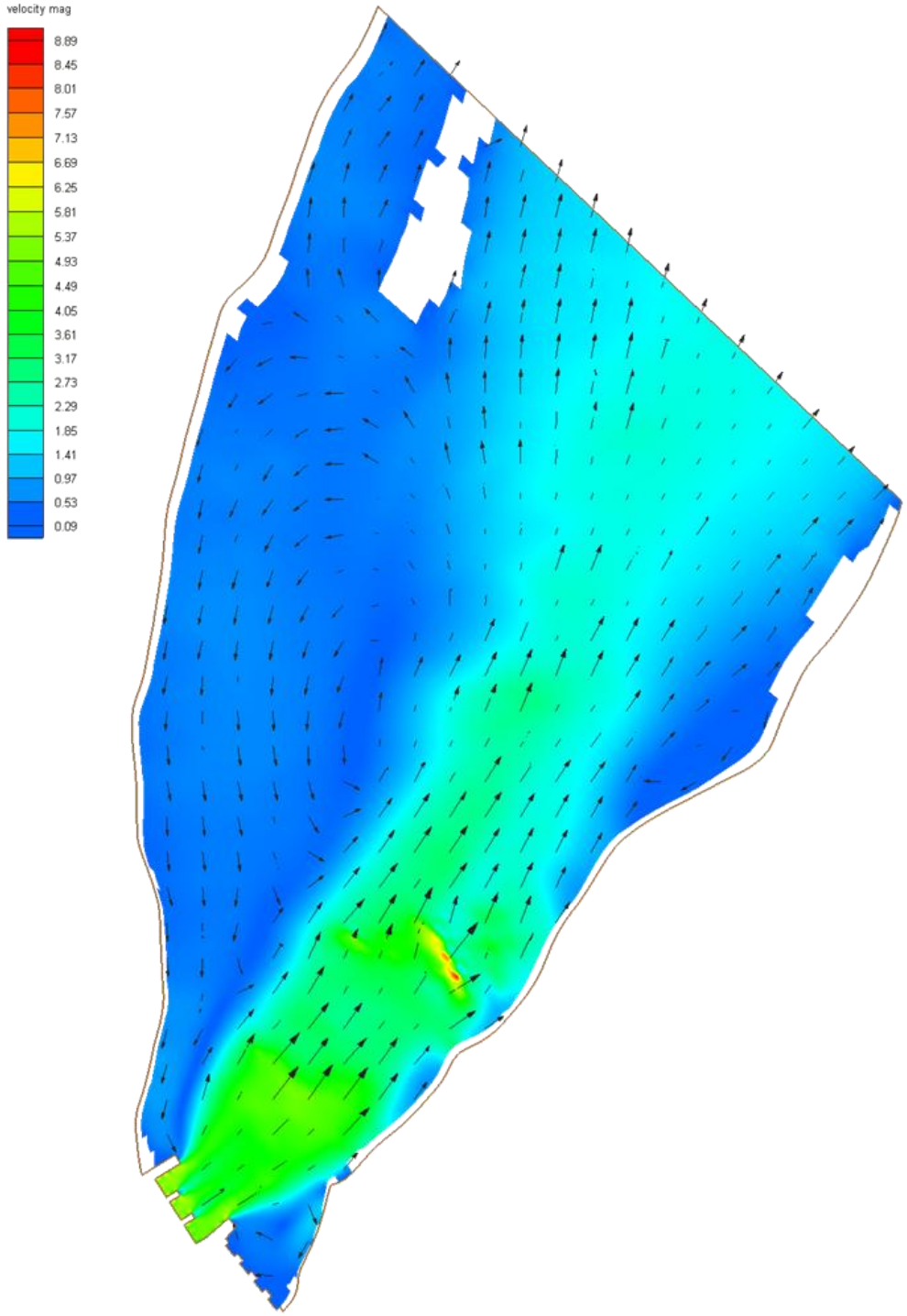

Figure 71. Velocity (m/s) distribution for DC3 in the pre-construction model.

8.1.3.2 Water depth

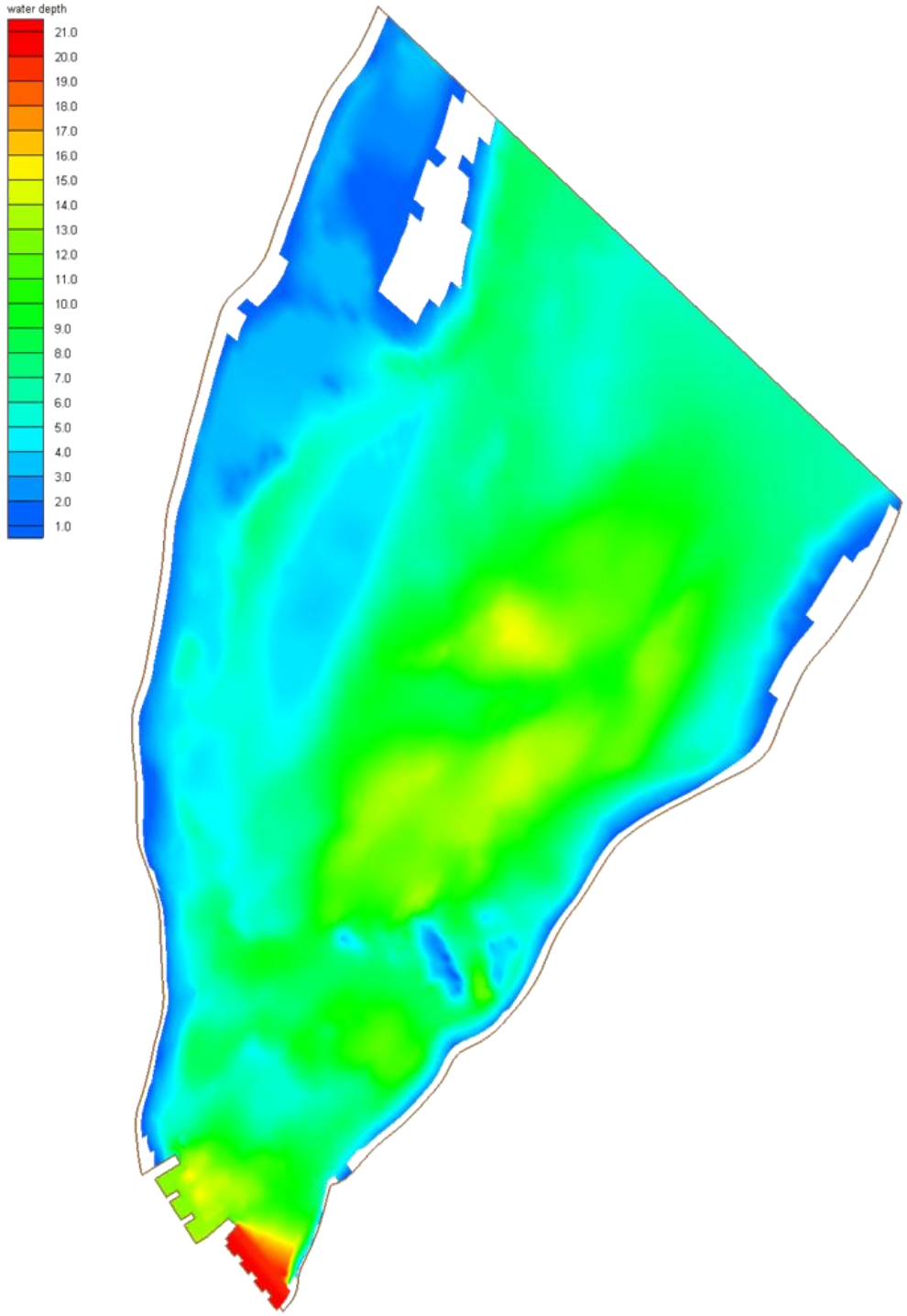

Figure 72. Water depth (m) distribution for DC3 in the pre-construction model.

8.1.3.3 Shear stress

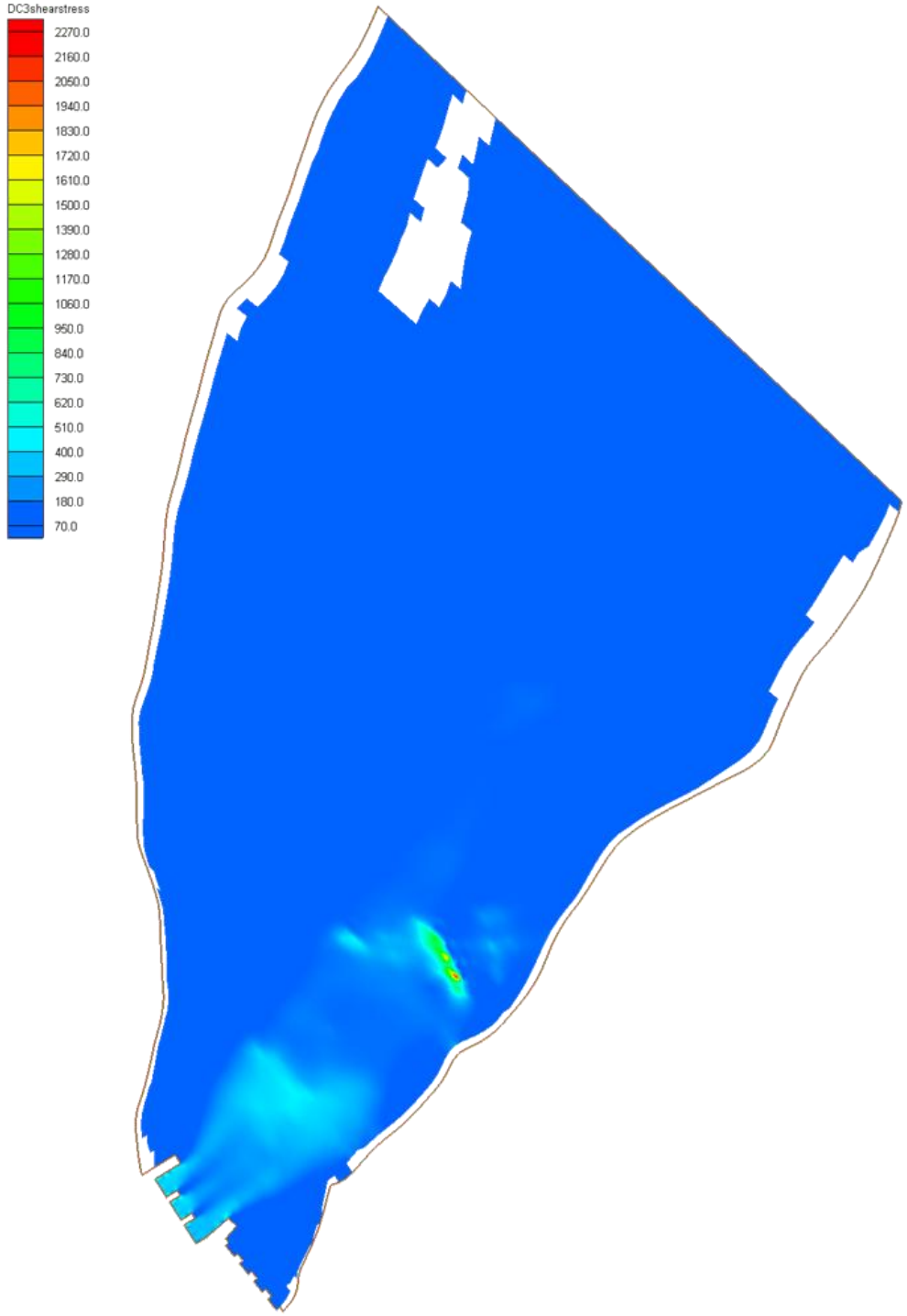

Figure 73. Shear stress (N/m^2) distribution for DC3 in the pre-construction model.

8.1.3.4 Critical particle diameter

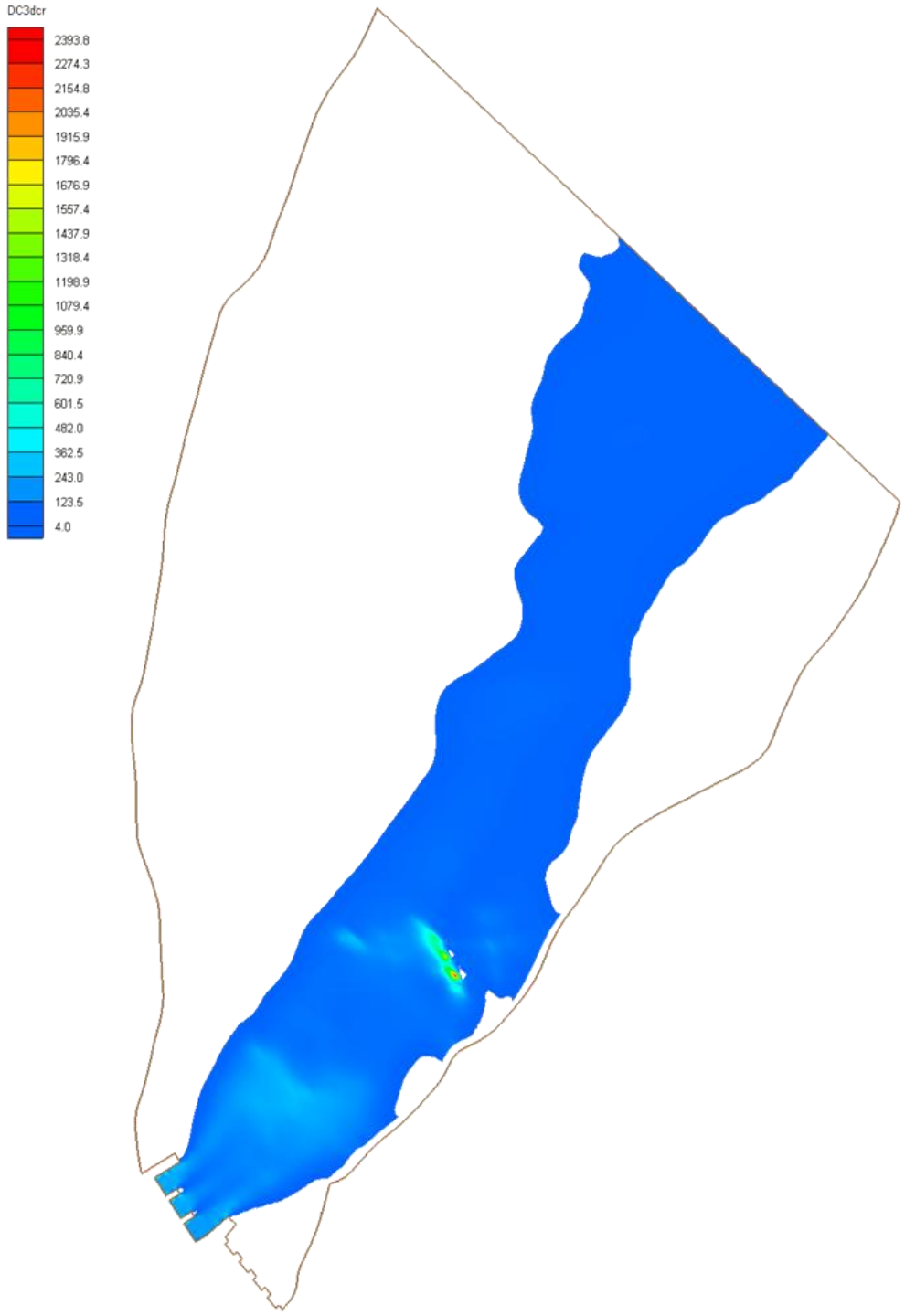

Figure 74. Critical particle diameter (mm) distribution for DC3 in the pre-construction model.

8.2 Post-construction situation

8.2.1 DC4

This DC includes a flow from power station of 840 m^3/s.

8.2.1.1 Velocity

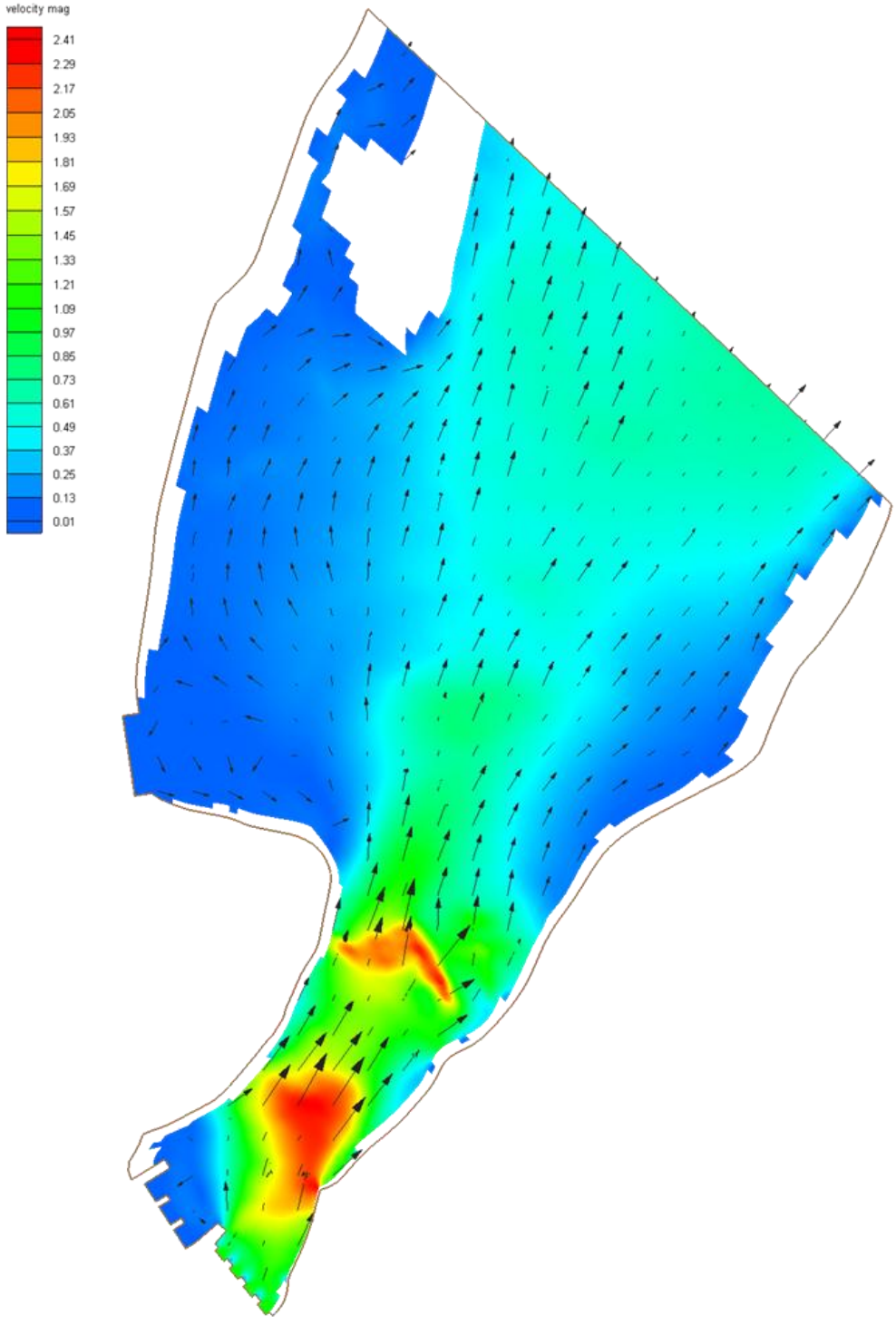

Figure 75. Velocity (m/s) distribution for DC4 in the post-construction model.

8.2.1.2 Water depth

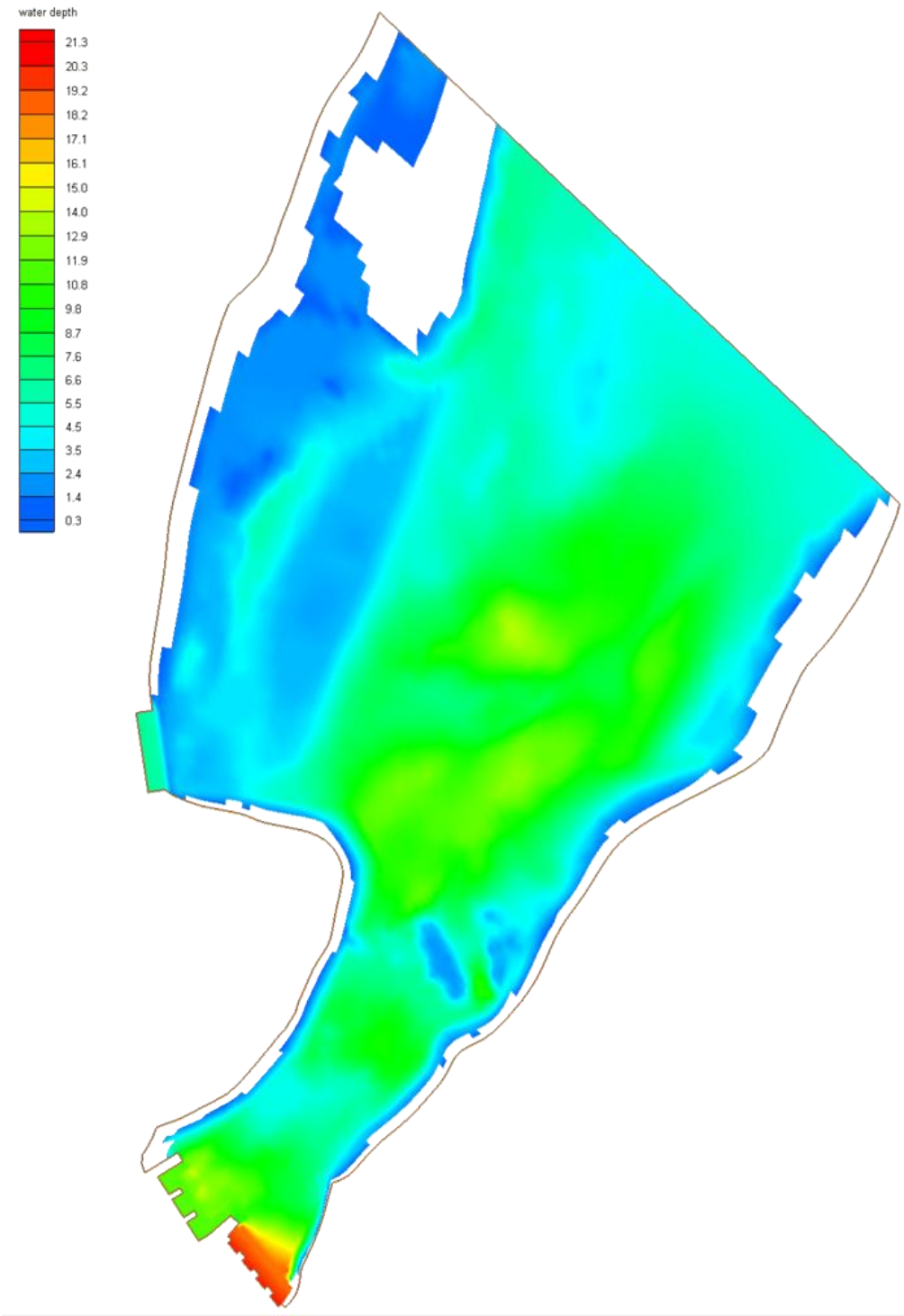

Figure 76. Water depth (m) distribution for DC4 in the post-construction model.

8.2.1.3 Shear stress

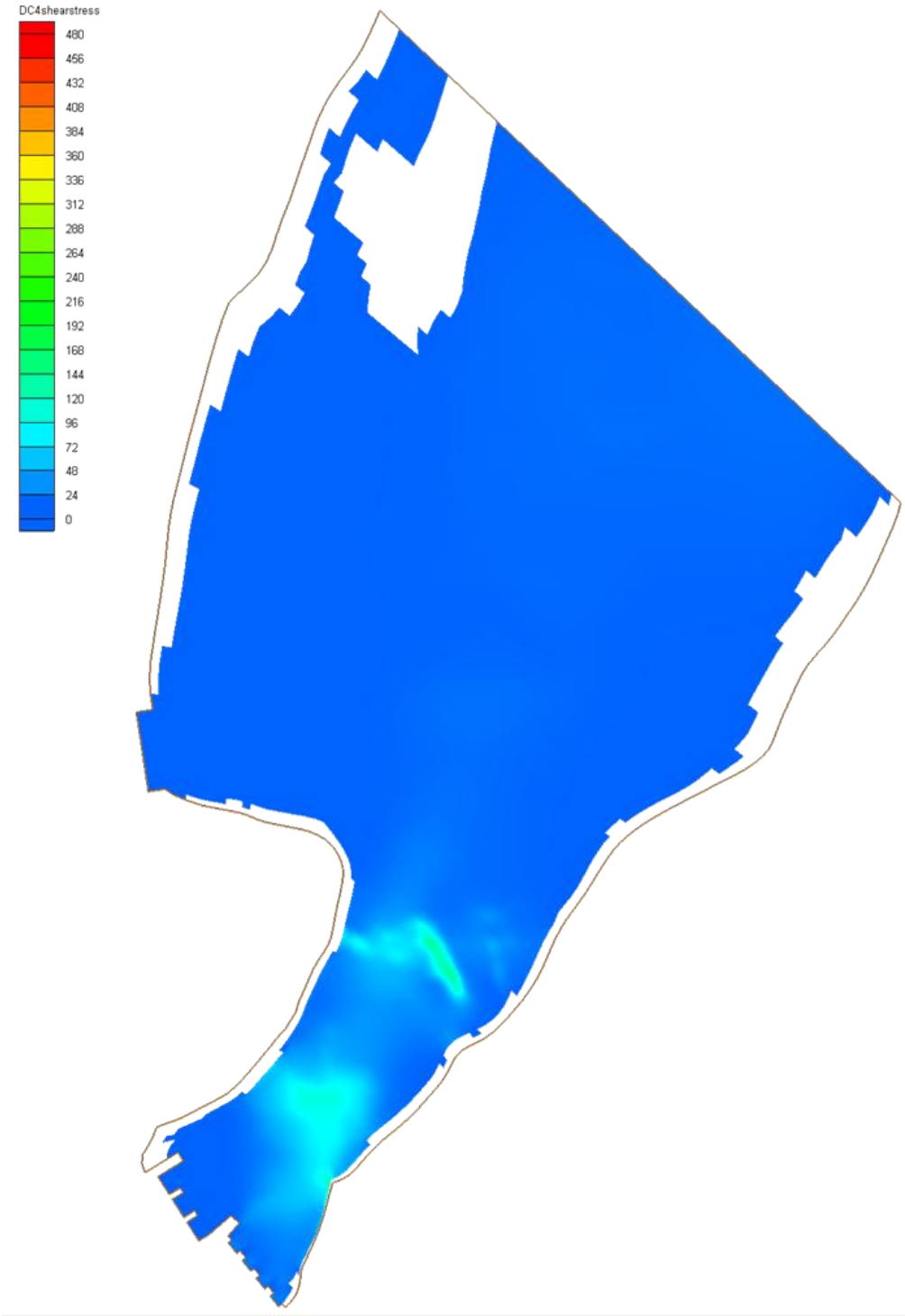

Figure 77. Shear stress (N/m^2) distribution for DC4 in the post-construction model.

8.2.1.4 Critical particle diameter

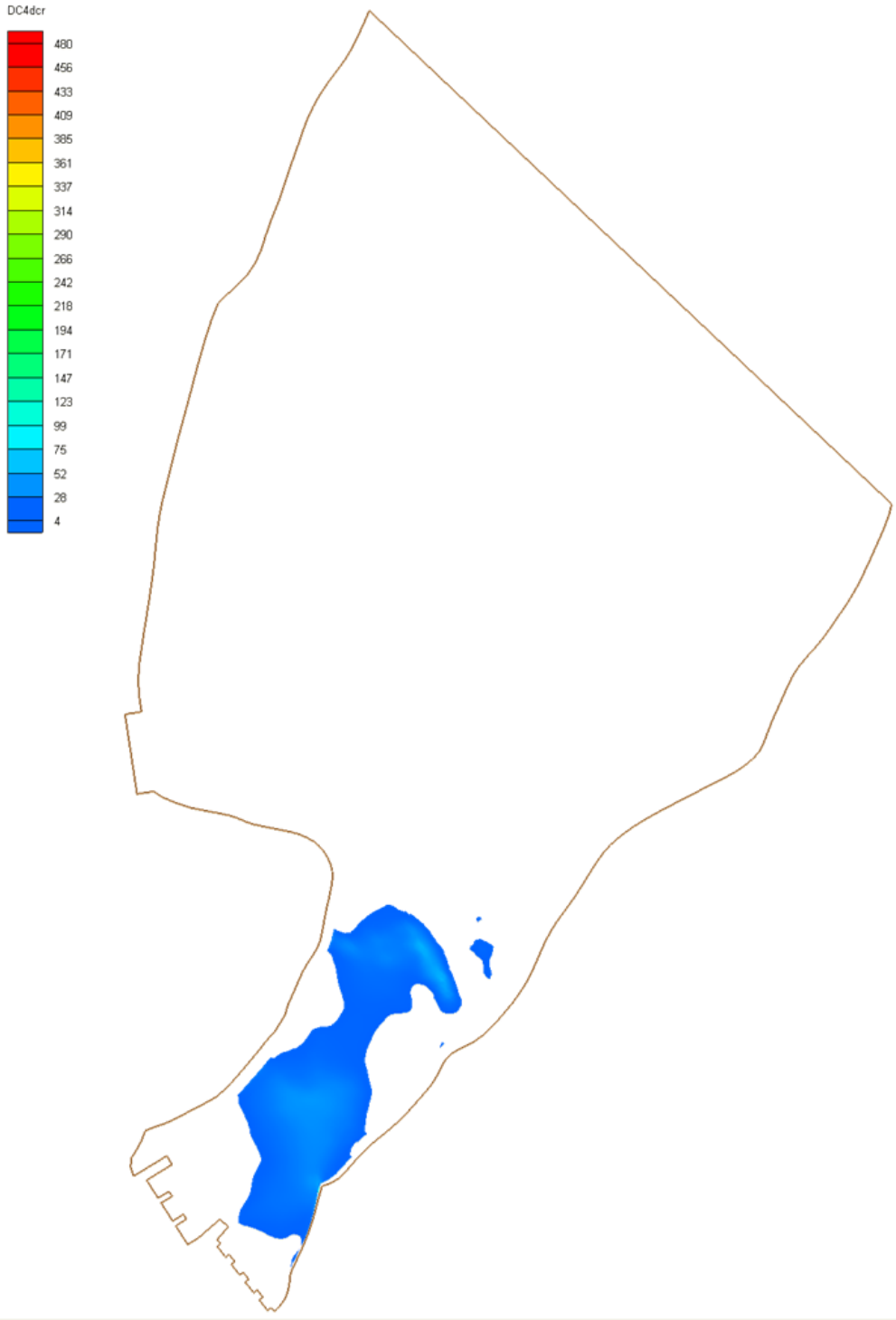

Figure 78. Critical particle diameter (mm) distribution for DC4 in the post-construction model.

8.2.2 DC5

This DC includes a flow from existing spillway of 2300 m^3/s.

8.2.2.1 Velocity

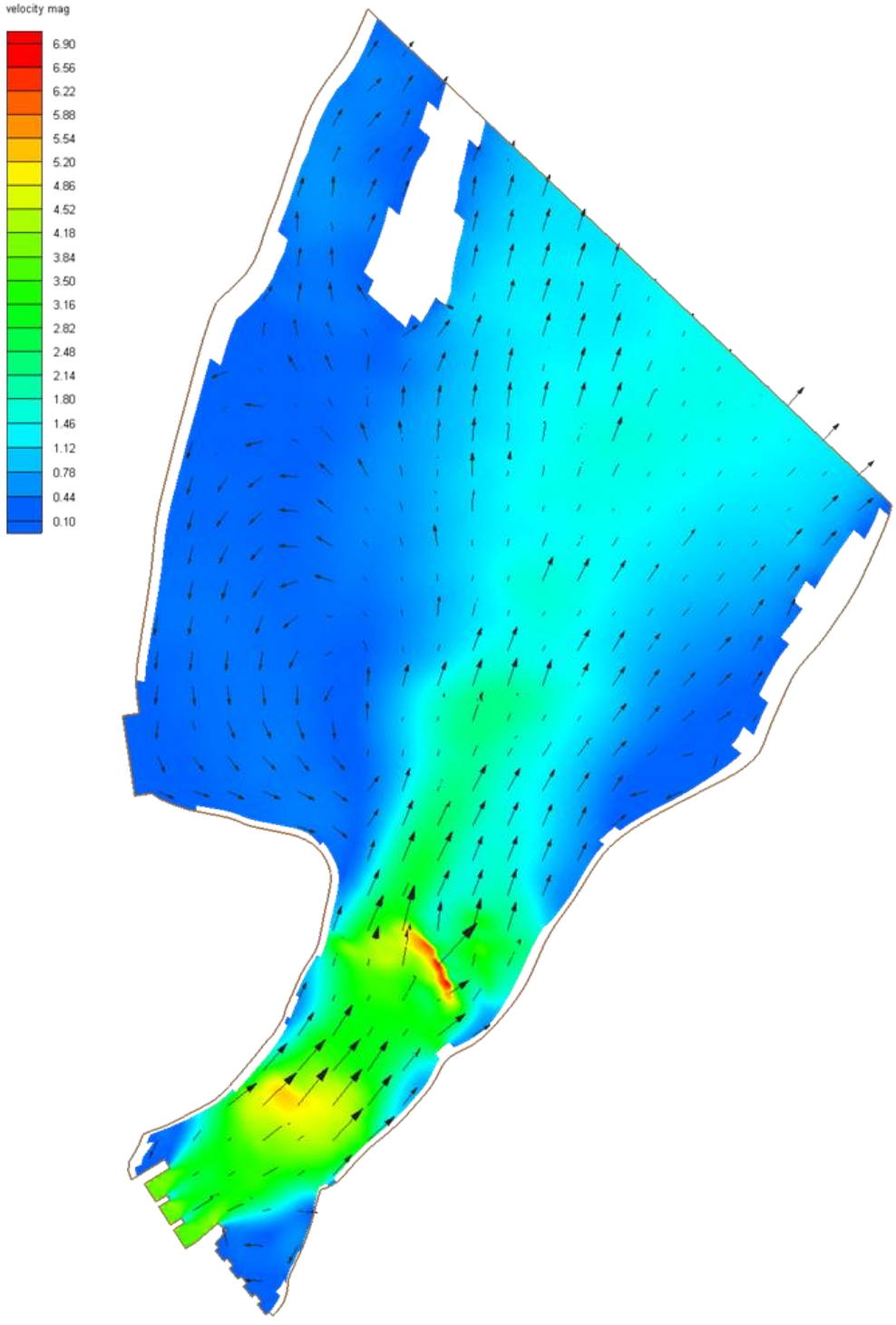

Figure 79. Velocity (m/s) distribution for DC5 in the post-construction model.

8.2.2.2 Water depth

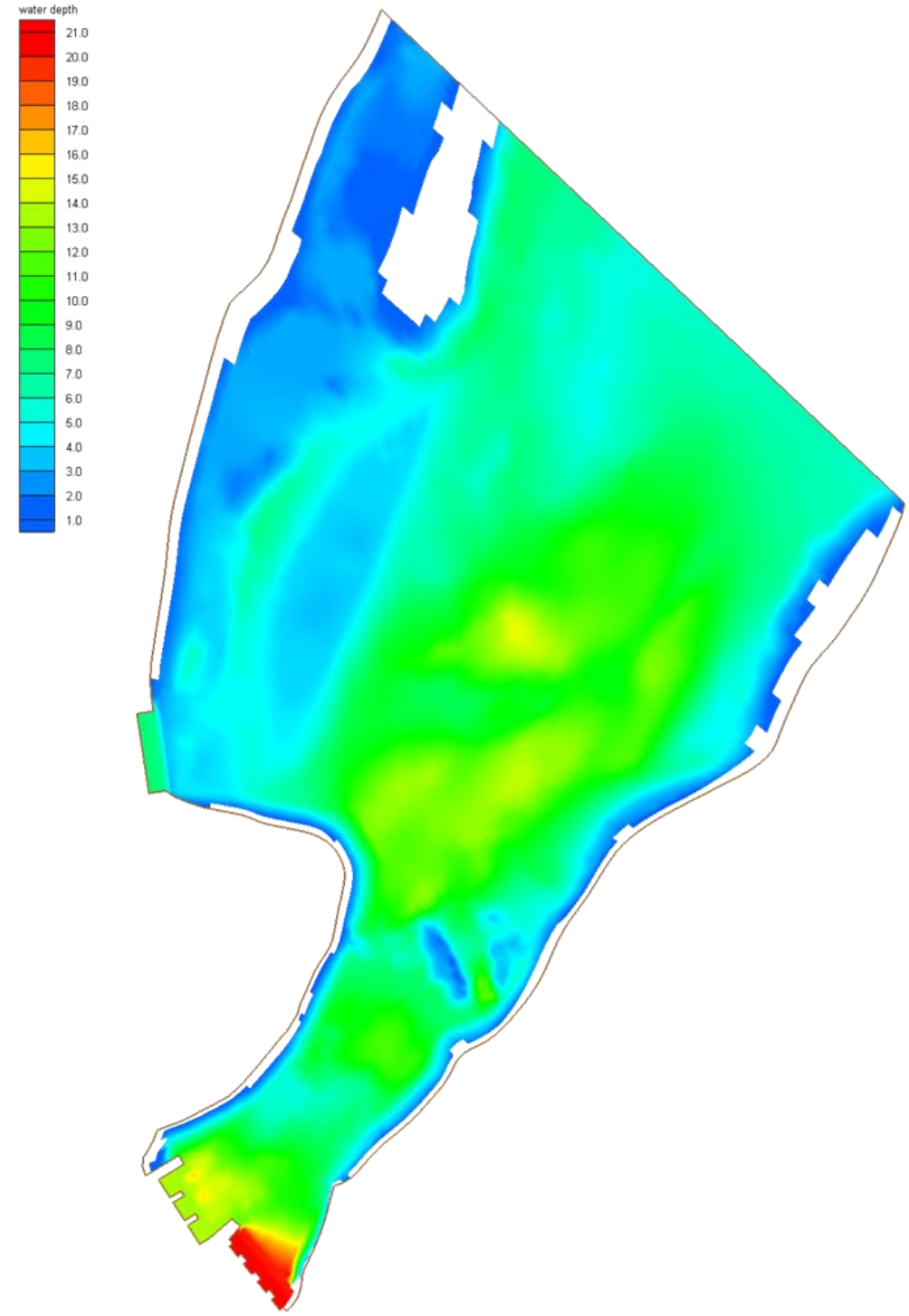

Figure 80. Water depth (m) distribution for DC5 in the post-construction model.

8.2.2.3 Shear stress

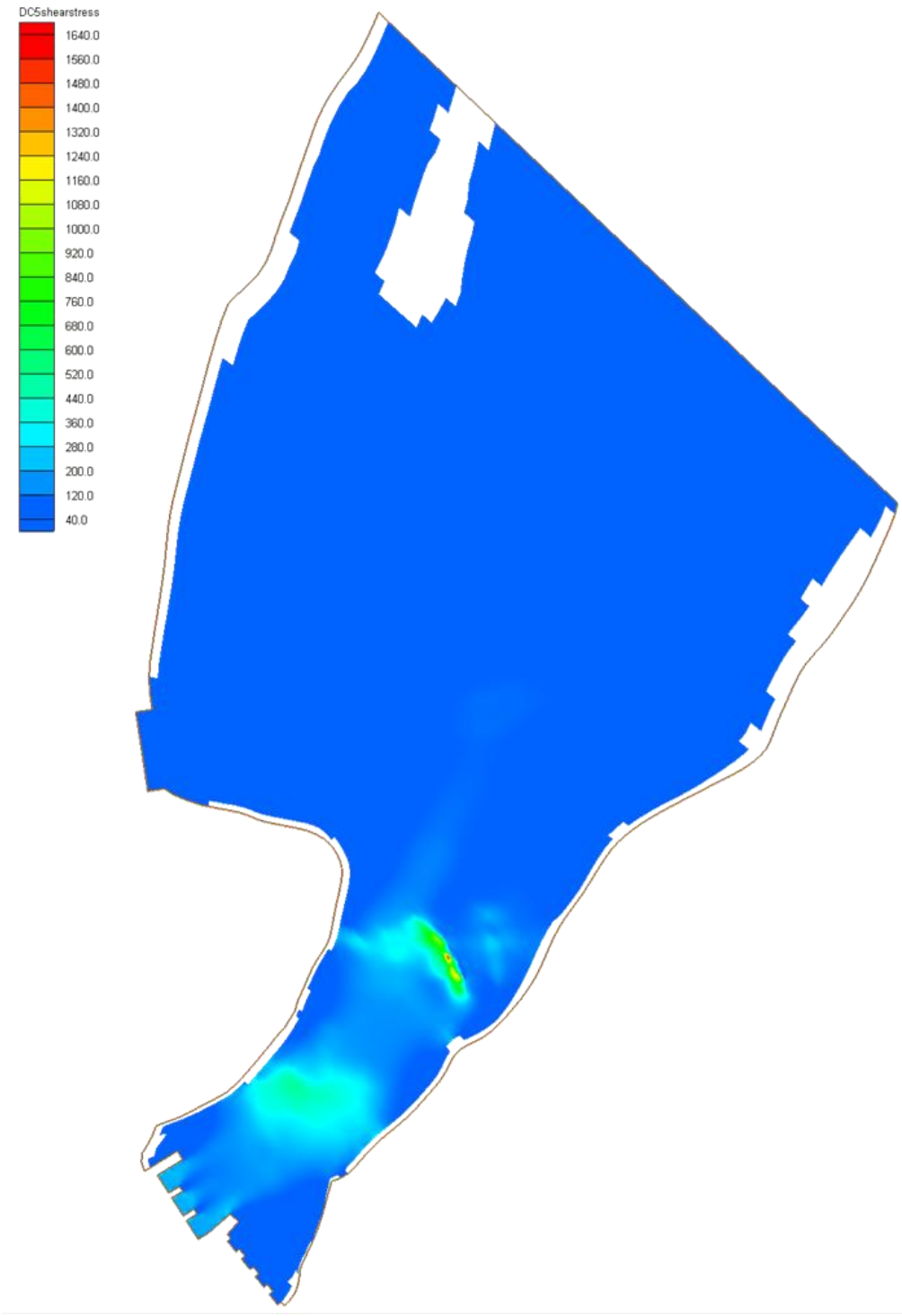

Figure 81. Shear stress (N/m^2) distribution for DC5 in the post-construction model.

8.2.2.4 Critical particle diameter

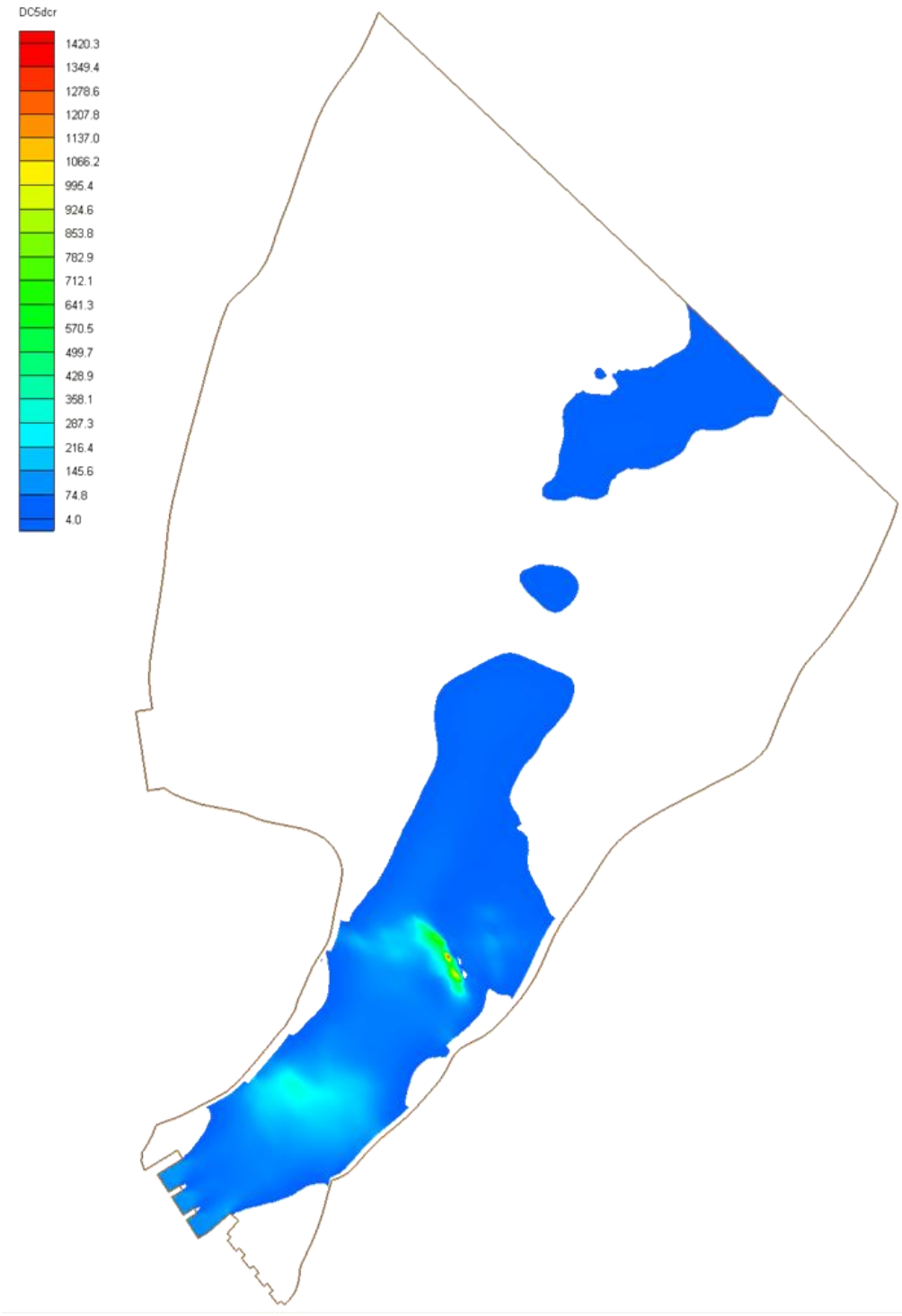

Figure 82. Critical particle diameter (mm) distribution for DC5 in the post-construction model.

8.2.3 DC6

This DC includes a flow from new spillway of 1500 m^3/s.

8.2.3.1 Velocity

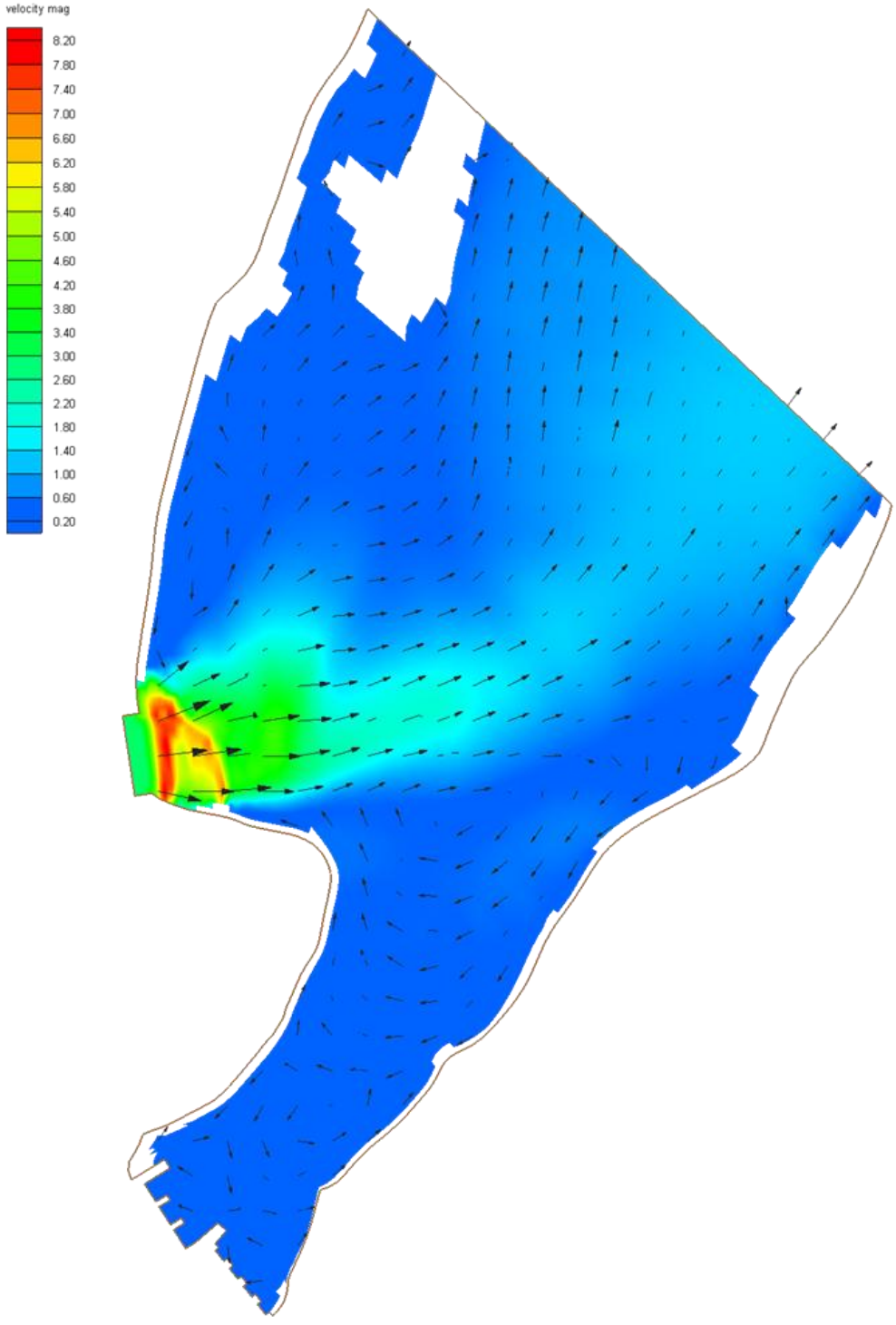

Figure 83. Velocity (m/s) distribution for DC6 in the post-construction model.

8.2.3.2 Water depth

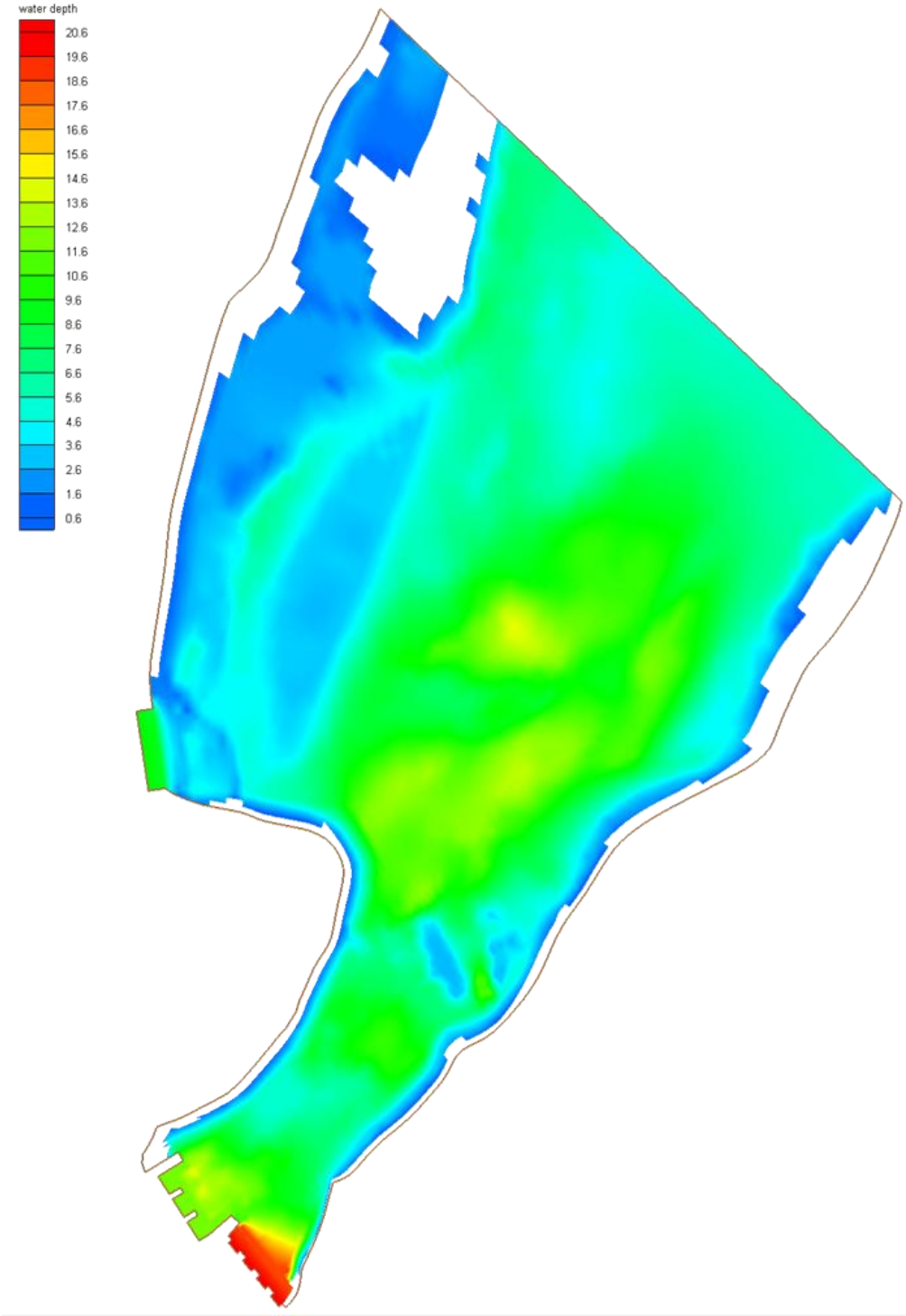

Figure 84. Water depth (m) distribution for DC6 in the post-construction model.

8.2.3.3 Shear stress

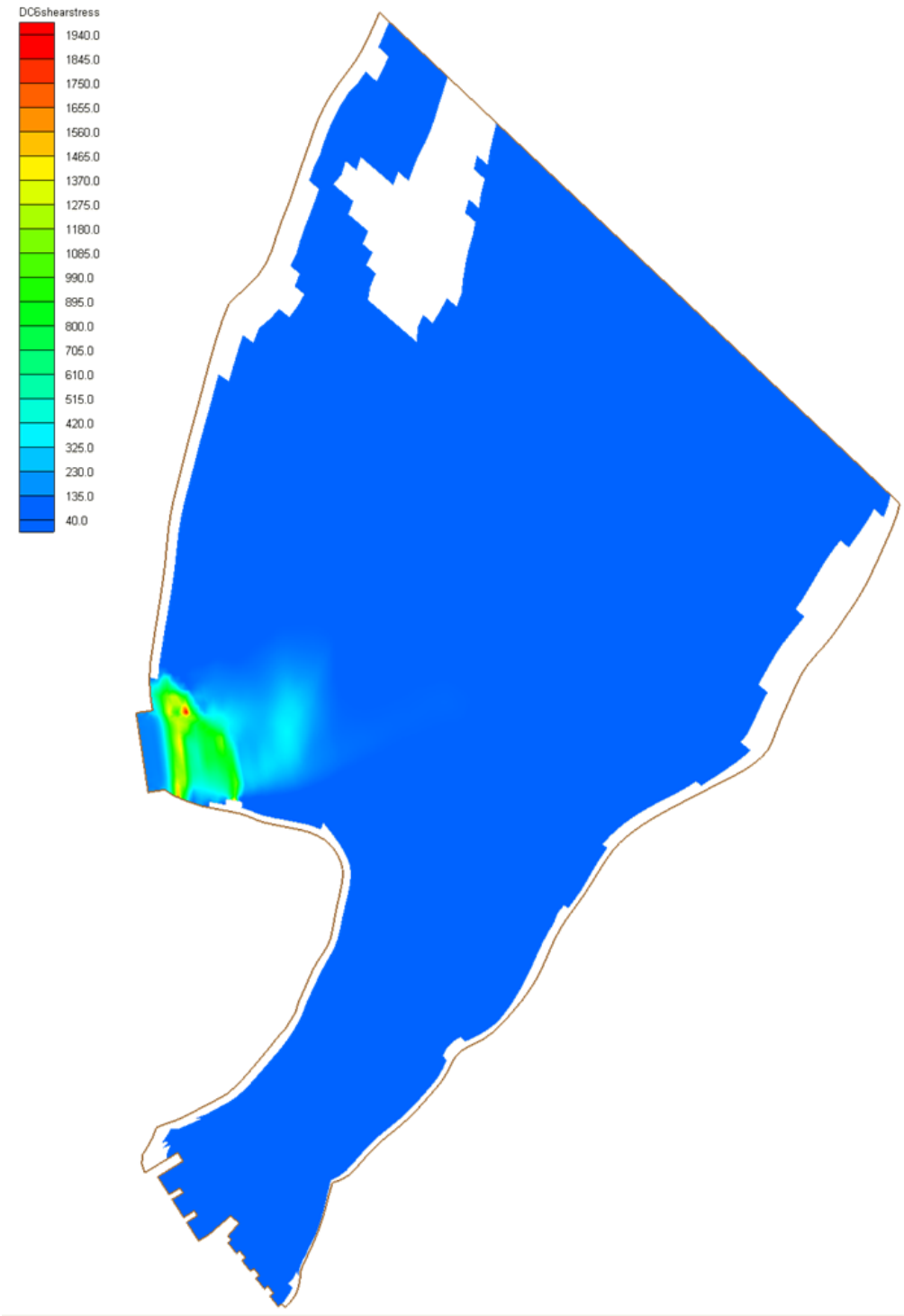

Figure 85. Shear stress (N/m^2) distribution for DC6 in the post-construction model.

8.2.3.4 Critical particle diameter

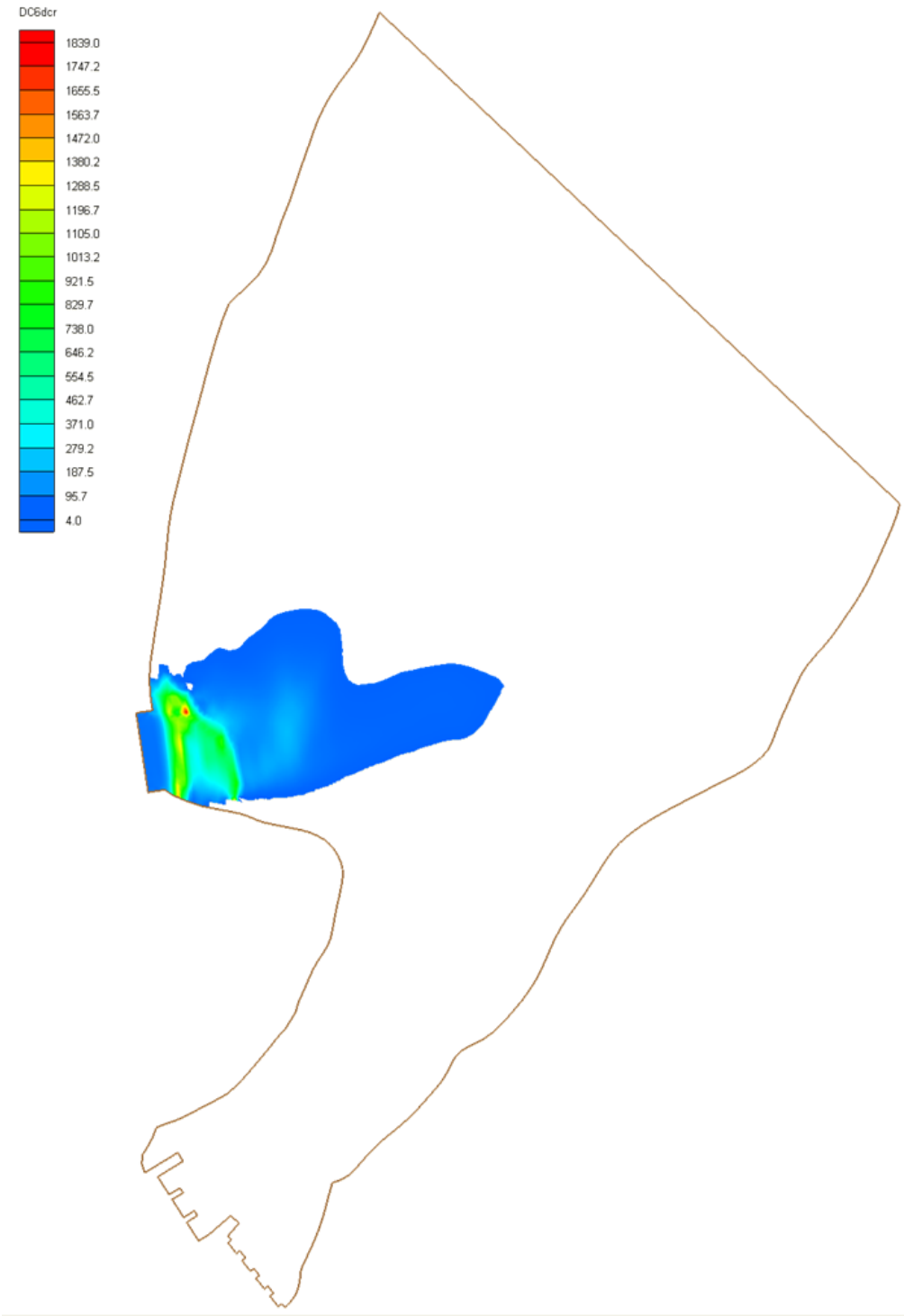

Figure 86. Critical particle diameter (mm) distribution for DC6 in the post-construction model.

8.2.4 DC7

This DC includes a flow from existing spillway of 1800 m^3/s and a flow from new spillway of 1500 m^3/s.

8.2.4.1 Velocity

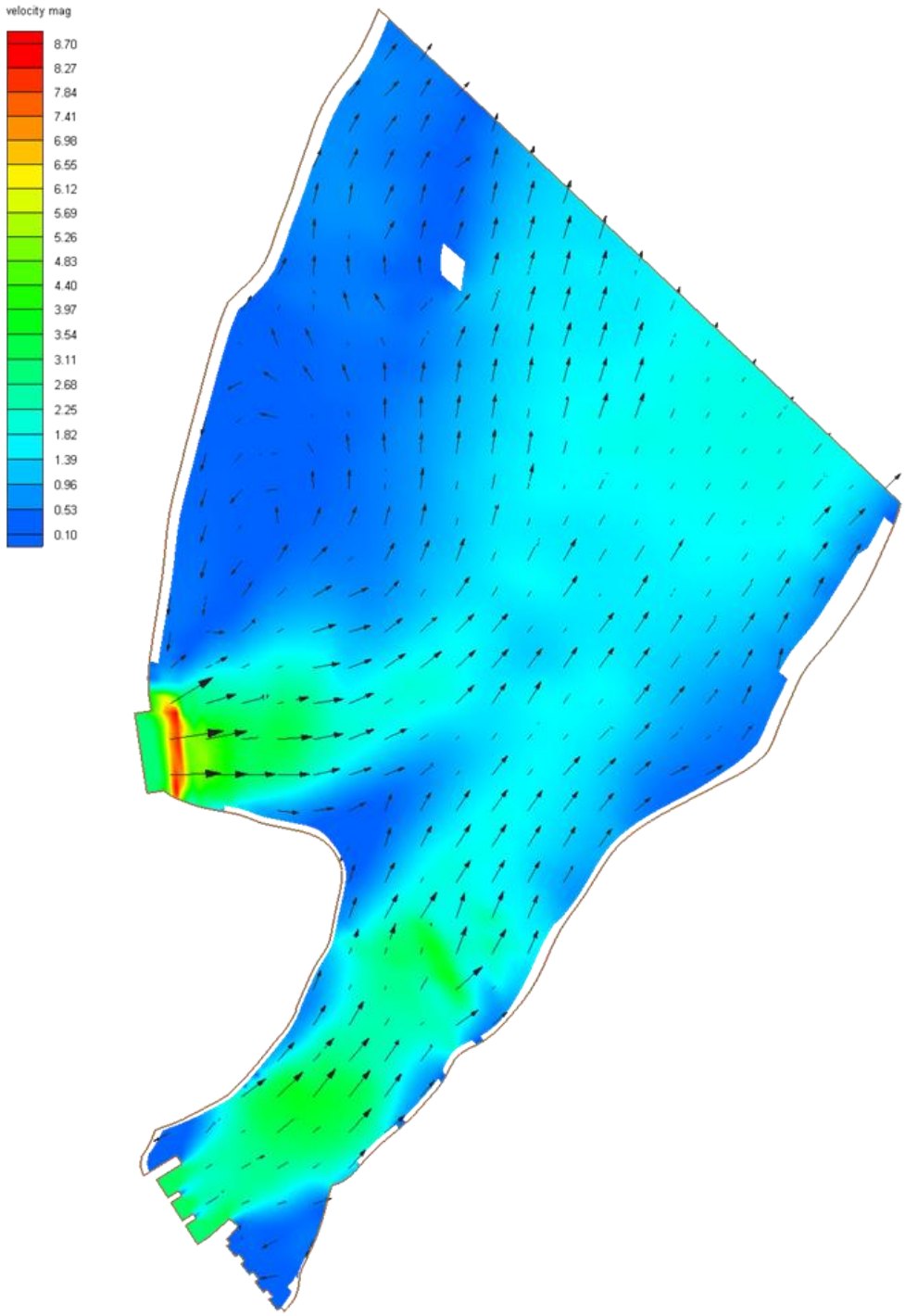

Figure 87. Velocity (m/s) distribution for DC7 in the post-construction model.

8.2.4.2 Water depth

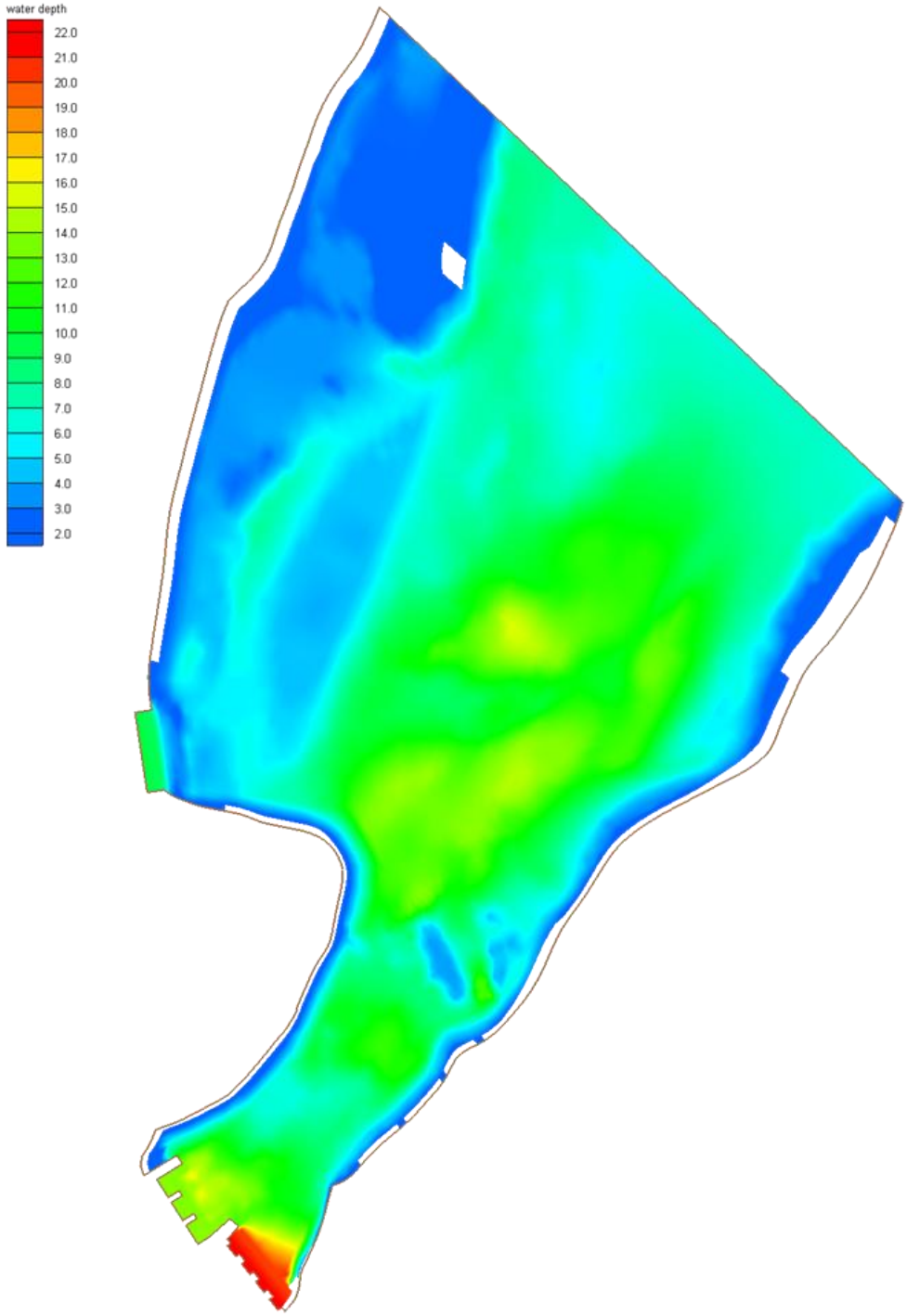

Figure 88. Water depth (m) distribution for DC7 in the post-construction model.

8.2.4.3 Shear stress

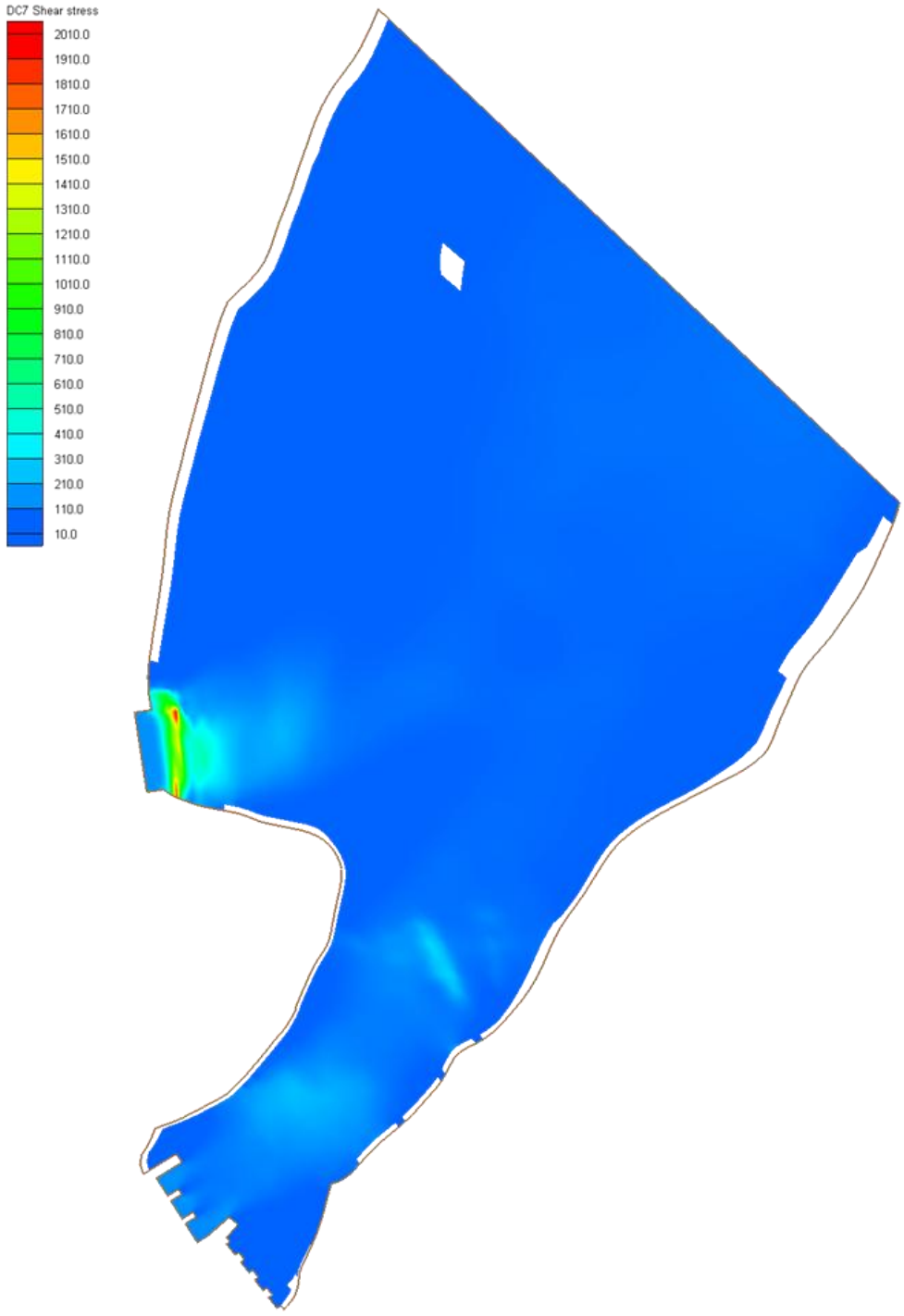

Figure 89. Shear stress (N/m^2) distribution for DC7 in the post-construction model.

8.2.4.4 Critical particle diameter

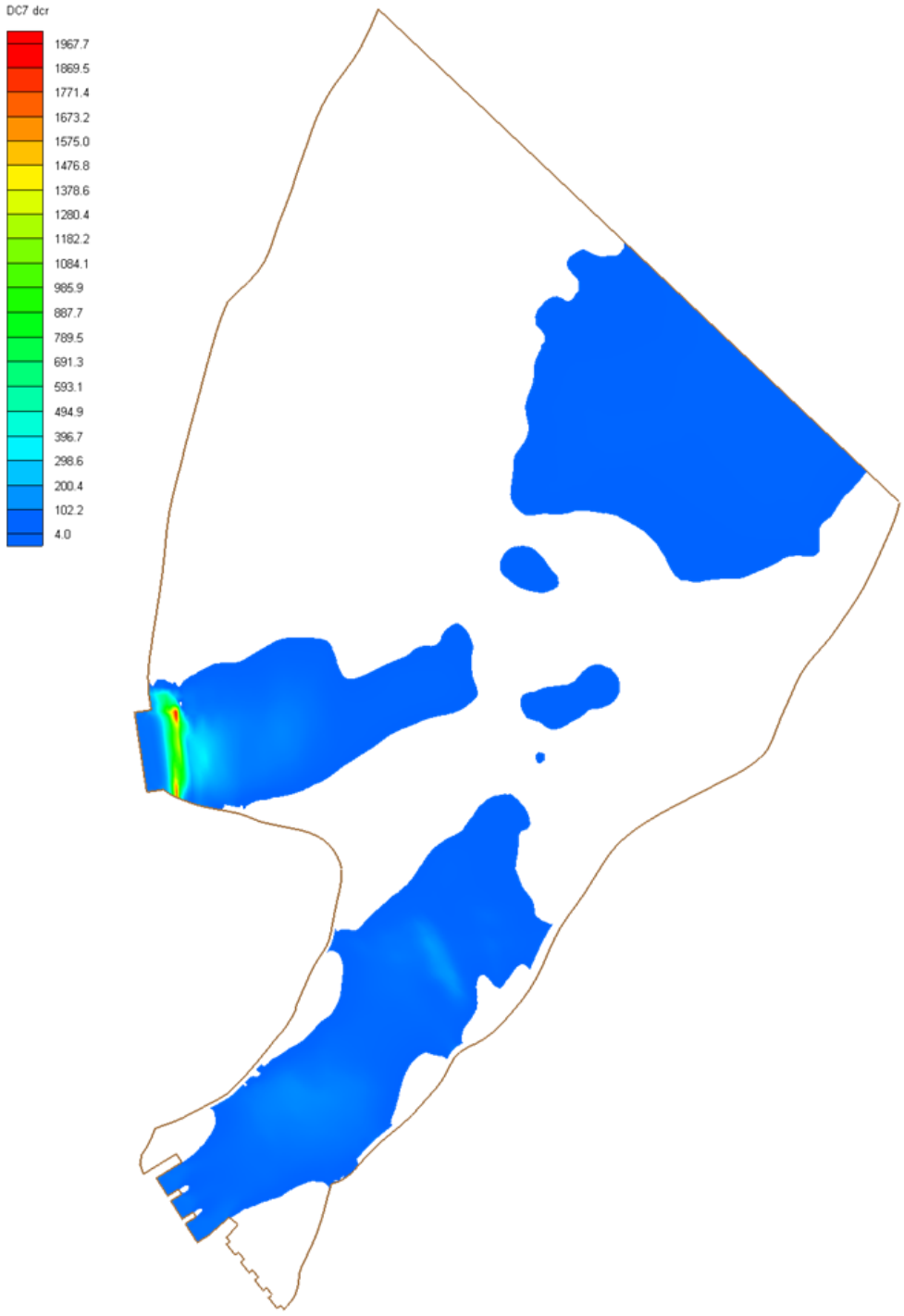

Figure 90. Critical particle diameter (mm) distribution for DC7 in the post-construction model.

8.2.5 DC8

This DC includes a flow from existing spillway of 2300 m^3/s and a flow from new spillway of 1700 m^3/s.

8.2.5.1 Velocity

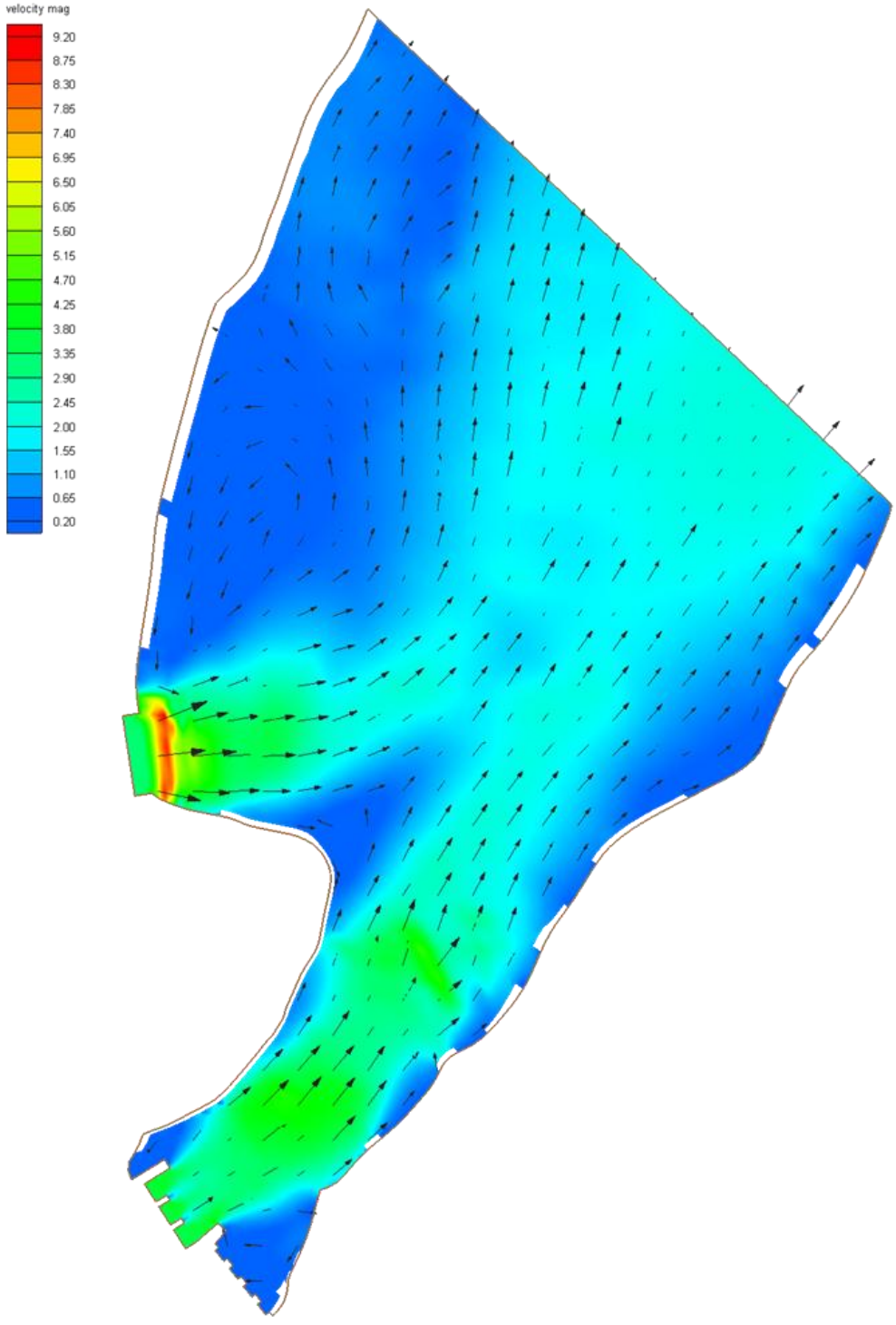

Figure 91. Velocity (m/s) distribution for DC8 in the post-construction model.

8.2.5.2 Water depth

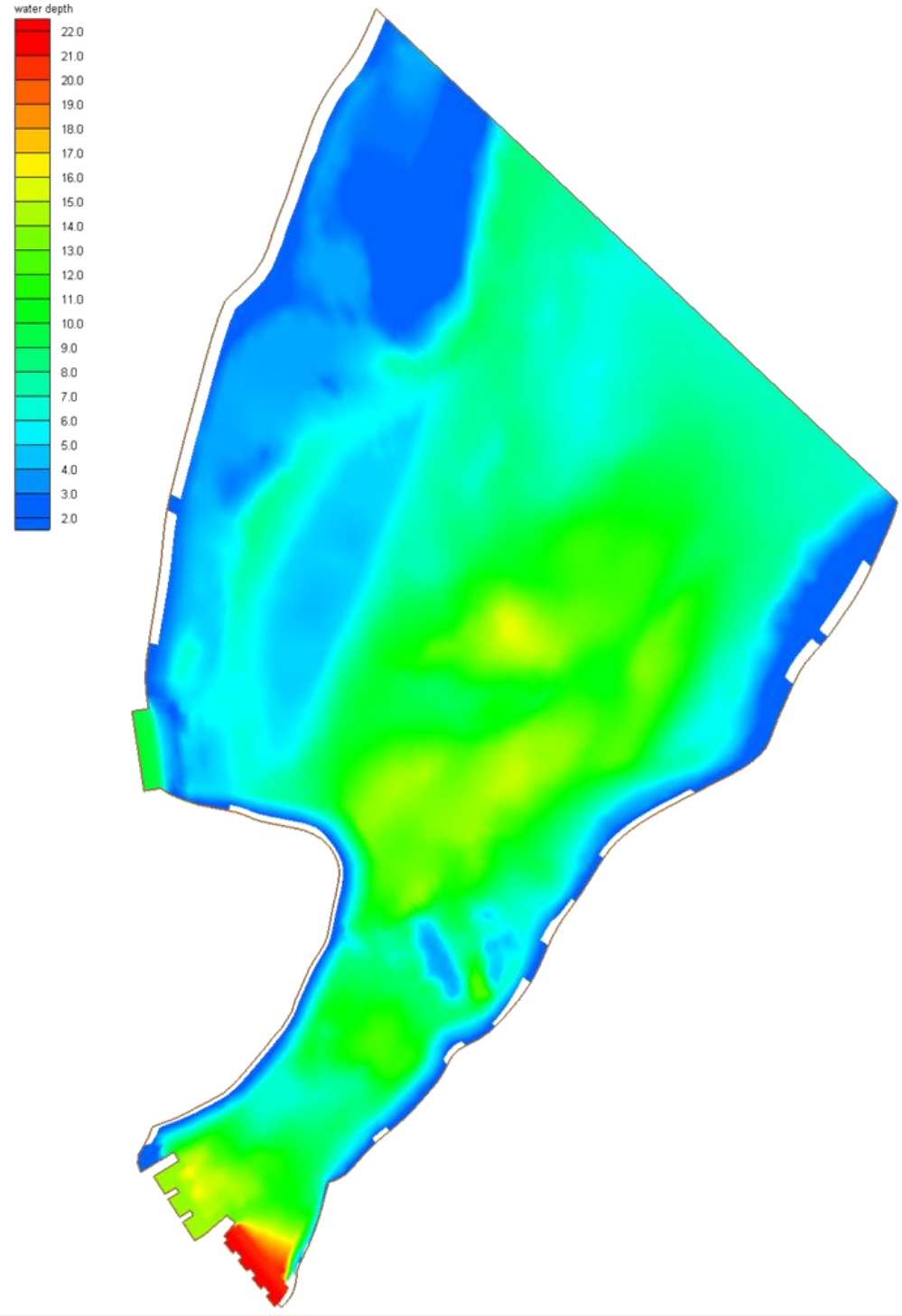

Figure 92. Water depth (m) distribution for DC8 in the post-construction model.

8.2.5.3 Shear stress

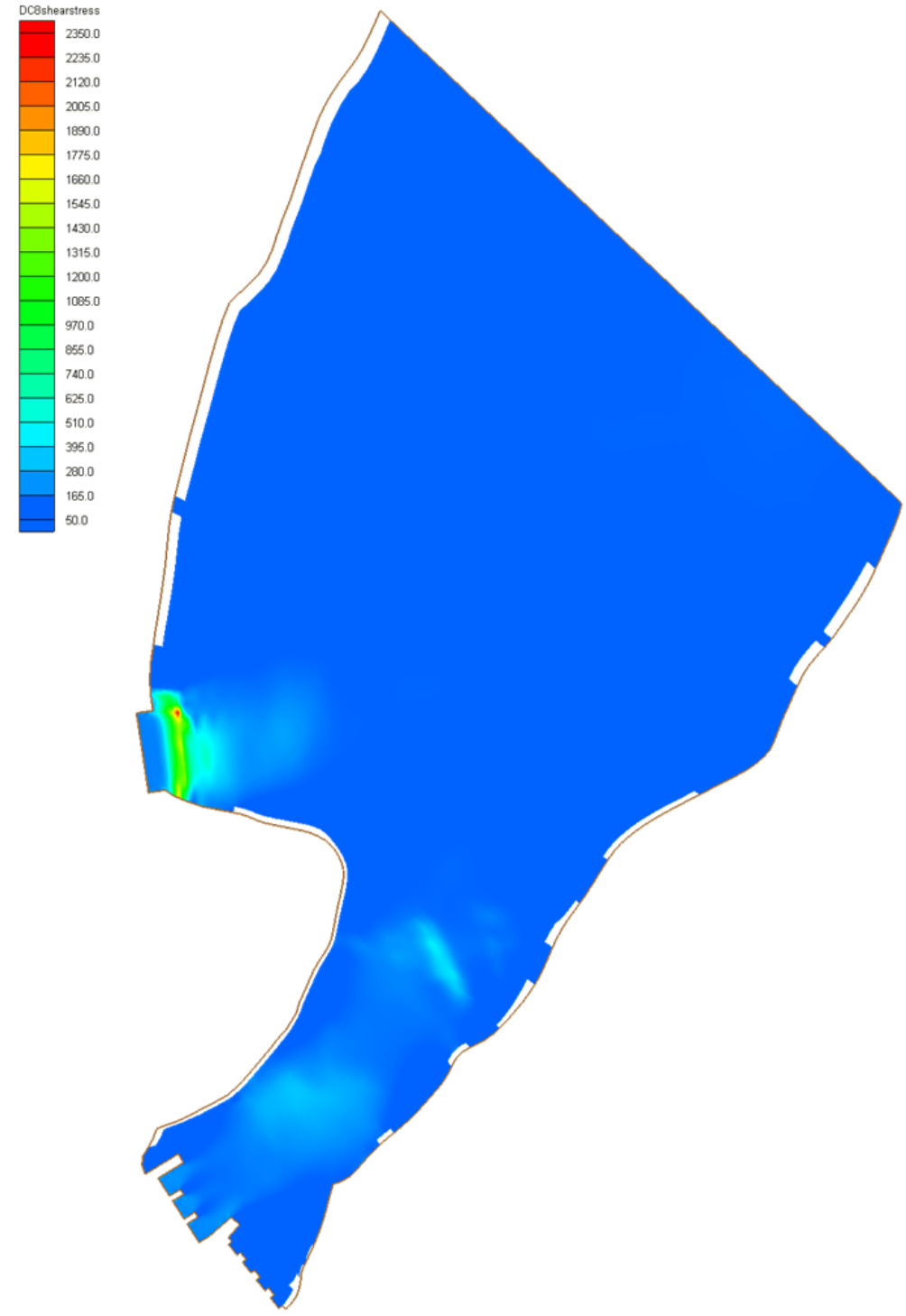

Figure 93. Shear stress (N/m^2) distribution for DC8 in the post-construction model.

8.2.5.4 Critical particle diameter

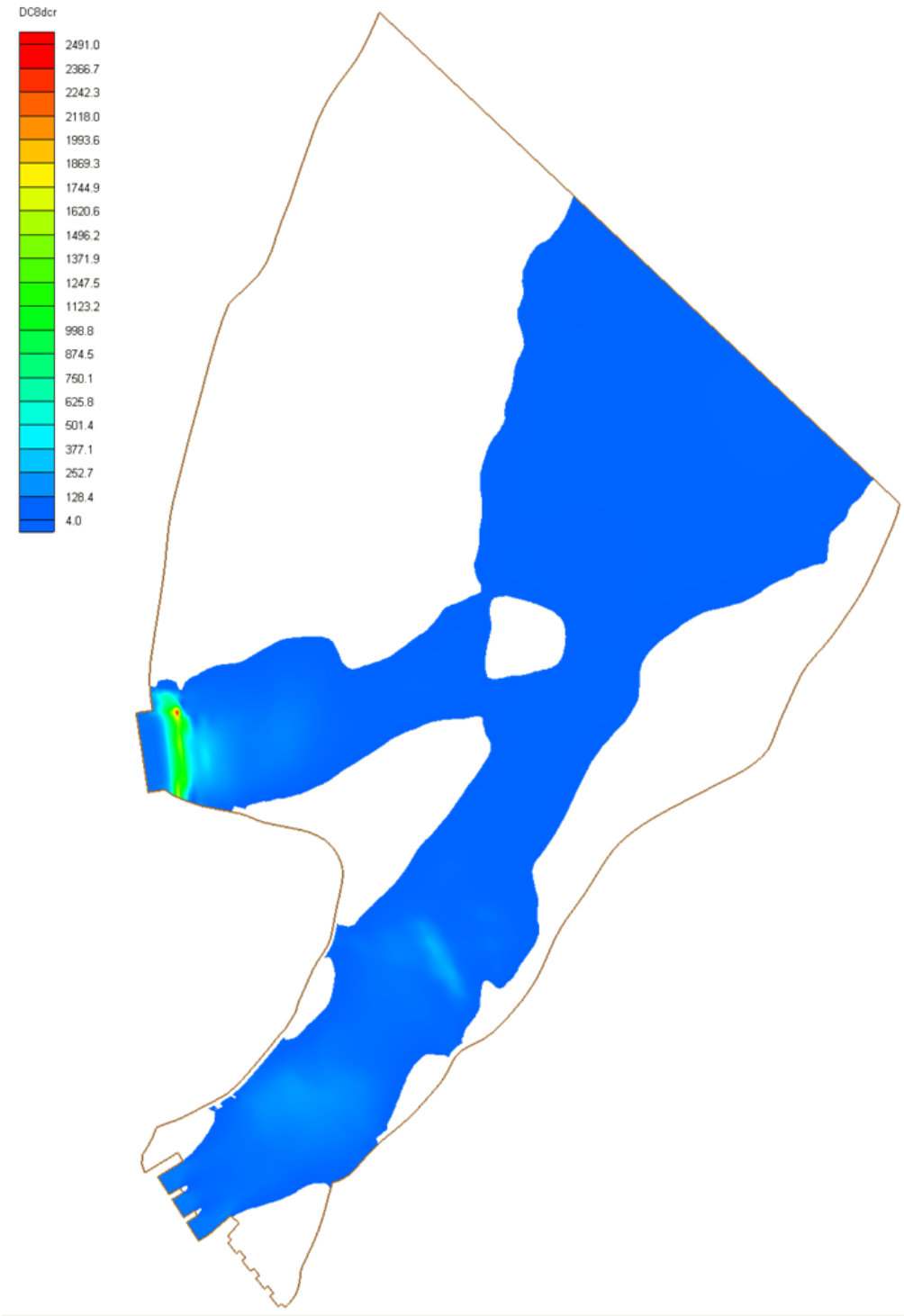

Figure 94. Critical particle diameter (mm) distribution for DC8 in the post-construction model.

8.3 Water depth profile at the power station outlet

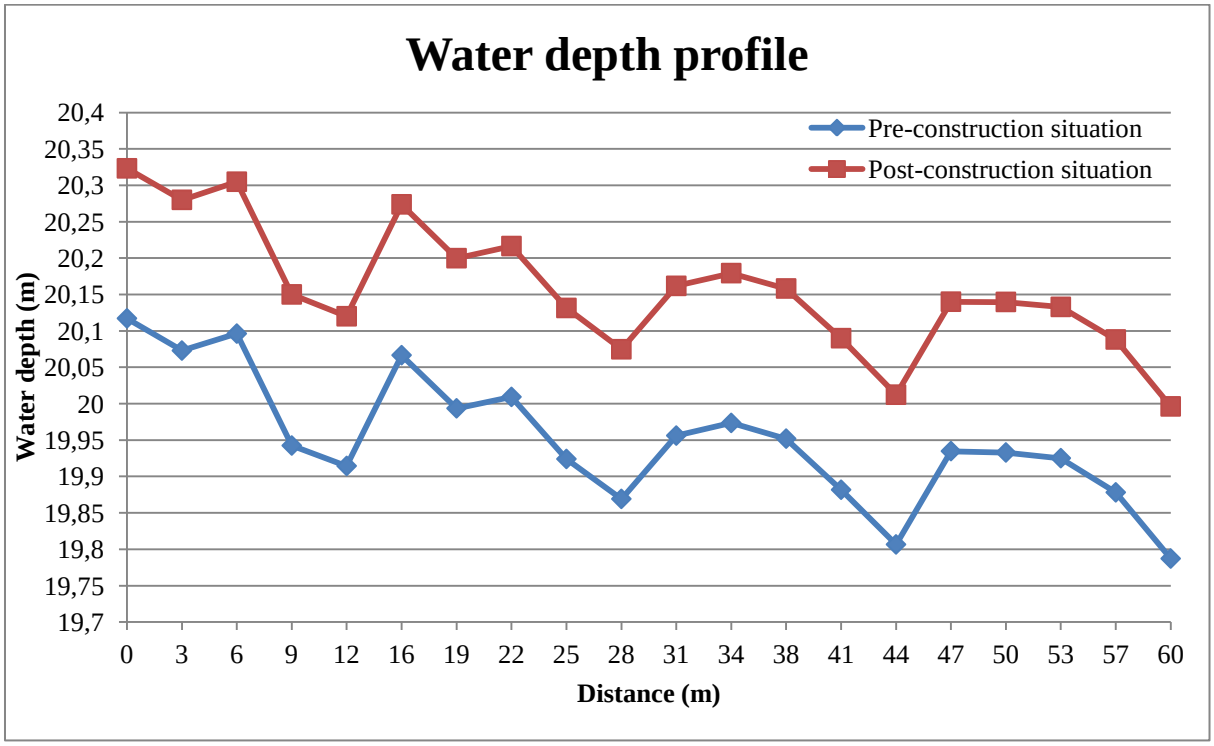

Figure 95. Water depth profile at the power station outlet in the pre- and post-construction models. The profile goes from the shoreline on the right side to the chutes on the left side.

The water depth profiles vary across the river width. However, by averaging all the values, the mean head loss can be calculated:

$\bar{h}_{pre} = 19{,}952\ meters$

$\bar{h}_{post} = 20{,}159\ meters$

$\Delta H = \bar{h}_{pre} - \bar{h}_{post} = -0{,}207\ meters$

Converting this value to power loss is done by using equation 27

Power output in pre- and post-construction (W)

$$P_{pre} = \frac{\rho g Q H_{pre}}{\varepsilon}$$

$$P_{post} = \frac{\rho g Q H_{post}}{\varepsilon}$$

dividing the equations above

$$\frac{P_{post}}{P_{pre}} = \frac{H_{post}}{H_{pre}} = \frac{23 - 0{,}207}{23} = 0{,}991$$

gives a power loss of 0,9% meaning a new power output of

$P_{post} = P_{pre} * P_{loss} = 735 * 0{,}991 = 728{,}39\ GWh/y$

9 Discussion

9.1 Verification process

The calibration and validation results presented in section 7.6 above are all reasonable good. Almost all values in the verification points stays within the set accuracy interval and the velocity profiles generally follows the ones received from the measurements in the physical model. The post-construction model follows the measured values better than the pre-construction model. This might be due to that the alteration of the spillways to keep subcritical flows affects the flows and velocities from the existing spillway more than from the new spillway. Other reasons might be higher accuracy in the measurements, better placements of the observation points or the altered Manning's roughness coefficients. In the validation of the post-construction model, a lower uncertainty interval could have been used. However, as more or less all computed velocities tend to be below the observed ones, especially in the pre-construction model, and since RMA2 is very sensitive to higher velocities i.e. low tuning parameters, the verification process turns into a procedure of finding the lowest possible tuning parameters that would allow the model to converge rather than tuning the parameters up and down to find the optimal values.

It is also important to point out that the combination of the tuning parameters used in this verification process is not the most optimal and there are many combinations that would have led to the same results. The increase in tuning parameters in the post-construction model compared to the pre-construction is probably because the channel cross-section, and thereby the wetted area, from the existing spillway towards the downstream end is severely decreased due to the excavated material zone placed on the left shore. This decrease in area leads to an increase in Froude's number and thereby supercritical flow if the same tuning parameters would have been used (as explained in section 7 above).

Another aspect is that one should be reserved when it comes to tune a numerical model by using roughness and viscosity parameters unless very good data is available. This could lead to a fake sense of reliability towards the model performance. Therefore, the parameter values presented in section 7.6 above should not be regarded as absolute. Furthermore, the tuning parameters might need to be changed as the flow and water depth is altered to match the new conditions and reflect the actual situation. However, due to the lack of data on material properties, this has not been done in this project.

9.2 Flow conditions

First of all, it should be mentioned that the values of the parameters presented in the figures above are not to be regarded as absolute and cannot be considered to be completely reliable due to the modifications of the models to maintain subcritical flows.

For DC1 (figure 63 to 66), the normal situation with a flow from the power station, the velocities are low ranging between 0-2,5 m/s with the highest present in the area around the power station and on the right shoreline where the bathymetry is relatively high. Quite a number of elements are dry due to the low flow, especially in the upper left model area where an island is formed. In figure 22, showing a satellite photo taken during a normal flow situation (DC1), it can be seen that there are some islets and shallow banks in this area which creates the continuous island present in the results. If the resolution of the finite element mesh had been higher, some elements in the area might had been kept wet,

thereby dividing the large island into several small ones and giving a more exact representation of the area. The shear stress follows the velocity profile and ranges from 0-10 N/m^2 in the major part of the investigated area. It becomes highest around the right shoreline next to the power station with 120 N/m^2 and remains around 30-50 N/m^2 a little further out in the channel. The critical particle diameter follows the trends of the shear stress and ranges from 4-10 mm in general. In the area next to the power station it increases up to 80 mm with a maximum of 135 mm at the right shoreline.

Comparing the results from DC1 with DC4 shows that the velocity increases with 0,5-1 m/s in the narrow passage between the power station and the new spillway due to the decreased river width. There is also a change in the flow pattern along the left shoreline close to the new spillway as a circulation zone is formed. This is most likely due to the more sudden expansion after the narrow passage of the jet stream flowing from the outlet, which causes turbulence and circulation in the areas outside of the jet where the water levels are higher and the velocities lower. The shear stresses stay the same in the major part of the area except around the right shoreline next to the power station where it increases with around 70% due to the higher velocities. As a consequence, the critical particle diameter in the area increases with up to 100%.

The change in water depth between DC1 and DC4 (figure 75 to 78) was computed in order to investigate possible head losses at the power plant and is displayed in figure 95. The results points toward an increase in water depth with 20,7 centimeters at the downstream end after the construction of the new spillway, giving a new water head of 22,8 meters and a power loss of 0,9% or 6,62 GWh per year. This loss is much higher than expected and the questionable results are probably due to the enforced subcritical conditions throughout the model but also the depth convergence parameter, the Manning's roughness coefficient and eddy viscosity values as well as the mesh resolution. This could be a subject to investigate further in future studies.

DC2 (figure 67 to 70) is a flow from the existing spillway where the velocities ranges from 0-5,5 m/s with the highest near the chutes and the shallower areas in the first 200 meters of the model. Due to the high flow, the number of dry elements at the shorelines and the island in the upper left corner are decreased. In the deeper, calmer left side of the river there is a large circulation zone formed which flows counterclockwise with velocities of 0-1 m/s. The shear stress follows the velocity profile and ranges from 0-20 N/m^2 in the major part of the area. It becomes highest in the shallower areas about 200 meters downstream of the chutes with 450 N/m^2 and in the general area just downstream the spillway with 200-300 N/m^2. The critical particle diameter follows the same pattern and is relatively high in the shallower areas with 470 mm.

Comparing the results from DC2 and DC5 (figure 79 to 82) shows that the velocities increase with 1-1,5 m/s in the narrow passage downstream the existing spillway and reaches up to 7 m/s in the shallower areas about 200 meters downstream. The large circulation zone present in DC2 is removed by the excavated material placed on the left side of the river as planned. Instead, there is a smaller circulation zone formed in the deeper areas next to the new spillway further downstream, same as in DC4. In DC5 the shear stress increases radically, especially around the existing spillway (around 200%) and in the shallower parts 200 meters downstream (up to 500%). The critical particle diameter increases both in affected model area and in magnitude with an increase of up to 550% in the shallower areas. This is most likely due to the decreased river width and removal of the circulation zone which increases the velocities.

For DC3 (figure 71 to 74), the velocities range from 0-9 m/s, the shear stress from 0-2300 N/m^2 and the critical particle diameter from 0-2600 mm. Comparing with DC2, this is an increase in velocity

with 60% and in shear stress and critical particle diameter with over 500%. The flow pattern and the points of high velocities and shear stress are the same as in DC2.

For DC6 (figure 83 to 86), with a flow from the new spillway, the velocities ranges between 0-8,5 m/s. The highest velocities are found in the shallower areas near the new spillway outlet. There is one circulation zone formed on the left river side upstream of the new spillway flowing counterclockwise, one at the end of the narrow passage leading from the existing spillway flowing clockwise, one further upstream in the narrow passage flowing counterclockwise and two on the left and right river side flowing clockwise. The shear stress ranges from 0-100 N/m^2 in the major part of the area and is highest around the new spillway where it ranges between 1000-2800 N/m^2. The new spillway is planned with erosion protection banks on both sides of the outlet which will most likely prevent erosion from these high shear stresses. The critical particle diameter follows the same pattern and has a maximum value of 2800 mm near the new spillway.

DC7 (figure 87 to 90) is a combined flow from the new and existing spillway where the velocities range between 0-8,7 m/s. The velocities are highest around the new spillway outlet and somewhat lower in the passage from the existing spillway. There is a circulation zone flowing counterclockwise formed on the left river side upstream of the new spillway and the previous island in the upper left corner is almost completely flooded. The shear stress ranges from 0-100 N/m^2 in the major part of the area and is highest around the new spillway outlet (1000-2000 N/m^2) and lower in the passage from the existing spillway (0-400 N/m^2). The same goes for the critical particle diameter which reaches a maximum of 1970 mm at the outlet of the new spillway.

Comparing the results from DC7 and DC8 (figure 91 to 94) it can be seen that the velocities are slightly increased throughout the model (0-5%). The same goes for the shear stress and the critical particle diameter which increases with 20% and 30% respectively. The flow pattern and the points of high velocities are the same in the two simulations.

9.3 Erosion

As there is no information regarding the particle size distribution in the investigated area, it is difficult to analyze the erosion potential. Since the majority of the riverbanks are protected with erosion resistant material, especially around the spillways and the power station, it is believed that there will be very little or no erosion of the bed material on the riversides, except during very high flows such as 3000-4000 m^3/s. However, these high flows will occur once every 10 000 years or less. Nevertheless, the computed bed shear stresses and critical particle diameters from the simulations could work as an indicator of what kind of erosion protection material that needs to be placed in that particular area to prevent future erosion. Even though the absolute values are not reliable the different areas can be related to each other, as exemplified above, in order to get a feel for the relative erosion potential. The areas of highest potential can then be investigated more thoroughly in further studies.

One such area is the shallow banks about 200 meters downstream of the existing spillway. It is unclear whether these areas are sufficiently protected or not as they are exposed to very high velocities and shear stresses in several cases. During high flow, the bed material in these areas might be transported further downstream and cause problems.

9.4 SMS numerical modeling

The capabilities of the subcritical numerical model RMA2 is not enough to completely reflect the flow conditions as the high initial velocities in the jet streams leads to supercritical flow in several sections. This in turn leads to a necessary simplification of the spillway inlets which affects the initial flow momentums and velocities. Therefore, the velocities and the flow pictures are most likely not correctly depicted in the near field areas. In order to capture and investigate the flow around these areas, a supercritical/subcritical two or three-dimensional model has to be applied. The high vertical velocity variations at the spillways could be separately evaluated by a three-dimensional model such as RMA10. As mentioned in section 4.1, if detailed boundary conditions and data are available, a three-dimensional model has improved predictive ability when a two-dimensional model does not try to correct for the effects of secondary circulation on the depth-averaged flow field. It is also better at estimate the correct bed shear stress and mixing processes.

Nevertheless, the general flow patterns and trends received from the RMA2 simulations correlates very well with what has been found in previous studies and will function as a good complement to the future tests in the physical hydraulic model in the laboratory at Vattenfall R&D.

10 Conclusions

To sum up, the construction of the new spillway and the placement of the excavated material on the left riverside will lead to an increase in velocities, shear stresses and critical particle diameters. This increase will be most pronounced in the vicinity of the spillways and the power station outlet. A subject for further investigations is the increase of the downstream water depth after the construction. The loss is much higher than expected and the questionable results may be due to a number of factors related to the numerical model.

Not any clear conclusions can be drawn regarding the erosion potential as there is no information regarding the particle size distribution in the investigated area. However, the bed shear stress and critical particle diameter values in the different areas may be related to each other in order to get a feel for the relative erosion potential. They could also work as an indicator of what kind of erosion protection material that needs to be placed in that particular area in order to prevent future erosion. Another topic for further investigations is whether the shallow areas about 200 meters downstream of the existing spillway are sufficiently protected or not as they are exposed to very high velocities and shear stresses in several situations.

Regarding the numerical model, the capabilities of RMA2 are not enough to completely reflect the flow conditions, especially in the area around the spillways. Even so, the general flow patterns and trends received from the simulations will function as a good complement to the future tests in the physical hydraulic model.

Finally, it should be mentioned that the purpose of numerical modeling as stated by W.A. Thomas, a retired research hydraulic engineer from US Army Corps of Engineers Waterways Experiment Station, is to “gain insigth, not answers”. In this respect, the project should be regarded as successful.

References

Printed

Andréasson, J. et al., 2004. Hydrological Change: Climate Change Impact Simulations for Sweden. *Ambio*, 33(4/5), pp.228-34.

Bates, P.D. & Anderson, M.G., 1993. A Two-Dimensional Finite-Element Model for River Flow Inundation. *Proceedings: Mathematical and Physical Sciences*, 440(1909), pp.481-91.

Bechara, T.A., Boudreault, A., Corfa, G. & Leclerc, M., 1995. Two-Dimensional Hydrodynamic Modeling: A Neglected Tool in the Instream Flow. *Transactions of the American Fisheries Society*, 124(5), pp.645-62.

Bergström, S., Harlin, J. & Lindström, G., 1992. Spillway design floods in Sweden. I: New guidelines. *Hydrological Sciences*, 37(5), pp.505-19.

Blackburn, J. & Steffler, P., 2002. *River 2D: Two-Dimensional Depth Averaged Model of River Hydrodynamics and Fish Habitat - Introduction to Depth Averaged Modeling and User's*. University of Alberta.

BOSS International, 1999. *Surface water modeling system version 6.0 - User's manual*.

Bradbrook, K.F. et al., 1999. The application of computational fluid dynamics to natural river channels: three-dimensional versus two-dimensional approaches. *Geomorphology*, 29, pp.1-20.

Chow, V.-T., 1959. *Open Channel Hydraulics*. New York: McGraw-Hill.

Coufal, R., 1997. *Bed changes and sediment transport at river mouth*. Gdansk: IBW PAN.

Ekström, I., Yang, J.X.L. & Berg, M., 2011. *Improving spillway discharge saftey at Bergeforsen*. Älvkarleby: Vattenfall Research and Development AB.

Elforsk, 2011. Dimensionerande flöden för dammanläggningar för ett klimat i förändring - metodutveckling och scenarier. *Elforsk*, 25.

Frisk, A., Wänn, A. & Yang, J.X.L., 2010. *Bergeforsens nya tunnelsutskov, hydrauliska modellförsök sommaren 2010*. Älvkarleby: Vattenfall Research and Development AB.

Hamill, L., 2001. *Understanding hydraulics*. 2nd ed. New York: Palgrave Macmillan.

Hudson, N.W., 1993. *Field measurement of soil erosion and runoff*. Ampthill: Food and Agriculture Organization of the United Nations.

KFR, 2007. *Riktlinjer för bestämning av dimensionerande flöden för dammanläggningar - Nyutgåva 2007*. Svensk energi, Svenska kraftnät, SveMin.

King, I., 2005. *Users Guide to RMA2 WES - Version 4.5*. New York: WexTech Systems, Inc.

Lysne, D.K., Glover, B., Stole, H. & Tesaker, E., 2003. *Hydraulic Design*. 8th ed. Trondheim: Norwegian University of Science and Technology - Department of Hydraulic and Environmental Engineering.

Soulsby, R., 1997. *Dynamics of marine sands - A manual for practical applications*. London: Thomas Telford.

US Army Corps of Engineers Waterways Experiment Station, Hydraulics Laboratory, n.d. *Users Guide to GFGEN - Version 4.27*.

USBR, 2001. *USBR Water Measurement Manual*. Washington: USDA.

Wänn, A. & Yang, J.X.L., 2010. *Bergeforsen dammsäkerhet, hydrauliska modellförsök*. Älvkarleby: Vattenfall Research and Development AB.

Yang, J.X.L., 2000. *Hydrauliska studier för Bergeforsens kraftstation, Indalsälven*. Älvkarleby: Vattenfall Research and Development AB.

Internet

Bergeforsfisket, 2012. *Nyheter*. [Online] Available at: http://www.bergeforsfisket.com/nyheter.php [Accessed 19 April 2012].

Google, 2011. *Google Maps*. [Online] Available at: http://maps.google.se/ [Accessed 18 January 2012].

SCB, 2011. *Tätorter; arealer, befolkning*. [Online] Available at: http://www.scb.se/Pages/ProductTables____13001.aspx [Accessed 18 January 2012].

SMHI, 2009. *Om flödestatistik för Sveriges vattendrag*. [Online] Available at: http://www.smhi.se/klimatdata/hydrologi/vattenforing/1.8369 [Accessed 19 January 2012].

SMHI, 2012. *Vattenwebb*. [Online] Available at: http://vattenweb.smhi.se/ [Accessed 18 January 2012].

Sundsvalls tidning, 2012. *Klart med brobygget i Bergeforsen*. [Online] Sundsvalls tidning Available at: http://st.nu/medelpad/timra/1.4570349-klart-med-brobygget-i-bergeforsen [Accessed 19 April 2012].

Svenska kraftnät, 2011. *Lagar, förordningar och riktlinjer*. [Online] Available at: http://www.svk.se/Om-oss/Var-verksamhet/Dammsakerhet/Lagar-forordningar-och-riktlinjer-/ [Accessed 20 January 2012].

Vattenfall, 2010. *Bergeforsen*. [Online] Available at: http://produktion.vattenfall.se/powerplant/bergeforsen [Accessed 18 January 2012].

Vattenfall, 2012a. *Indalsälven*. [Online] Available at: http://www.vattenfall.se/sv/file/indalsalvensvpdf_11336352.pdf [Accessed 18 January 2012].

Vattenfall, 2012b. *Bergeforsen kraft AB*. [Online] Available at: http://bergeforsenskraft.se/ [Accessed 19 April 2012].

Other

Yang, J.X.L., 1998. *Pre-construction physical hydraulic model.* [photograph].

Yang, J.X.L., 2012. Discussion regarding erosion and sediment transport. [conversation] (Personal communication, 2 February 2012).